# AN EXPERIMENTAL STUDY OF A PLANE TURBULENT WALL JET USING PARTICLE IMAGE VELOCIMETRY

A Thesis Submitted to the College of

Graduate Studies and Research

in Partial Fulfillment of the Requirements

for the Degree of Master of Science

in the Department of Mechanical Engineering

University of Saskatchewan

Saskatoon

By

Matthew Dunn

## PERMISSION TO USE

In presenting this thesis in partial fulfillment of the requirements for a Postgraduate degree from the University of Saskatchewan, I agree that the Libraries of this University may make it freely available for inspection. I further agree that permission for copying of this thesis in any manner, in whole or in part, for scholarly purposes may be granted by the professor or professors who supervised my thesis work or, in their absence, by the Head of the Department or the Dean of the College in which my thesis work was done. It is understood that any copying or publication or use of this thesis or parts thereof for financial gain shall not be allowed without my written permission. It is also understood that due recognition shall be given to me and to the University of Saskatchewan in any scholarly use which may be made of any material in my thesis.

Requests for permission to copy or to make other uses of materials in this thesis in whole or part should be addressed to:

Head of the Department of Mechanical Engineering
57 Campus Drive
University of Saskatchewan
Saskatoon, Saskatchewan S7N 5A9
Canada

# Abstract

This thesis documents the design and fabrication of an experimental facility that was built to produce a turbulent plane wall jet. The target flow was two-dimensional with a uniform profile of the mean streamwise velocity and a low turbulence level at the slot exit. The design requirements for a flow conditioning apparatus that could produce this flow were determined. The apparatus was then designed and constructed, and measurements of the fluid flow were obtained using particle image velocimetry (PIV). The first series of measurements was along the slot width, the second series was along the slot centerline and the third was at 46 slot heights off the centerline. The Reynolds number, based on the slot height and jet exit velocity, of the wall jet varied from 7594 to 8121. Data for the streamwise and transverse components of velocity and the three associated Reynolds stress components were analyzed and used to determine the characteristics of the wall jet.

This experimental facility was able to produce a profile of the mean streamwise velocity near the slot exit that was uniform over 71% of the slot height with a streamwise turbulence that was equal to 1.45% of the mean velocity. This initial velocity was maintained to 6 slot heights. The fully developed region for the centerline and the off-centerline measurements was determined to extend from 50 to 100 slot heights and 40 to 100 slot heights, respectively. This was based on self-similarity of the mean streamwise velocity profiles when scaled using the maximum streamwise velocity and the jet half-width. The off-centerline Reynolds stress profiles achieved a greater degree of collapse than did the centerline profiles.

The rate of spread of the wall jet along the centerline was 0.080 in the self-similar region from 50 to 100 slot heights, and the off-centerline growth rate was 0.077 in the self-similar region from 40 to 100 slot heights. The decay rate of the maximum streamwise velocity was -0.624 within the centerline self-similar region, and -0.562 within the off-centerline self-similar region. These results for the spread and decay of the wall jet compared well with recent similar studies.

The two-dimensionality was initially assessed by measuring the mean streamwise velocity at 1 slot height along the entire slot width. The two-dimensionality of this wall jet was further analyzed by comparing the centerline and off-centerline profiles of the mean streamwise velocity at 2/3, 4, 50, 80, and 100 slot heights, and by comparing the growth rates and decay rates. Although this facility was able to produce a wall jet that was initially two-dimensional, the two-dimensionality was compromised downstream of the slot, most likely due to the presence of return flow and spanwise spreading. Without further measurements, it is not yet clear exactly how the lack of complete two-dimensionality affects the flow characteristics noted above.

# Acknowledgements

Thank you Professor Bugg and Professor Bergstrom for your advice, guidance, financial support and understanding during the course of this program. You waited patiently while I pursued my extra-curricular interests and kept me motivated to finish this thesis. I know that I would not have finished without your continued support.

I would like to thank my advisory committee: Professor Sumner, Professor Mazurek, Professor Chen and Professor Torvi for the time you put into this thesis. Your suggestions and insights helped to improve the overall quality of this study.

I would also like to thank David Deutscher, Henry Berg and Kevin Jeffery for their technical expertise, and Sherri Haberman, Janai Simonson, April Wettig and Kelley Neale for their help throughout the years.

I gratefully acknowledge the financial support from the University of Saskatchewan Graduate Scholarship, the Department of Mechanical Engineering, University of Saskatchewan, and from the National Aboriginal Achievement Foundation.

Finally, I would like to thank my family and friends for their emotional support and for putting up with my continued absence while I finished this thesis.

# Dedication

To my parents and Vangool.

# Table of Contents

# List of Tables

# List of Figures

# Nomenclature

**Roman**

| | |
|---|---|
| $A$ | Growth rate of the wall jet |
| $a$ | Width of a flow conditioner wall [m] |
| $b$ | Height of a flow conditioner wall [m] |
| $C$ | Orifice plate discharge coefficient |
| CBC | Correlation-based-correction |
| CNN | Cellular neural network |
| $D$ | Pipe diameter [m] |
| DNS | Direct numerical simulation method used for computational studies |
| $d$ | Orifice plate diameter [m] |
| $d_{sc}$ | Mesh screen wire diameter [m] |
| $E$ | Modulus of elasticity [Pa] |
| FFT | Fast Fourier transform |
| $H$ | Slot height [m] |
| $h$ | Thickness of a flow conditioner wall [m] |
| $L_{st}$ | Length of straightening vanes [m] |
| $L_1$, $L'_2$ | Orifice plate constants that depend on the pressure tap arrangement |
| LDA | Laser Doppler anemometry |
| LES | Large eddy simulation method used for computational studies |
| $l_{sc}$ | Length of screen mesh [m] |
| $M_{jet}$ | Momentum of the wall jet per unit mass [kg·m/s] |
| $M_{loss}$ | Momentum loss at the ground plane per unit mass [kg·m/s] |

| | |
|---|---|
| $M_0$ | Momentum at the slot exit per unit mass [kg·m/s] |
| $\dot{m}$ | Mass flow rate [kg/s] |
| $\dot{m}_e$ | Mass flow rate of the entrained fluid [kg/s] |
| $\dot{m}_{jet}$ | Mass flow rate of the wall jet [kg/s] |
| $\dot{m}_0$ | Mass flow rate at the slot exit [kg/s] |
| $n$ | Decay rate of the wall jet |
| PIV | Particle image velocimetry |
| $\Delta P$ | Measured pressure differential across the orifice plate [Pa] |
| $\Delta P_{sc}$ | Pressure drop across the mesh screens [Pa] |
| $\Delta P_{slot}$ | Pressure drop across the slot exit [Pa] |
| $\Delta P_{st}$ | Pressure drop across the straightening vanes [Pa] |
| $Q$ | Volumetric flow rate [L/s] |
| $Q_{st}$ | Volumetric flow rate through the straightening vanes [$m^3$/s] |
| $q$ | Uniform pressure distribution on the flow conditioner walls [Pa] |
| $R_c$ | Radius of curvature of the inside corner of the slot [m] |
| $Re$ | Reynolds number |
| $Re_D$ | Reynolds number based on the bulk velocity in the pipe and pipe diameter |
| $Re_s$ | Reynolds number based on the slot height and jet exit velocity |
| $r_{st}$ | Radius of straightening vanes [m] |
| $T$ | Fluid temperature [$^oC$] |
| $t$ | Time [s] |
| $\Delta t$ | PIV image time separation [s] |

| | |
|---|---|
| $U_e$ | Local freestream velocity [m/s] |
| $U_{internal}$ | Internal velocity of the flow conditioner [m/s] |
| $U_{slot}$ | Velocity exiting the flow conditioner [m/s] |
| $u_m$ | Maximum streamwise velocity [m/s] |
| $u_{mean}$ | Mean streamwise velocity [m/s] |
| $u_0$ | Maximum streamwise velocity at the slot exit [m/s] |
| $u_x$, $u_y$ | Streamwise and vertical components of the particle velocity [m/s] |
| $u_*$ | Friction velocity [m/s] |
| $u^+$ | Inner velocity scale [m/s] |
| $V$ | Orifice voltage [volts] |
| $V_b$ | Bulk velocity in the pipe [m/s] |
| $\overline{u'u'}$, $\overline{v'v'}$ | Normal stress components of the Reynolds stress per unit mass [$m^2/s^2$] |
| $\overline{u'v'}$ | Reynolds shear stress per unit mass [$m^2/s^2$] |
| $W$ | Slot width [m] |
| $u$, $v$, $w$ | Streamwise, transverse and spanwise components of velocity [m/s] |
| $u$', $v$', $w$' | Streamwise, transverse and spanwise fluctuating components of velocity [m/s] |
| $x$, $y$, $z$ | Cartesian coordinate system [m] |
| $x_0$ | Distance from the slot exit to the virtual origin of the wall jet [m] |
| $\Delta x$ | Streamwise particle displacement [pixels] |
| $\Delta y$ | Vertical particle displacement [pixels] |
| $y_{1/2}$ | Wall jet half-width measured at $0.5u_m$ [m] |
| $y^+$ | Inner length scale [m] |

**Greek**

| | |
|---|---|
| $\alpha$ | Numerical factor based on the ratio of *b*/*a* |
| $\beta$ | Constant based on the orifice plate diameter and pipe diameter |
| $\beta_i$ | Scaling constant used by Barenblatt et al. (2005) |
| $\beta_{sc}$ | Constant based on the mesh screen length and diameter |
| $\delta$ | Deflection of the flow conditioner walls [m] |
| $\mu$ | Dynamic viscosity of the fluid [kg/m·s] |
| $\nu$ | Kinematic viscosity of the fluid [$m^2/s$] |
| $\rho$ | Fluid density [$kg/m^3$] |
| $\tau_w$ | Wall shear stress [Pa] |

# Chapter 1

# Introduction and Theory

The following sections provide the appropriate theory and background information related to turbulent plane wall jets. This includes a full description of plane wall jets, the corresponding transport equations, and the characteristics used to assess the quality of the flow.

## 1.1 Motivation

Launder & Rodi (1981) defined a wall jet as "a shear flow directed along a wall where, by virtue of the initially supplied momentum, at any situation, the streamwise velocity over some region within the shear flow exceeds that in the external stream." Wall jets have engineering applications in heating and film cooling, as well as in momentum and mass transfer. A wall jet can be used to improve the thermal performance of gas turbines by preventing excess heat transfer to the surface of a turbine blade or to the walls of the combustion chamber (Launder & Rodi, 1983). Applying a plane wall jet to the surface of an airplane wing can help delay separation by transferring momentum to the air next to the surface. A common example of a plane wall jet is a car windshield defroster, which is used to remove frost from the glass surface. Wall jets can be produced by discharging fluid through a rectangular slot, a round hole, or by the impingement of fluid on a surface. An unintentional example of impingement occurs when the air discharging from a vertical take-off and landing (VTOL) aircraft engine impacts the ground and spreads laterally (Tachie, 2000). Studying wall jets can provide further

understanding of the fundamental nature of the flow, leading to improvements in the various practical applications. Knowledge of wall jet characteristics such as the rate of spread and the decay rate of the maximum velocity, can potentially extend the life of gas turbines, provide greater maneuverability of aircraft, increase the efficiency of automobile defrosters, and determine the aerodynamic loading that VTOL aircraft impart on buildings and ground personnel.

### 1.2 Plane Wall Jet

Figure 1.1 is an isometric schematic of a plane wall jet facility. At the slot exit $x = 0$, at the surface of the ground plane $y = 0$, and $z = 0$ at the middle of the slot width. The $x$-direction, $y$-direction and $z$-direction will hereafter be referred to as the streamwise, tranverse and spanwise directions, respectively. The mean velocity components are $u$, $v$ and $w$, and the fluctuating velocity components are $u'$, $v'$ and $w'$, in the streamwise, transverse and spanwise directions, respectively.

A wall jet is formed when a fluid is discharged through a slot into a volume of the same fluid that is either stagnant or moving. The jet of fluid exits the slot and uses the initially supplied momentum to flow across a surface that can be either flat or curved (Launder & Rodi, 1981). The ideal plane wall jet has an infinite slot width and is discharged into a body of fluid that has no restrictions in the streamwise and transverse directions (George et al., 2000). In practical settings, the slot can be a variety of shapes, however in order to achieve two-dimensional flow a rectangular shape with a large slot width, $W$, to height, $H$, ratio is required. The boundary condition above the slot can be either a lip with a certain thickness or it can be a vertical wall.

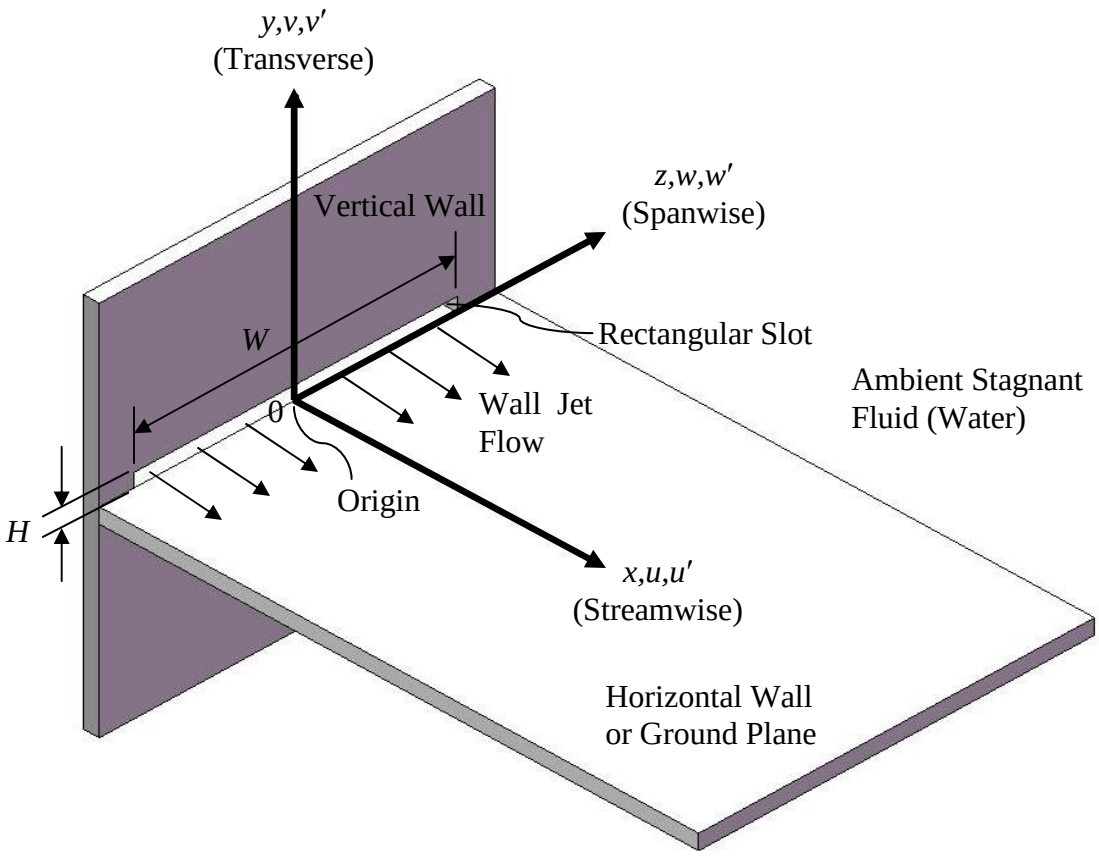


Figure 1.1: Isometric view of the geometry for creating a plane wall jet.

The wall jet studied here is discharged from a rectangular slot into stagnant water, has a vertical wall above the slot exit, and travels in the streamwise direction across a flat, horizontal smooth ground plane. The jet of fluid then interacts with the stagnant fluid and the wall, eventually developing into the wall jet sketched in figure 1.2. The wall jet velocity profile has a location of maximum velocity, $u_m$, and two locations of zero velocity. The velocity is zero at the wall due to the no-slip condition of viscous flow, and is zero at a certain transverse distance away from the wall where the outer edge of the wall jet meets the stagnant fluid. Below $u_m$ is the inner region of the wall jet, which is similiar to a boundary layer flow, and above $u_m$ is the outer region, which is similar to a free jet flow. The location where the velocity is reduced to one half of the maximum

velocity in the outer region is the jet half-width, $y_{1/2}$ (George et al., 2000). The jet half-width is used to describe the transverse extent of the wall jet.

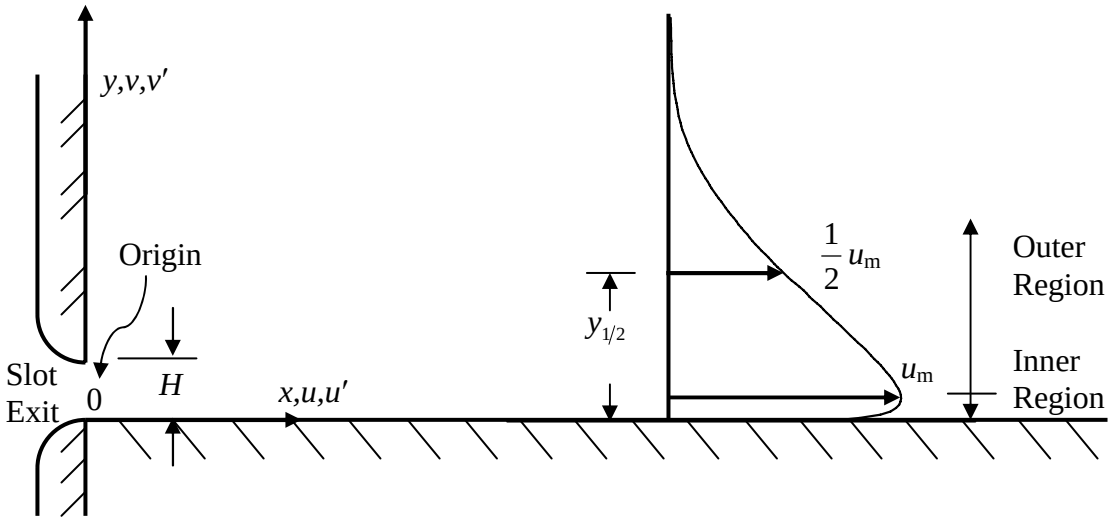


Figure 1.2: Side view of a plane wall jet.

### 1.2.1 Conservation of Mass

The fluid exiting the slot develops into a wall jet as it travels in the streamwise direction due to its interaction with the wall and the surrounding stagnant fluid. The process whereby the stagnant fluid gets drawn into the developing wall jet is known as entrainment (Kundu & Cohen, 2008). In laminar flows entrainment is due to viscosity, whereas for turbulent flows it is the result of turbulent mixing.

There are three transport equations that can be used to describe a turbulent plane wall jet. These are the continuity equation, the Reynolds-averaged Navier-Stokes equation, and the momentum integral equation.

The continuity equation is derived from the principle of conservation of mass and for steady two-dimensional incompressible flow is of the form

$$\frac{\partial u}{\partial x} + \frac{\partial v}{\partial y} = 0 \tag{1.1}$$

where $u$ is the streamwise velocity and $v$ is the transverse velocity. Figure 1.3 presents a control volume drawn around a portion of a plane wall jet. For this control volume, the streamwise mass fluxes include the fluid exiting the slot, $\dot{m}_o$, and the local wall jet mass flux, $\dot{m}_{jet}$. The transverse mass flow rate is due to the entrained fluid, $\dot{m}_e$. Applying equation (1.1) to a plane wall jet and integrating yields

$$\dot{m}_{jet} = \dot{m}_o + \dot{m}_e . \tag{1.2}$$

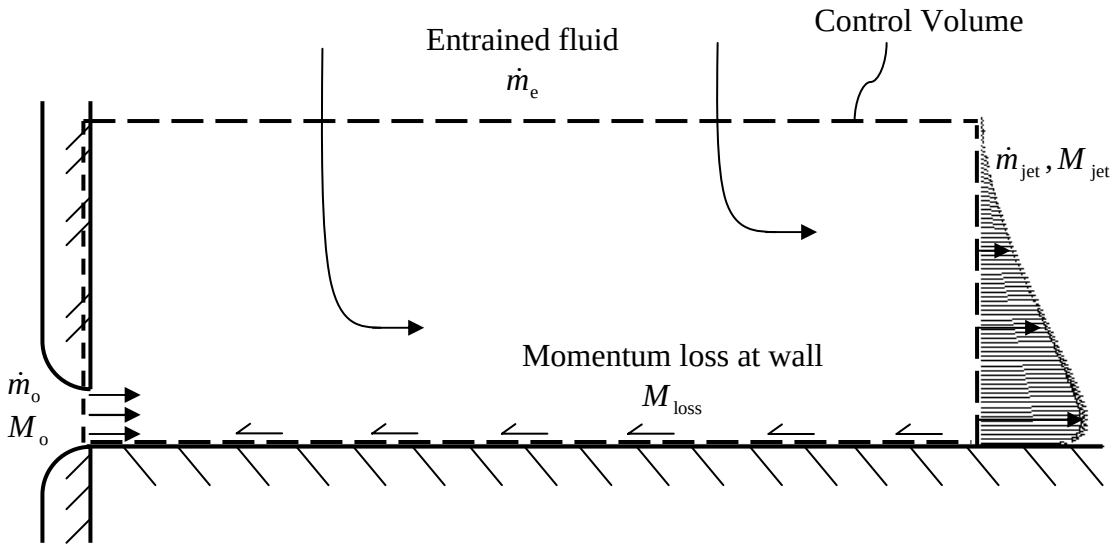


Figure 1.3: Control volume for a plane wall jet.

1.2.2 Conservation of Momentum

The Reynolds-averaged Navier-Stokes equation is derived from the principle of conservation of momentum and is used for turbulent flows. Irwin (1973) showed that the appropriate momentum equation for a steady two-dimensional plane wall jet is of the form

$$u\frac{\partial u}{\partial x}+v\frac{\partial u}{\partial y}=\frac{\partial}{\partial y}\left[-\overline{u'v'}+\nu\frac{\partial u}{\partial y}\right]-\left[\frac{\partial}{\partial x}\left(\overline{u'u'}-\overline{v'v'}\right)\right]. \tag{1.3}$$

The Reynolds shear stress per unit mass, $\overline{u'v'}$, and normal stresses per unit mass $\overline{u'u'}$ and $\overline{v'v'}$ represent effective turbulent stresses. The viscous shear stress per unit mass is $\nu\frac{\partial u}{\partial y}$, where $\nu$ is the kinematic viscosity, and the boundary conditions are $u\to 0$ as $y\to 0$ and $u\to 0$ as $y\to\infty$. For a turbulent wall jet the laminar stress is negligible (except at the wall) and the normal stress terms are negligible to second order (George et al., 2000), so that equation (1.3) reduces to

$$u\frac{\partial u}{\partial x}+v\frac{\partial u}{\partial y}=\frac{\partial}{\partial y}\left[-\overline{u'v'}\right]. \tag{1.4}$$

Equation (1.4) can be integrated from the slot to a location $x$ to obtain the momentum integral equation in the form of

$$\int_0^\infty\left[u^2\right]dy=M_o-\int_0^x\frac{\tau_w}{\rho}dx \tag{1.5}$$

where $\tau_w$ is the wall shear stress, $\rho$ is the fluid density, and the right hand side of the equation is the momentum per unit mass supplied at the slot exit minus $\int_0^x \frac{\tau_w}{\rho} dx$, which is the momentum loss due to friction at the wall, $M_{loss}$.

### 1.2.3 Region of Initial Development

The region of initial development is the region adjacent to and downstream of the slot where the wall jet transitions into a fully developed flow. The initial development of a wall jet on a plane surface is shown schematically in figure 1.4.

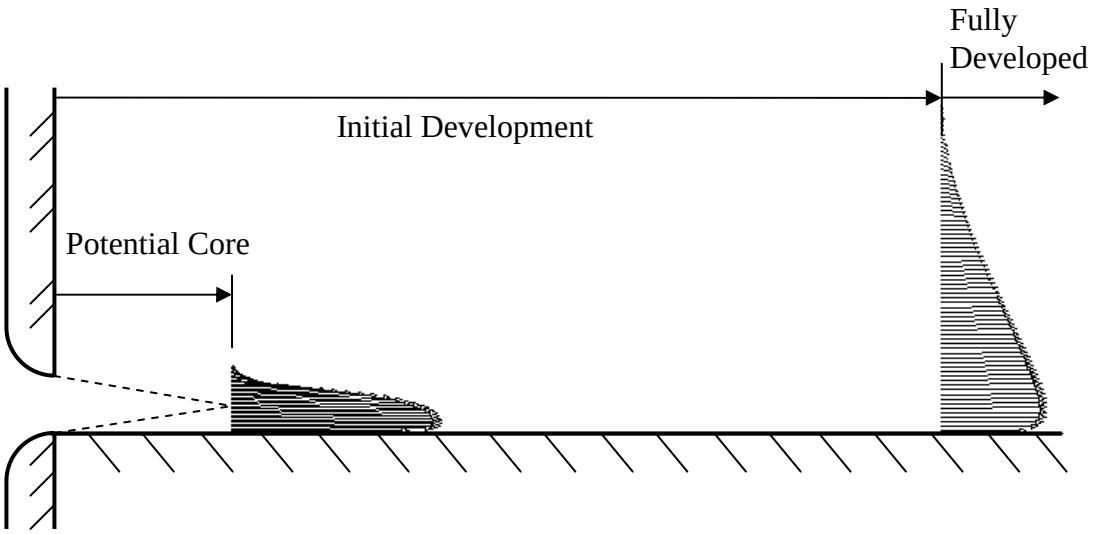


Figure 1.4: Initial development region of a plane wall jet.

### 1.2.4 Initial Conditions

George et al. (2000) were unable to remove a dependency on the initial conditions on the wall jet development downstream of the slot. Shinneeb (2006) also determined that the initial conditions at the slot exit affect the downstream flow. The proper

documentation of a wall jet should therefore include velocity and turbulence profiles at or near the slot exit in order to facilitate useful comparisons to previous results.

Figure 1.5 shows the fluid discharged through a slot that has an inside corner with a curved profile. Ideally, the contraction ratio and the shape of the orifice are designed so that the jet has a uniform velocity profile at the slot exit. The internal design of the apparatus should also reduce the turbulence intensity of the fluid, resulting in a relatively low value for the streamwise turbulence intensity at the slot exit.

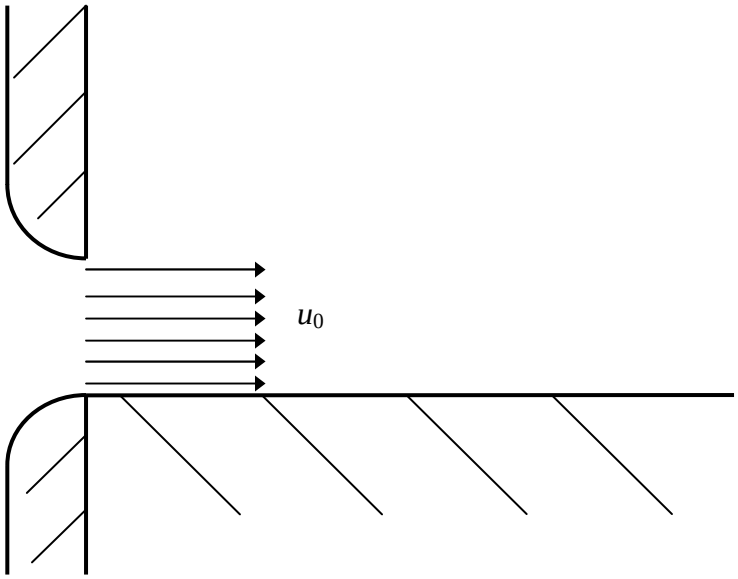


Figure 1.5: Uniform streamwise velocity profile.

### 1.2.5 Potential Core

Downstream of the slot, the flat section of the velocity profile is known as the "core" of the jet. As the wall jet travels downstream, it interacts with the wall and stagnant fluid above. A boundary layer develops in the inner region while a mixing layer occurs in the outer region. This lateral transfer of momentum causes the core of the jet to

decrease in size, while at the same time increasing the transverse extent of the wall jet (see figure 1.6). Eventually the maximum velocity is reduced to less than its initial value throughout the flow, signifying the loss of the potential core (Rajaratnam, 1976). Downstream of this location the maximum velocity is always less than the initial maximum velocity at the slot exit. Rajaratnam (1976) found that for plane wall jets the potential core varied from $x/H$ = 6.1 to 6.7 for $Re = 10^4$ to $10^5$.

### 1.2.6 Fully Developed Region

Velocity profiles are said to be self-similar when they can be non-dimensionalized to collapse on to a common curve. Typically, velocity profiles are non-dimensionalized using a characteristic length scale and velocity scale. The traditional scales used in the outer region of a wall jet are the maximum streamwise mean velocity, $u_m$, and the jet half-width, $y_{1/2}$ (Rajaratnam, 1976). The scales used in the inner region near the wall are $u_*$ and $l = \nu/u_*$, where the friction velocity is defined as $u_* = \sqrt{\tau_w/\rho}$.

The wall jet continues to develop as it flows in the streamwise direction. Once the wall jet has achieved self-similiar mean velocity and turbulence profiles, it has reached a state of dynamic equilibrium, which is also known as self-preservation (Kundu & Cohen, 2008). The streamwise region where this occurs can be used to assess if the flow is fully developed.

### 1.2.7 Spread Rate

As the wall jet flows downstream it spreads in the wall normal direction. This is due to the growth of the boundary layer at the wall as well as the entrainment of stagnant

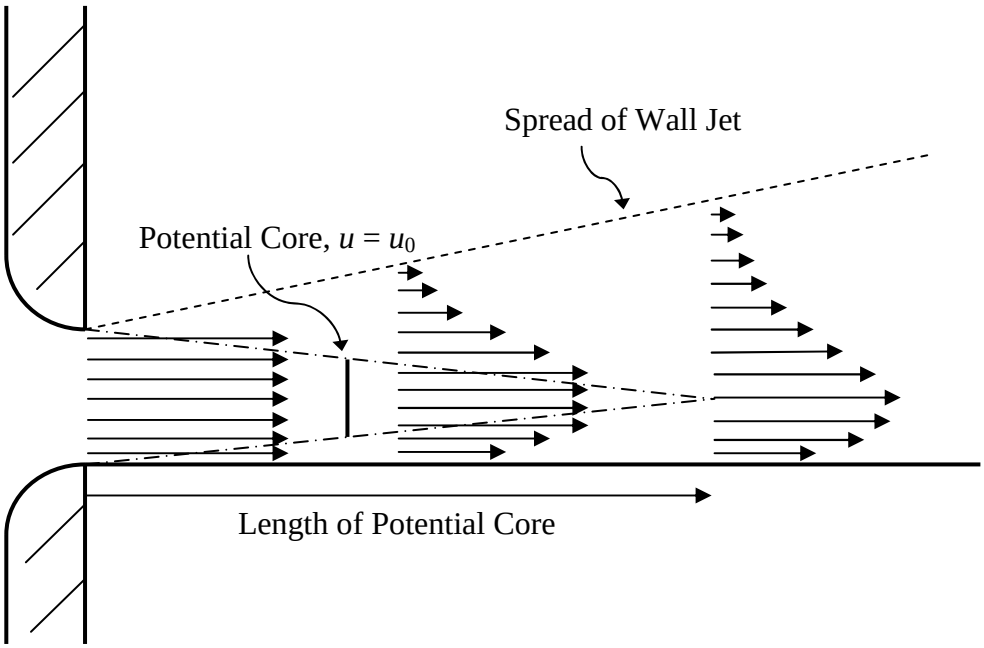


Figure 1.6: The potential core region of a plane wall jet.

fluid in the outer region (Rajaratnam, 1976). The jet half-width is used to define the rate of spread by plotting its value as a function of the streamwise location and determining the slope, $dy_{1/2}/dx$, of a linear regression applied to the fully developed region (Launder & Rodi, 1981). The equation of this line is of the form:

$$y_{1/2} = A(x + x_0) \tag{1.6}$$

where $x_0$ is the virtual origin and $A = dy_{1/2}/dx$.

### 1.2.8 Decay Rate

The spread of the wall jet and the loss of momentum at the wall cause the maximum velocity, $u_m$, to decrease. This decay of the wall jet is obtained by plotting the maximum velocity as a function of the streamwise location in the fully developed region

and determining the slope, $du_m/dx$. The streamwise location can also be represented by the jet half-width using equation (1.7), allowing the decay rate to be determined by plotting $u_m$ as a function of $y_{1/2}$ in logarithmic form and solving for $n = d(\log(u_m))/d(\log(y_{1/2}))$,

$$\frac{u_m}{u_0} = B\left(\frac{y_{1/2}}{H}\right)^n, \tag{1.7}$$

where $B$ is a constant (George et al., 2000).

### 1.2.9 Return Flow

If the wall jet is discharged into a sufficiently large volume of stagnant fluid then the jet will continue to grow as its initial momentum is transferred to the entrained fluid and also dissipated at the wall as heat due to the wall shear stress. In a water tow tank with a vertical wall above the slot exit, a recirculating flow will be present due to entrainment from a finite volume of stagnant fluid (Eriksson et al., 1998). This recirculating flow, also called a return flow, could potentially alter the shape of the wall jet's velocity profile, e.g. creating a negative streamwise velocity at large tranverse values as shown in figure 1.7.

### 1.2.10 Reynolds Stress Profiles

The Reynolds stresses that are present in equation (1.3) characterize the turbulence structure of a flow. For a two-dimensional flow, the components of the Reynolds stress tensor are the normal stresses in the streamwise and transverse directions,

$\overline{u'u'}$ and $\overline{v'v'}$, and the Reynolds shear stress, $\overline{u'v'}$. The variance of the streamwise and transverse velocity components can be experimentally determined, which allows the Reynolds stresses to be presented in terms of the profiles $\overline{u'u'}/u_m^2$, $\overline{v'v'}/u_m^2$ and $\overline{u'v'}/u_m^2$ (Eriksson et al., 1998).

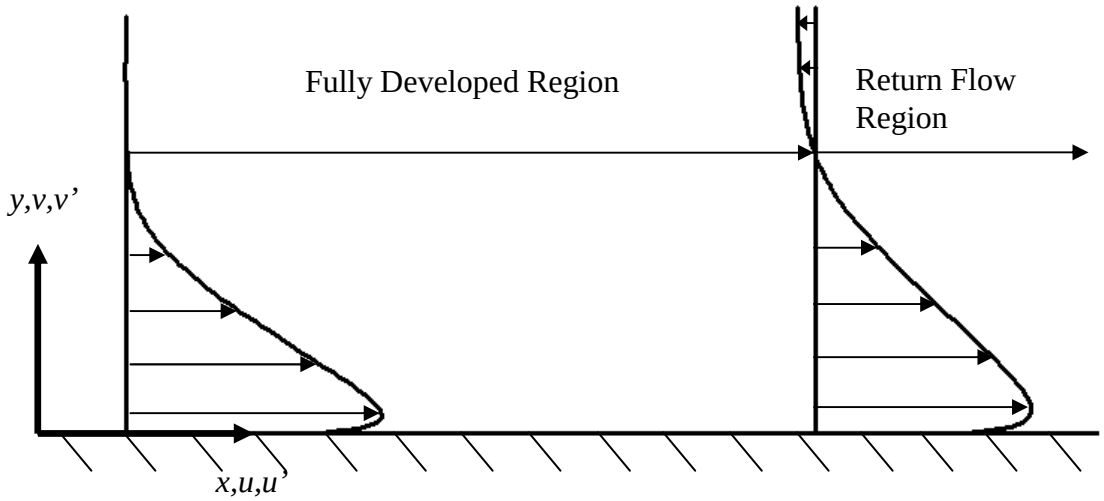


Figure 1.7: Regions of fully developed flow and return flow.

### 1.3 Objectives

The purpose of this thesis is to document the design and fabrication of an experimental facility that has the capability to produce a turbulent plane wall jet, and to determine the flow characteristics of the wall jet using particle image velocimetry (PIV).

The objectives can be summarized as:

1. Design and build an experimental apparatus to produce a turbulent plane wall jet;

2. Assess the flow characteristics at the slot exit by documenting the initial conditions and the two-dimensionality of the wall jet;
3. Investigate the experimental facility by taking measurements of the fluid flow with a PIV system and comparing the wall jet characteristics to previous established results.

### 1.4 Scope

This study examines a water jet that is discharged from a rectangular slot and flows across a smooth horizontal glass wall that is flush with the bottom of the slot. A vertical wall is present above the exit of the slot, and the flow apparatus is contained within a water tow tank. A 1.1-kW centrifugal pump and a piping system are used to transport water from the far end of the tank into the flow apparatus. A large Reynolds number is desired so that this wall jet can be compared to previous experiments. A PIV system is used to take measurements along the slot width, along the centerline and 0.275 m off of the centerline in order to determine the quality of the plane turbulent wall jet that this facility produces.

The scope can be summarized as:

- A wall jet with a Reynolds number that is based on the slot height and jet exit velocity and varies from 7594 to 8121 was studied.
- Three series of measurements were taken. The first series of measurements provided data at $x/H = 1$ along the entire slot width. The second series was along the slot centerline and the third was 0.275 m ($z/H = 46$) off the centerline. Seven

flow field measurements were obtained from $x/H$ = 0 to 100 for the second and third series and additional flow fields were measured at the slot exit to improve the precision in that region.

- Two thousand images were acquired using the PIV system for each field of view to determine the average streamwise velocity, as well as the streamwise and wall normal turbulence intensities and Reynolds shear stress. The spanwise velocity is not measured to keep the scope at an appropriate size. Previous studies have shown that means converge with 2000 images (Shinneeb, 2006); additional images were not obtained due to the computational expense required for analysis when using PIV.

## 1.5 Outline

The appropriate theory and background information have been provided in this chapter. A literature review will be presented in Chapter 2. The design and construction of a flow conditioning apparatus will then be described in Chapter 3, followed by an overview of the experimental facility and an outline of the measurements that were obtained. The experimental results will then be used in Chapter 4 to assess the characteristics of the plane wall jet that has been produced. Finally, conclusions about the experimental apparatus and the flow characteristics of the plane wall jet will be made and recommendations for future work will be provided in Chapter 5.

# Chapter 2

# Literature Review

A review of the literature on plane wall jets has been performed to provide information on the design of experimental facilities used to produce two-dimensional turbulent plane wall jets, the characteristics that have been obtained in prior studies, and the scaling that has been used. The experimental studies will be presented first, followed by theoretical and computational studies.

## 2.1 Experimental Studies

### 2.1.1 The turbulent wall jet, Launder & Rodi (1981)

The first comprehensive critical review of the existing experimental literature on turbulent wall jets was performed by Launder & Rodi (1981).

Launder & Rodi (1981) had four main criteria for assessment of the quality of a turbulent wall jet:

(a) “For two-dimensional cases there should be strong direct or indirect evidence that the flow achieved good two-dimensionality. The principal test applied was the close satisfaction of the two-dimensional momentum integral equation.”

(b) “The flow conditions should be well defined and good experimental practice should be conveyed by the author's documentation of the work.”

(c) “The experimental data should display good internal consistency and should preferably include measurements of turbulence quantities as well as those for the mean flow.”

(d) “The experimental data should exhibit general credibility in comparison with established results in similar flows.”

Of the over two hundred experimental studies that they found, approximately seventy were aerodynamic studies with uniform thermophysical properties. Further refining the search to the two-dimensional wall jet on a plane surface resulted in forty-six sources that they referenced and subdivided as follows: the wall jet in still air, the wall jet in a moving stream, the wall jet in a uniform velocity stream, and the wall jet in an adverse pressure gradient. The wall jet in still air, which is the focus of this study, had fifteen literature sources that met their assessment criteria. Of those sources, eight provided values for characteristics that are applicable to this current study. Table 2.1 lists the characteristics and initial conditions for these wall jet studies.

Launder & Rodi (1981) determined that the appropriate range of values for the growth rate $\mathrm{d}(y_{1/2})/\mathrm{d}(x)$ was $0.073 \pm 0.002$. This was based on the experiments of Tailland & Mathieu (1967), Bradshaw & Gee (1960), Verhoff (1970) and Patel (1962).

The streamwise mean velocity profiles of Tailland & Mathieu (1967), Guitton (1968), and Sigalla (1958) achieved a satisfactory collapse when scaled with $u_{\mathrm{m}}$ and $y_{1/2}$.

The turbulence profiles were scaled with $u_m$ and $y_{1/2}$. The streamwise turbulence profiles of Giles et al. (1966), Guitton (1968), and Wilson & Goldstein (1976) collapsed reasonably well in the region from $0.2 < y/y_{1/2} < 1.2$. Reasonable agreement for the collapse of the transverse turbulence profiles was not observed, however the Reynolds stress profiles of Tailland & Mathieu (1967), Giles et al. (1966), Guitton (1968), and Wilson & Goldstein (1976) collapsed fairly well in the region from $0.1 < y/y_{1/2} < 0.6$.

Table 2.1 Characteristics of plane wall jets in a stagnant fluid compiled by Launder & Rodi (1981).

| Reference | *Re* | Slot dimension (m) | Range $(x/H)$ | $\frac{d(y_{1/2})}{d(x)}$ | $\frac{\overline{v'v'}}{u_m^2}$ (max) | $\frac{\overline{u'v'}}{u_m^2}$ (max) |
|---|---|---|---|---|---|---|
| Sigalla (1958) | 20,000-40,000 | $H$ = 0.008<br>$W$ = 0.132 | 4-70 | 0.064 | | |
| Bradshaw & Gee (1960) | 6,080 | $H$ = 4.6E-4<br>$W$ = 2.5E-4 | 339-1459 | 0.071 | 0.0122 | 0.0165 |
| Patel (1962) | 30,000 | $H$ = 0.0051 | 32-92 | 0.071 | | |
| Giles et al. (1966) | 20,000-100,000 | | | 0.0766 | 0.011 | |
| Tailland & Mathieu (1967) | 11,000<br>18,000<br>25,000 | $H$ = 0.006<br>$W$ = 0.900 | 33-200 | 0.076<br>0.074<br>0.073 | 0.29 | 0.012 |
| Guitton (1968) | 30,800 | $H$ = 0.0077<br>$W$ = 0.760 | 26-209 | 0.071 | 0.014 | 0.013 |
| Verhoff (1970) | 10,300<br>12,100 | $H$ = 0.00122<br>$H$ = 0.00178 | 57-410 | 0.0816<br>0.0766 | | |
| Wilson & Goldstein (1976) | 13,000 | $H$= 0.00609<br>$W$=0.508 | 23-125 | 0.076 | 0.018 | 0.013 |

2.1.2 Laser Doppler measurement of turbulence parameters in a two-dimensional plane wall jet, Schneider & Goldstein (1994)

Schneider & Goldstein (1994) performed an experimental study of a turbulent plane wall jet in still air using a single-component laser Doppler anemometry (LDA) system. Particular interest was paid to the turbulence parameters to see how the LDA results compared to hot-wire measurements, which are known to be affected by flow reversals in turbulent flow. They found that the LDA measurements of the streamwise turbulence intensity were slightly higher and the Reynolds shear stress was significantly higher in the outer region when compared to hot-wire measurements.

The Reynolds number based on the slot height was $Re$ = 14000. They measured a uniform velocity profile at the slot exit with a turbulence intensity of 0.3% over the central region. This low turbulence level was achieved by placing screens and honeycomb-shaped flow straighteners prior to the slot exit, as well as by having a contraction ratio of 35:1. The contraction had a convex shape with a radius of curvature of 0.102 m. The spanwise dimension of the slot was 0.483 m and the slot height was 0.0054 m, which resulted in a slot aspect ratio of 90:1. This ratio was large enough for the wall jet to achieve two-dimensionality at the slot exit, as evidenced by a streamwise velocity variation of $\pm 0.1\%$ over the central 0.32 m of the slot width. Downstream of the slot the conservation of momentum from one streamwise location to the next was determined to be acceptable enough to assure the two-dimensionality of the wall jet.

LDA measurements were taken at $x$ = 45H, 75$H$, and 110$H$. The conventional outer scaling coordinates of $u_{\mathrm{m}}$ and $y_{1/2}$ were used. The streamwise mean velocity

profiles achieved a reasonable collapse, as did the streamwise turbulence profiles. The Reynolds stress profiles achieved a reasonable collapse for $y/y_{1/2}$ values less than 0.6. Schneider & Goldstein (1994) expressed the growth of a wall jet with the equation

$$\frac{y_{1/2}}{H} = A\left(\frac{x}{H} + \frac{x_0}{H}\right) \tag{2.1}$$

where the growth rate, $d(y_{1/2})/d(x) = A$, was found to be 0.077, and the value for the normalized virtual origin ($x_0/H$) was -8.7. The decay rate of the wall jet was determined to be -0.608 by plotting $u_m/u_0$ as a function of $x/H$ in logarithmic form.

2.1.3 An experimental study of a two-dimensional plane turbulent wall jet, Eriksson, Karlsson & Persson (1998)

Eriksson et al. (1998) used a two-component LDA system to obtain a comprehensive set of data on the mean velocities and turbulence quantities for a plane wall jet at a relatively high Reynolds number. The wall jet was discharged into stagnant water with a Reynolds number based on the inlet of $Re$ = 9600. Upstream of the slot exit a large contraction and a screen were utilized to reduce the turbulence levels and to produce a uniform streamwise velocity profile at the slot exit. Eriksson et al. (1998) looked at the initial development of the wall jet, as well as the region of fully developed flow. Special attention was given to the near-wall region due to the high-spatial resolution that the LDA system provided. They determined the wall shear stress by measuring the mean velocity gradient using data below $y^+ = 4$, which enabled them to use the friction velocity, $u_*$, as an inner velocity scale and $u_*/\nu$ as an inner length scale.

Previous experiments had been unable to measure $u_*$ without resorting to empirical relations.

Eriksson et al. (1998) also compared their turbulence data to previous experiments that had used hot-wire measurements in order to determine the potential effect of reverse flows on hot-wires. They found that large differences between the LDA and hot-wire turbulence data were present in the outer region, which they attributed to the inability of the hot-wires to measure the reverse flows that are present in turbulent flow. The difference between the peak values for the transverse turbulence intensity and the Reynolds shear stress was 40% and 20%, respectively.

Measurements were taken at the slot exit and a uniform velocity profile was obtained with a turbulence intensity of less than 1%. Downstream of the slot, measurements were taken at 5*H*, 10*H*, 20*H*, 40*H*, 70*H*, 100*H*, and 200*H*. The fluid temperature and initial velocity were regularly checked and there were no changes during individual measurements. However the value of *Re* varied by up to 3% between sets of measurements.

The two-dimensionality of the wall jet was initially checked by taking spanwise measurements at multiple streamwise locations. They noticed a variation of the wall jet thickness, possibly due to a $\pm 1\%$ variation of the slot height, and took their main set of measurements at a spanwise location where the "average properties" of the wall jet prevailed. They later used Launder & Rodi's (1981) criteria of satisfying the momentum integral equation to verify the range of flow that was two-dimensional. They found that

the wall jet achieved a satisfactory momentum balance as far downstream as 100 slot heights.

The region of fully developed flow was determined using two methods. The first was a quantitative analysis of the degree to which the mean velocity and turbulence intensity profiles collapsed using either inner or outer scaling. The streamwise mean velocity profiles collapsed from 20$H$ to 150$H$ using the outer scaling of $u_m$ and $y_{1/2}$. The turbulence intensity profiles collapsed from 40$H$ to 150$H$ using the outer scaling, but only after the "extra" turbulence from outside the jet was subtracted to prevent the profiles from increasing in magnitude as the streamwise distance increased. The turbulence intensity profiles were then scaled using the inner coordinates of $u/u_*$ and $y^+ = y \cdot u_*/\nu$. The streamwise turbulence intensity profiles collapsed from 40$H$ to 150$H$, but only to a $y^+$ value of approximately 8. The transverse turbulence intensity profiles collapsed from 40$H$ to 150$H$ up to a $y^+$ value of approximately 30. The Reynolds shear stress profiles collapsed out to a $y^+$ value of approximately 100 for $x/H$ = 40 to 100.

The second method used to determine the fully developed region was to plot $\log(u_m)$ as a function of $\log(y_{1/2})$ and see which data points aligned with an applied linear regression. This method was based on the similarity theory proposed by George et al. (2000) which will be reviewed later in this chapter. The measurements from 40$H$ to 150$H$ were found to be in agreement with the similarity theory.

Eriksson et al. (1998) determined that their growth rate, $d(y_{1/2})/d(x)$, was equal to 0.078 in the region from 20*H* to 150*H*, and calculated their decay rate, $d(\log(u_m))/d(\log(y_{1/2}))$, to be equal to -0.57 in the region from 40*H* to 150*H*.

Based on their overall analysis, Eriksson et al. (1998) produced a fully developed two-dimensional plane wall jet from 40*H* to 100*H*. The wall jet was in the initial development stage from the slot exit to 40*H*, and a return flow began to affect the further development of the wall jet in the range of 100*H* to 150*H*.

2.1.4 Open channel turbulent boundary layers and wall jets on rough surfaces, Tachie (2000)

Tachie (2000) focused his thesis on an experimental investigation of turbulent near-wall flows. In particular, he studied turbulent boundary layers and wall jets in stagnant water using both smooth and rough surfaces. The wall jet facililty had a slot height of 0.01 m with a contraction ratio of 9:1 and a slot width to slot height ratio of 79:1. The initial turbulence of the wall jet was reduced by preceeding the slot exit with plastic drinking straws. As opposed to a vertical wall above the slot exit, there was an upper lip that had a thickness of 0.006 m. The presence of a slot lip and a relatively low contraction ratio produced a mean velocity profile at the exit that was only flat over the central 30-40%. The profile of the streamwise turbulence intensity was flat over the central 20% and varied from 3-5%. Tachie (2000) applied an approximate momentum balance and determined that satisfactory two-dimensionality was achieved for streamwise locations less than 100*H*.

The mean streamwise velocity was measured using a one component laser Doppler velocimeter at $x/H$ = 10, 30, 40, 50, 60, 70, 80, and 100. The profiles collapsed reasonably well at $x/H \geq 30$ when scaled with $u_m$ and $y_{1/2}$, however there was a return flow present in the outer region. The infuence of the return flow became more pronounced at $x/H \geq 60$, especially for $y/y_{1/2}$ values > 2. The turbulence profiles were measured at the same streamwise locations using a two-component LDA system. When they were scaled with $u_m$ and $y_{1/2}$, the streamwise and transverse turbulence profiles collapsed reasonably well in the region from 30$H$ to 60$H$, and the profiles of the Reynolds shear stress collapsed reasonably well from 30$H$ to 80$H$, especially at $y/y_{1/2}$ values less than 0.8.

The growth rates obtained by Tachie (2000) varied from 0.085 to 0.090. These were obtained using the scaling of $y/y_{1/2}$ and $x/H$. The decay rate, $\frac{d\left(\frac{u_m \nu}{M_o}\right)}{d\left(\frac{y_{1/2} M_o}{\nu^2}\right)}$, was found using the method recommended by George et al. (2000) and was equal to -0.521.

2.1.5 Summary of Previous Experimental Results

The experimental results obtained by Schneider & Goldstein (1994), Eriksson et al. (1998), and Tachie (2000) are summarized in Tables 2.2 and 2.3. Table 2.2 summarizes the set-up of each experiment, the initial conditions that were obtained, the scaling used, and the region of fully developed flow. Table 2.3 summarizes the characteristics that were obtained and the two-dimensionality of the plane wall jet. The

Table 2.2 Experimental set-up, initial conditions, scaling and fully developed region for previous experiments.

| Reference | Experimental method (fluid) | *Re* | Slot dimension (m) | Range (*x/H*) |
|---|---|---|---|---|
| Schneider & Goldstein (1994) | LDA (air) | 14000 | $H = 0.0054$<br>$W = 0.483$ | 43-110 |
| Eriksson et al. (1998) | LDA (water) | 9600 | $H = 0.0096$<br>$W = 1.45$ | 0-200 |
| Tachie (2000) | LDA (water) | 13400 | $H = 0.010$<br>$W = 0.8$ | 0-100 |
| Reference | Uniform streamwise velocity profile | Streamwise turbulence intensity (%) | Scaling | Fully developed region (*x/H*) |
| Schneider & Goldstein (1994) | yes | 0.3 | $y_{1/2}$, $U_m$ | |
| Eriksson et al. (1998) | yes | 1 | $y_{1/2}$, $u_m$ and $y^+$, $u^+$ | 40-150 |
| Tachie (2000) | no | 3-5 | $y_{1/2}$, $U_m$ | 30-100 |

decay rates for Schneider & Goldstein (1994), Eriksson et al. (1998), and Tachie (2000) were found using $\frac{d(\log(u_m/u_0))}{d(\log(x/H))}$, $\frac{d(\log u_m)}{d(\log y_{1/2})}$, and $\frac{d\left(\frac{u_m \nu}{M_o}\right)}{d\left(\frac{y_{1/2} M_o}{\nu^2}\right)}$, respectively.

The comprehensive critical review of the experimental literature on turbulent wall jets performed by Launder & Rodi (1981) provided criteria for assessing the quality of a turbulent wall jet, as well as a range of values for the spread rate. Schneider & Goldstein (1994) provided information on the design of an experimental facility that was able to produce a two-dimensional wall jet with a uniform profile of the streamwise velocity and a low turbulence intensity. They also provided characteristics for comparison such as the rate of spread, the decay rate, the streamwise turbulence intensity, and the Reynolds shear

Table 2.3 Characteristics and two-dimensionality for previous experiments.

| Reference | Growth Rate | Decay Rate | $\frac{\overline{u'u'}}{u_m^2}$ [max] | $\frac{\overline{v'v'}}{u_m^2}$ [max] | $\frac{\overline{u'v'}}{u_m^2}$ [max] | Two-dimensionality |
|---|---|---|---|---|---|---|
| Schneider & Goldstein (1994) | 0.077 | -0.608 | 0.051 | | 0.015 | Established at slot exit and maintained downstream based on an acceptable momentum balance |
| Eriksson et al. (1998) | 0.078 | -0.57 | 0.045 | 0.028 | 0.015 | Maintained at $x/H \leq$ 150 based on momentum balance |
| Tachie (2000) | 0.085-0.090 | -0.521 | 0.04 | 0.036 | 0.02 | Maintained at $x/H \leq$ 100 based on an approximate momentum balance |

stress. Eriksson et al. (1998) provided the same characteristics for comparison as Schneider & Goldstein (1994), and also provided the transverse turbulence intensity and the region of fully developed flow. Tachie (2000) provided the same characteristics as Eriksson et al. (1998) as well as information on the design of an experimental facility that produced a two-dimensional wall jet; however the profile of the streamwise velocity was not uniform and had a larger turbulence intensity than Schneider & Goldstein (1994) and Eriksson et al. (1998).

## 2.2. Theoretical and Computational Studies

### 2.2.1 A similarity theory for the turbulent wall jet without external stream, George, Abrahamsson, Eriksson, Karlsson, Loefdahl & Wosniak (2000)

George et al. (2000) presented a new theory for the turbulent wall jet in still surroundings that was based on a similarity analysis of the governing equations. They

used the asymptotic invariance principle (AIP) to determine the proper scaling that would provide similarity solutions in the limit of infinite Reynolds number. The inner and outer regions of the wall jet were analyzed separately. Their analysis showed that the appropriate velocity and length scales in the inner region were $u_*$ and $\nu/u_*$, respectively. The appropriate velocity and length scales in the outer region were the conventional outer coordinates of $u_m$ and $y_{1/2}$, however the Reynolds shear stress was found to scale with $u_*$. Their theory indicated a power law relation between $u_m$ and $y_{1/2}$ in the form of $u_m \sim (y_{1/2})^n$ in order for similarity to be achieved. The value of $n$ needed to be less than $-0.5$ and had to be determined from experimental data.

They found their new theory to be in agreement with previous experimental data, in particular that of Eriksson et al. (1998) and Abrahamsson, Johansson & Loefdahl (1994). The latter experiment studied a wall jet in air using hot-wire measurements and achieved very similar inlet conditions to that of Eriksson et al. (1998). When they applied a power law relation between $u_m$ and $y_{1/2}$ they obtained a best-fit value for $n$ of -0.528. While the value for $n$ appeared to be universal for the data considered, they were unable to remove the possibility of a dependence on the initial conditions at the slot exit.

2.2.2 The turbulent wall jet: A triple-layered structure and incomplete similarity, Barenblatt, Chorin, & Prostokishin (2005)

Barenblatt et al. (2005) hypothesized that the flow region of a turbulent wall jet consists of three layers: a top layer above the location of maximum velocity, a near-wall layer below the location of maximum velocity, and an intermediate layer in the region

where the velocity is near its maximum value. They also proposed that a turbulent wall jet has the property of incomplete similarity at large Reynolds numbers, which implies that the height of the slot affects the development of the wall jet. They introduced a new scaling technique where the slot height was incorporated into the length scale by replacing $y_{1/2}$ with $(x/H)^{\beta i}$. Additionally, a jet half-width in the inner region of the wall jet was introduced as a length scale. Consequently there were two values for $\beta_i$: one in the inner region and another in the outer region. The values for $\beta_i$ were determined by plotting $\ln(y_{1/2})$ as a function of $\ln(x/H)$ for both the inner and outer jet half-widths and calculating the slope, $\beta_i$, of a linear fit applied in the fully developed region.

Barenblatt et al. (2005) applied their scaling technique to the previous experimental results of Karlsson et al. (1991) and obtained a collapse of the data in the inner region when using the inner jet half-width, and a collapse of the data in the outer region when using the outer jet half-width. They determined that the wall jet has the property of incomplete similarity by plotting $\ln(u_m/u_o)$ as a function of $\ln(x/H)$ and calculating the value of the slope of the linear fit applied to the data. They noted that the value of the slope should be -0.5 for complete similarity, whereas the value they obtained for the slope was -0.6. This differs from the definition of complete similarity that was proposed by George et al. (2000).

### 2.2.3 Large eddy simulation of a plane turbulent wall jet, Dejoan & Leschziner (2004)

Dejoan & Leschziner (2004) undertook a computational study of a plane wall jet in stagnant surroundings using the large eddy simulation (LES) method. The purpose of

their study was to further explore scaling and similarity as well as the initial development of the jet, and to determine the turbulence stress budgets which had not been available from previous experiments. They stated that the direct numerical simulation (DNS) method was preferable due to the detailed and physically reliable information it provided, however it was too computationally expensive at the relevant Reynolds numbers.

Dejoan & Laschziner (2004) made direct comparisons to the experimental results of Eriksson et al. (1998) and as such used the same boundary and initial conditions: a wall jet with a $Re$ = 9600 being discharged into stagnant water, a vertical wall above the slot exit, and an initial uniform streamwise velocity profile with a turbulence intensity of less than 1%. Previous experimental results found that a plane wall jet begins to reach a fully developed state at streamwise distances larger than 20$H$. The flow domain used by Dejoan & Laschziner (2004) had a height of 10$H$, a length of 22$H$, and a spanwise depth of 5.5$H$, which then allowed them to make comparisons in a small range of streamwise values that were close to becoming fully developed.

The results they obtained appeared to agree with the experimental results of Eriksson et al. (1998) in most respects. They also provided results for the budgets for the turbulence kinetic energy and Reynolds stresses, which allowed them to look at the processes that are responsible for the interaction between the inner and outer wall jet layers. This interaction is beyond the scope of this thesis, however for future studies that are interested in this area of research the article by Dejoan & Leschziner (2004) appears to be an excellent resource.

## 2.3 Chapter Summary

The literature on previous experimental results provided information on the design of experimental facilities that this study will use to produce a plane wall jet that is two-dimensional and has an initial profile of the streamwise velocity that is uniform with a low turbulence intensity. The literature on previous theoretical and computational studies provided information on the scaling of wall jets, the criteria for self-similarity, and showed that there is a possible dependence of the initial conditions at the slot on the downstream development. This study will document the initial conditions at the slot and use the scaling coordinates of $u_{\mathrm{m}}$ and $y_{1/2}$.

# Chapter 3

# Experimental Apparatus and Instrumentation

## 3.1 Introduction

An experimental facility was designed and constructed to produce a plane turbulent wall jet. The components of this facility were an existing glass-walled water tank, a pump and piping system capable of transferring water from one end of the tank to the other end, an orifice plate to measure the flow, and a ground plane and flow conditioner that was designed to produce a plane turbulent wall jet with specific initial conditions.

The instrumentation used to obtain data for this study were a pressure transducer and volt meter to measure the flow rate through the orifice plate, and a particle image velocimetry (PIV) system that included seeding particles, dual Nd:YAG lasers, a pulse/delay generator, and a digital camera. The PIV system was controlled using a computer with in-house software.

The design and construction of the wall jet facility is the subject of the first section of this chapter. The next section discusses the PIV system that was used. The final section of the chapter outlines the series of measurements that were taken.

## 3.2 Overall Description of Wall Jet Facility

Figure 3.1 is a schematic of the overall experimental facility used in this study. The water is drawn from the far side of the tank and is pumped through the orifice plate and into the back of the flow conditioner, eventually being discharged through the slot at the front of the flow conditioner and flowing across the horizontal glass wall. The interior

dimensions of the water tank are a length of 4 m, a width of 1.04 m, and a depth of 0.7 m. The flow conditioner rests on the floor of the tank. There are steel bars that clamp around the flow conditioner that have a thin foam pad placed underneath to prevent any damage to the glass. The ground plane is a horizontal glass wall that was aligned to the slot exit and held in place with a steel frame that was suspended from angled brackets that rested on top of the water tank. The steel frame and brackets were connected by threaded steel rods, which allowed the height of the glass wall to be finely adjusted.

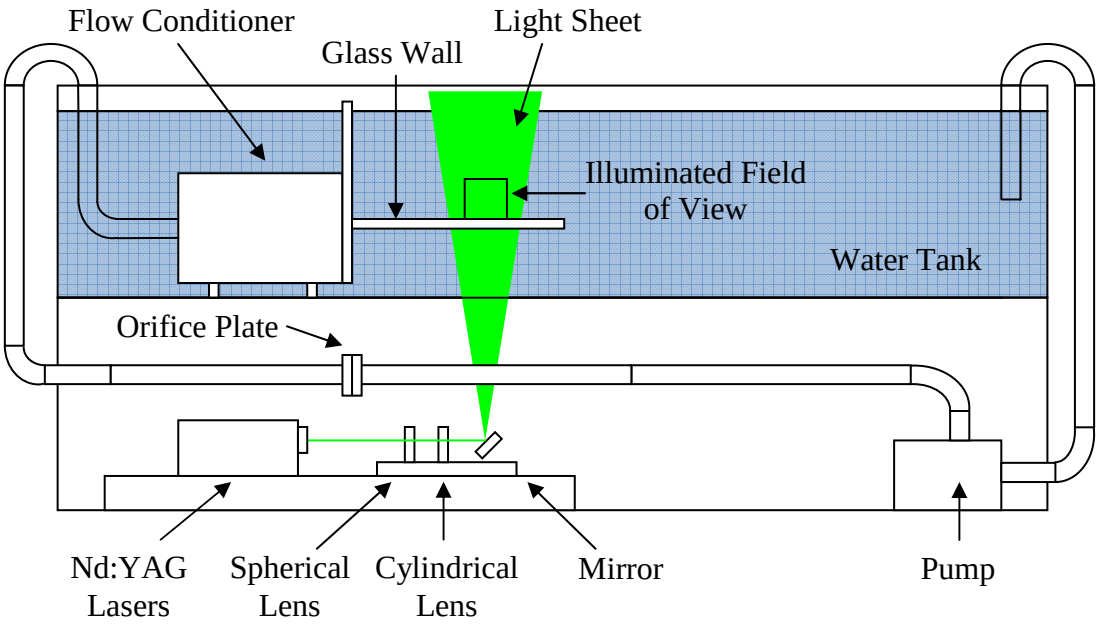


Figure 3.1: Schematic of experimental facility (not to scale).

## 3.3 Pump and Flow Measurement

### 3.3.1 Pump and Piping System

The layout of the pump and piping system that was designed to supply water to the inlet of the flow conditioner from the far end of the water tank can be seen in figure 3.1. A Goulds G&L series 1.1-kW centrifugal pump was able to supply a flowrate of 5.82 $x10^{-3}$ $m^3/s$, corresponding to a Reynolds number at the slot exit of 8100 based on the slot height. The flow resistance at the pump intake was reduced through the use of a larger inlet pipe and a bell mouth entry. PVC pipe was used to transport the water from the tank to the pump, and from the pump to the flow conditioner. Additionally, there was a valve and a section of flexible tubing that were used at the pump outlet, and an orifice plate section that was located between the pump and the flow conditioner. This section was composed of copper pipe with a diameter of 2 inches and the orifice plates. A manifold made of PVC pipe was designed to evenly supply fluid to the four holes in the back of the flow conditioner.

### 3.3.2 Orifice Plate

An orifice plate was installed between the pump and piping manifold to measure the flow rate. By measuring the pressure differential across the orifice plate the flow rate could be calculated based on ISO 5167-1 “Measurement of fluid flow by means of pressure differential devices” (1999). The dimensions of the orifice plate, the Reynolds number, the pressure tap arrangement and the measured pressure differential were used to calculate the flow rate based on equation (3.4),

$$Q = C\frac{\pi}{4}d^2\sqrt{\frac{2\Delta P\rho}{1-\beta^4}}, \tag{3.4}$$

where $Q$ is the volumetric flow rate, $C$ is the discharge coefficient, $d$ is the orifice plate diameter, $D$ is the pipe diameter, $\beta = d/D$, $\rho$ is the fluid density, and $\Delta P$ is the measured pressure differential across the orifice plate. The formula for the discharge coefficient is

$$C = 0.5959 + 0.0312\beta^{2.1} - 0.1840\beta^{8} + 0.0029\beta^{2.5}\left(\frac{10^6}{\mathrm{Re}_D}\right)^{0.75} + 0.0900 L_1 \beta^4 \left(1-\beta^4\right)^{-1} - 0.0337 L_2' \beta^3 , \tag{3.5}$$

where $L_1$ and $L'_2$ are constants that depend on the pressure tap arrangement, and the Reynolds number is based on the bulk velocity in the pipe, $V_b$, and diameter:

$$\mathrm{Re}_D = \frac{V_b D}{\nu} = \frac{4Q}{\pi \mu D}. \tag{3.6}$$

For this apparatus $L_1 = 0.4333$ and $L'_2 = 0.47$.

The equations for the volume flow rate, $Q$, and the discharge coefficient, $C$, were non-linear which required an iterative process to obtain the solution. This was accomplished using a spreadsheet. A typical value for $\Delta P$ was 25.7 kPa, which corresponded to a flow rate of 5.82 L/s.

### 3.4 Design of the Flow Conditioner

The initial conditions of a plane wall jet are known to affect its development downstream of the slot. By reproducing initial conditions that are similar to previous physical experiments and computational studies, more accurate comparisons of wall jet characteristics can be made. The conditions at the slot exit that this study attempted to reproduce are a uniform profile for the streamwise velocity, a vertical velocity component equal to zero, and a low value for the turbulence intensity, as indicated by the

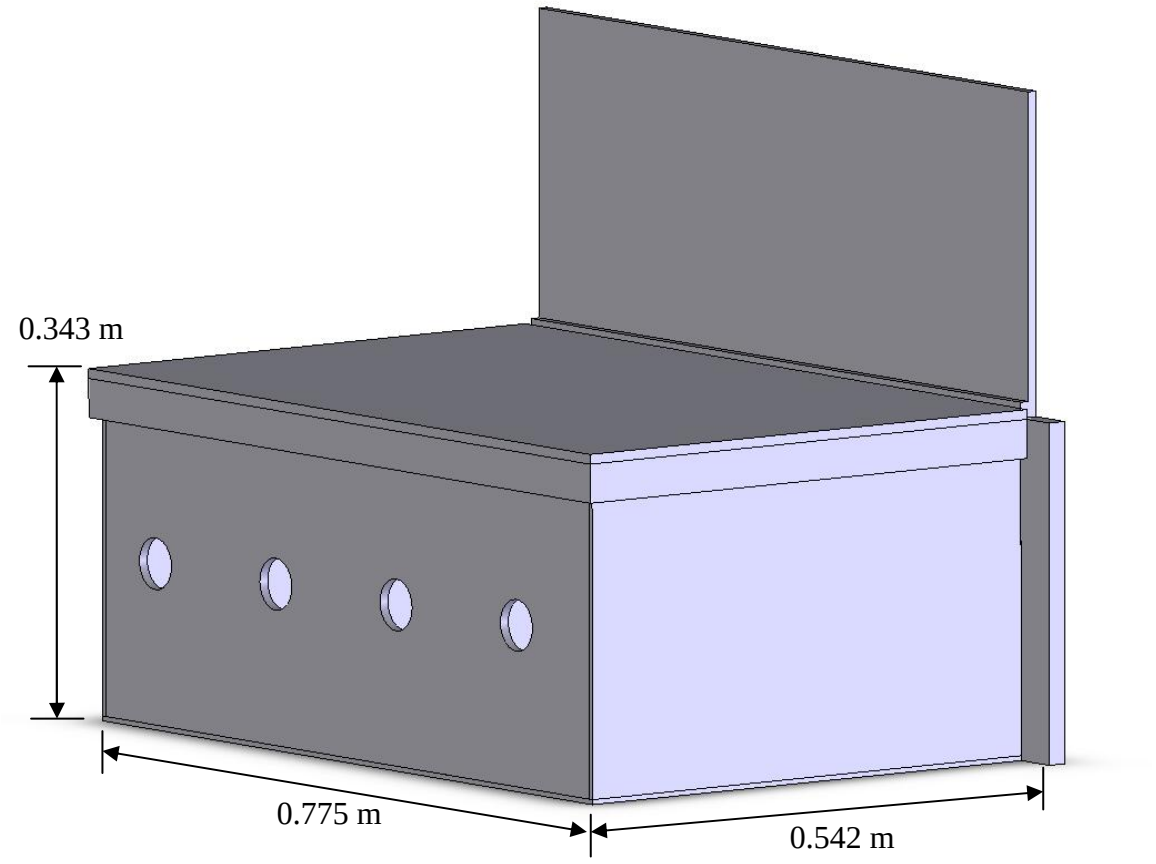


Figure 3.2: Isometric view of the back of the flow conditioner.

streamwise Reynolds stress component, $\overline{u'u'}$. In addition, producing a plane wall jet required the flow to be two-dimensional. This would allow comparison of the flow characteristics to previous plane wall jet studies.

Figures 3.2, 3.3 and 3.5 show the flow conditioner that was designed and built to produce a plane wall jet with the desired initial conditions. The water entered the back of the device through four inlet holes, flowed through multiple screens and straightening vanes, and was discharged from the front of the device through a slot. The design of this flow conditioner was guided by Shinneeb's (2006) design of a flow conditioner that was used to produce an axisymmetric jet. While a plane wall jet flow differs from the flow

within a wind tunnel, the design methods used for wind tunnels can also provide insight into the design of this experimental apparatus. The design and construction of each component of the flow conditioner will be discussed in the following sections.

### 3.4.1 Flow Conditioner Length

Farell (1996) experimented with the use of plastic straw honeycombs and wire mesh screens to reduce turbulence levels and non-uniformity of a wind tunnel flow. The results from that study showed that various combinations of honeycombs, screens and manipulator spacings were effective in reducing both the non-uniformity and turbulence level of the flow. A universal optimum combination was not determined, however a coarse screen followed by a honeycomb and one or more fine screens was found to be effective.

For the current study, water entered the flow conditioner through four holes in the back of the device (figure 3.2). There were four deflection plates inside the device that were attached to the holes. These circular plates helped to distribute the flow across the full width of the flow conditioner. The use of deflection plates was based on the design of Shinneeb's (2006) flow conditioner. Downstream of the deflection plates was a settling chamber followed by circular plastic drinking straws that filled the entire cross-section of the flow conditioner (see figure 3.3). The straws had a diameter of approximately 0.002 m and a length of 0.20 m, and were used as flow straightening vanes. The straws aligned the flow in the streamwise direction and reduced large vortical structures and related turbulence that would have been present downstream of the deflection plates. There were two screens that held the straws in place, and two additional screens between the straws

and the slot. The first two screens that held the straws in place had mesh numbers of 8 and 42. The mesh numbers refer to the number of wires that are contained within one inch of screen. Lower mesh numbers correspond to coarser screens. The remaining two screens also had mesh values of 8 and 42, and the coarser screen was placed downstream of the 42 mesh screen in order to prevent any deflection of the finer screen. The pressure drop across the screens helped to produce a uniform velocity at the exit face of the screen. The screens also helped to break up larger vortical structures that might be present in the flow, further reducing the turbulence intensity. An internal length of 0.516 m was chosen for the flow conditioner to accommodate the deflection plates, straws, screens and settling chamber (see figure 3.3).

### 3.4.2 Nozzle Design and Flow Conditioner Height

For subsonic flows, contractions accelerate the flow and tend to reduce the non-uniformity and turbulence intensity (Tavoularis, 2005). In wind tunnels the design of the contraction is dependent on the wall shape, Reynolds number and length of the contraction. Contractions that are too long will generate relatively large boundary layers at the slot exit, whereas short contractions have the potential for flow separation (Morel, 1975). The typical wall shape of a wind tunnel contraction is a concave section followed by a convex section.

Tavoularis (2005) advises following designs that have achieved the desired initial conditions under similar flow conditions. The design used by Shinneeb (2006) was used as a basis for the nozzle design of this flow conditioner since that study produced an

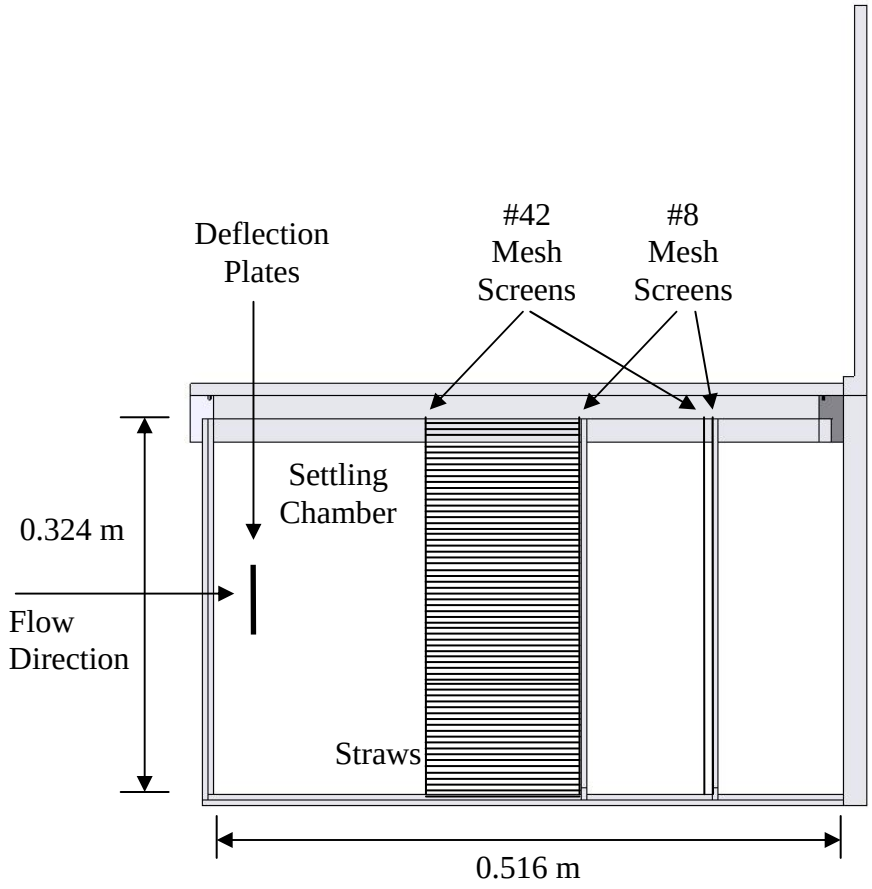


Figure 3.3: Side view of the flow conditioner.

axisymmetric wall jet with the desired initial conditions in the same water tank as the current study. Shinneb's (2006) flow conditioner was able to produce a uniform streamwise velocity profile at the slot exit that had a low turbulence intensity by using a convex section that had a nozzle radius equal to the height of the slot. The traditional concave section found in wind tunnels was replaced with a flat vertical section. This study used a similar design; the inside corner of the slot had a convex profile with a radius of curvature, $R_c$, equal to 0.0095 m (3/8 in), which is close to the maximum slot height of 0.009 m, and the section preceding the convex nozzle was a flat vertical wall (see figure 3.4).

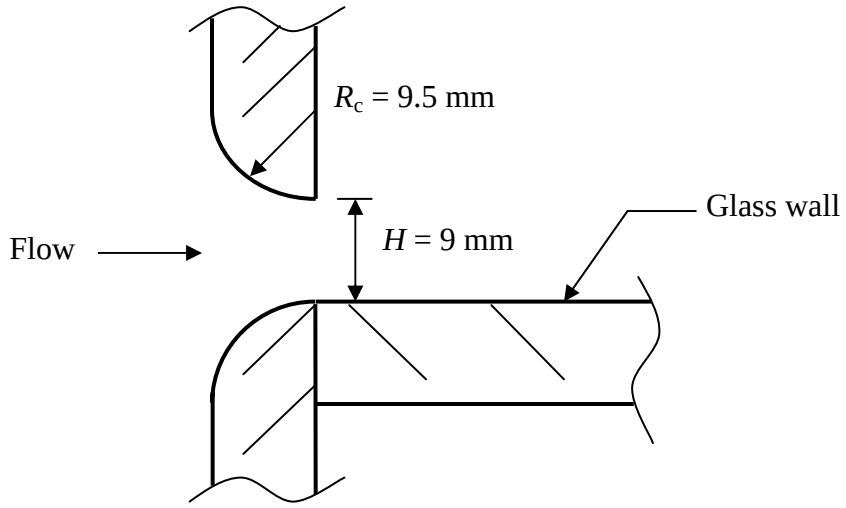


Figure 3.4: Section of slot exit showing circular arc profiles of top and bottom plates.

The height of the flow conditioner was governed by the contraction ratio, which is the ratio of the internal height to the slot height. Tavoularis (2005) recommended a contraction ratio that was as large as possible, with a value greater than or equal to 16 being generally sufficient. A large contraction ratio was used by Eriksson et al. (1998) and Schneider & Goldstein (1994) to produce a uniform streamwise velocity profile. Tachie (2000) did not achieve a uniform profile when using a smaller contraction ratio of 9:1. An internal height to slot height ratio of 36:1 was chosen for this flow conditioner, which is similar to the ratio of 35:1 used by Schneider & Goldstein (1994). To maintain this ratio at the maximum slot height of 0.009 m, the internal height of the flow conditioner was designed to be 0.324 m, as indicated in figure 3.3.

### 3.4.3 Flow Conditioner Width

Producing a plane wall jet required the flow to be two-dimensional. The width of the flow conditioner needed to be relatively large to achieve this. Previous researchers have shown that a large slot width to slot height ratio is necessary to avoid three-

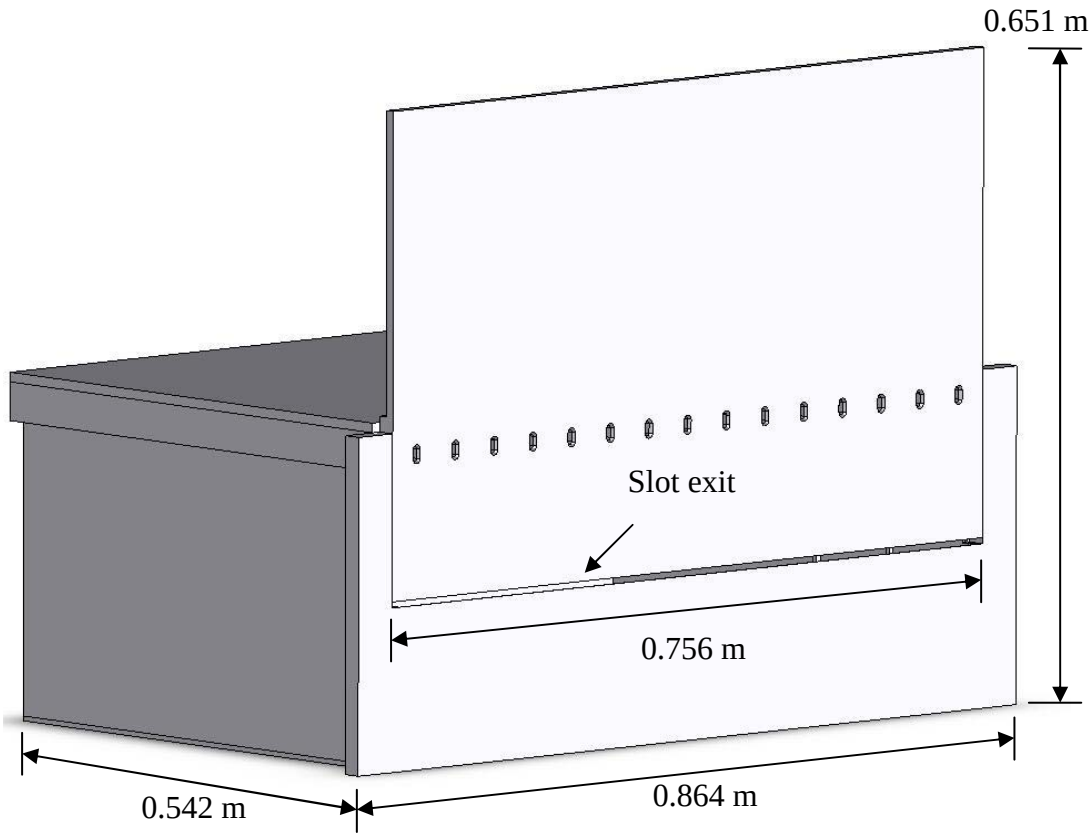


Figure 3.5: Isometric view of the front of the flow conditioner.

dimensional flows from forming. Eriksson et al. (1998) recommended a slot width to height ratio of 150:1, while Schneider & Goldstein (1994) were able to obtain an acceptable momentum balance downstream of the slot using a ratio of 90:1. The exterior width of the flow conditioner was chosen to be 0.864 m so that the flow conditioner would easily fit into the water tank which had a width of 1.04 m. This allowed the width of the slot to be 0.756 m (see figure 3.5). The height of the slot can be adjusted from a closed position to a height of 0.009 m. At 0.009 m, 0.006 m and 0.005 m slot heights, the width to height ratios are 84:1, 126:1 and 151:1, respectively. In this thesis, preliminary

measurements were taken at a slot height of 0.009 m, and the main series of measurements were taken with a slot height of 0.006 m.

### 3.4.4 Pressure Within the Flow Conditioner

The pressure inside the flow conditioner had to be estimated in order to calculate the wall deflection. There are three contributions to the pressure within the flow conditioner: the pressure drops across the mesh screens, the plastic drinking straws, and the slot exit. Based on a slot exit Reynolds number of 9600 and a slot height of 9 mm the flow rate through the flow conditioner is $7.26 \times 10^{-3}$ $m^3/s$. The streamwise velocity inside the flow conditioner is 0.030 m/s and the streamwise velocity exiting the slot is 1.067 m/s.

The pressure drop across the mesh screens was estimated using equation (3.1) proposed by Mehta (1985),

$$\Delta P_{sc} = \left( 6.5 \left[ \frac{1-\beta_{sc}}{\beta_{sc}^{\,2}} \right] \left[ \frac{u d_{sc}}{\beta_{sc} \nu} \right]^{-0.33} \right) \frac{1}{2} \rho U_e^{\,2}, \qquad (3.1)$$

where $d_{sc}$ is the mesh screen wire diameter, $u$ is the mean streamwise velocity, $U_e$ is the local freestream velocity, $\nu$ is the kinematic viscosity, $\rho$ is the density of the fluid, and $\beta_{sc} = \left( 1 - \frac{d_{sc}}{l_{sc}} \right)^2$, where $l_{sc}$ is the screen mesh length. In this situation, the local freestream velocity is assumed to be the same as the mean streamwise velocity. For a 42 mesh screen with a wire diameter of 0.0003 m and a screen mesh length of 0.0006 m, the pressure drop is 10.5 Pa. For an 8 mesh screen with a wire diameter of 0.0007 m and a screen mesh length of 0.0032 m, the pressure drop is 0.981 Pa.

The water flowing through the plastic straws had a Reynolds number of 59, which signified laminar flow and allowed the pressure drop across the straws to be estimated using equation 6.44 from White (1999) as follows: $\Delta P_{st} = \frac{8\mu L_{st} Q_{st}}{\pi (r_{st})^4} = 47$ Pa, where μ is the dynamic viscosity of the water, $L_{st}$ is the straw length, $Q_{st}$ is the flow rate through the straws, and $r_{st}$ is the straw radius.

The pressure drop across the slot exit was calculated using Bernoulli's equation in the form of $\Delta P_{slot} = \frac{1}{2}\rho\left(U_{slot}^2 - U_{internal}^2\right)$. For a slot height of 0.009 m the pressure drop was equal to 568 Pa, which is a significantly higher value than the pressure drop across the straws and screens combined. When the slot height is reduced to 0.005 m the pressure drop across the screens and straws remained the same, however the pressure drop across the slot increased to 1839 Pa.

The pressure inside the flow conditioner was equal to the sum of the pressure drops across the screens, the straws and the slot, which was approximately 2000 Pa for a slot height of 0.005 m. An internal pressure of 5000 Pa was used to calculate the minimum required thickness needed to prevent a significant deflection of the walls. This provided a safety factor of approximately 2.5 for a slot height of 0.005 m.

### 3.4.5 Walls of the Flow Conditioner

The walls of the flow conditioner were made out of grey PVC and composed of seven main pieces: the back wall, the two side walls, the bottom wall, the removable top wall, the bottom section of the front wall, and the adjustable top section of the front wall. Each of these pieces can be seen in figures 3.6 and 3.7.

There was a border glued to the top of the side walls and back wall that allowed the top wall to be screwed into place so that it could be removed when needed. To prevent leakage, a rubber gasket was placed between the border and the top wall. A rubber gasket was also placed between the side walls and the adjustable front wall to prevent leakage. The process of machining the slot into the top and bottom sections of the front wall caused the PVC material to warp. If the slot was left in this condition the two-dimensionality of the wall jet would be lost. This situation was remedied by embedding a flat piece of stainless steel on the inside of both front wall sections. These bars were held in place with bolts and did not increase the thickness of the front wall. There were also two smaller pieces of PVC that were attached to the front of the flow conditioner to help prevent the adjustable front section from deflecting.

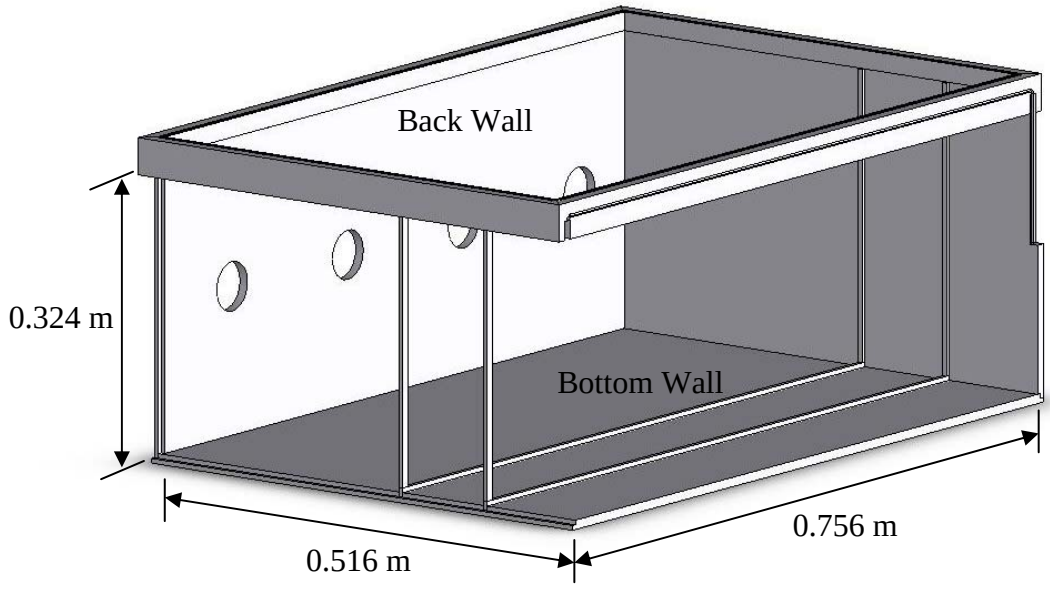


Figure 3.6: Isometric front view of top border, back, side, and bottom walls, and screen holders.

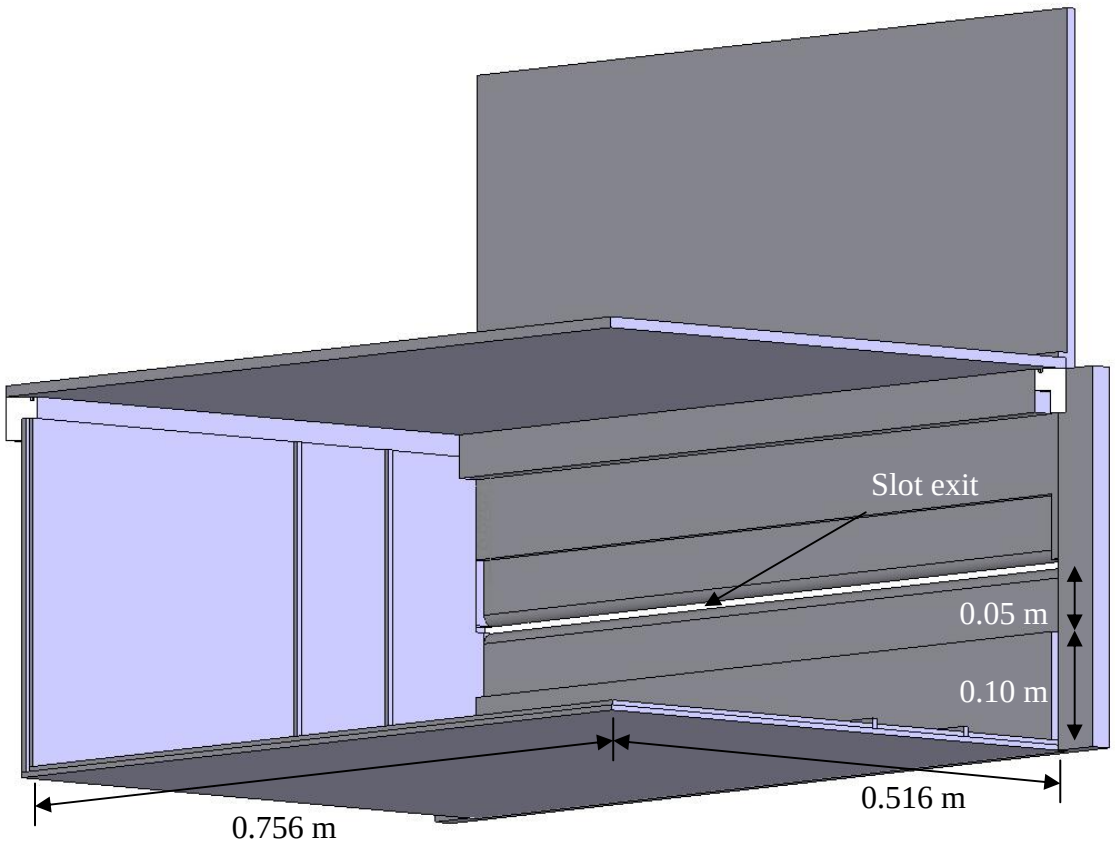


Figure 3.7: Isometric back view of removable top, bottom wall, side wall, fixed bottom section of front wall, adjustable top section of front wall, and inside view of curved slot.

The approximate deflection, $\delta$, of the front wall of the flow conditioner was calculated using equation (3.2), from Timoshenko (1955), for a plate with two opposing edges that are simply supported, a third edge that is fixed in place (either by clamping or gluing), and a fourth edge that is free to move. This corresponds to the boundary conditions for the front walls of the flow conditioner. The top section of the front wall has both side edges simply supported by a piece of PVC while the third edge of the wall is

bolted into place and the slot is left unsupported. The bottom section of the front wall has three edges that are glued in place while the slot edge is not supported.

$$\delta = \frac{\alpha q b^4}{E h^3} \tag{3.2}$$

In equation (3.2) the uniform pressure distribution on the wall $q$ = 5000 psi, the modulus of elasticity $E$ = 3.1 x $10^9$ Pa, $b$ is the height of the wall, $h$ is the thickness of the plate, and $\alpha$ is a numerical factor that is obtained from a table of values based on the ratio of $b/a$, where $a$ is the width of the wall.

Both sections of the front wall were further divided into section 1, which had a height $b_1$ = 0.10 m and thickness $h_1$ = 0.019 m, and section 2, which had a height $b_2$ = 0.05 m and thickness $h_2$ = 0.0095 m (see figure 3.7). The deflection of the top and bottom sections was then calculated as the sum of the section 1 and section 2 deflections as follows:

$$\delta_{\text{top}} = \delta_{\text{bottom}} = \delta_1 + \delta_2 = \frac{\alpha q b_1^4}{E h_1^3} + \frac{\alpha q b_2^4}{E h_2^3} = 0.029\,\text{mm} + 0.015\,\text{mm} = 0.044\,\text{mm}.$$

The deflection for each of the front wall section was less than one mm, which was considered sufficiently low.

The deflection of the remaining walls was calculated using equation (3.3), which is for a plate that is built-in (fixed in place) at the edges.

$$\delta = \frac{\alpha q a^4}{E h^3} \tag{Eqn 3.3}$$

The thickness of each of the walls was 0.0095 m. The deflection of the side walls and back wall were 0.512 mm and 0.576 mm, respectively. The deflection of the top and bottom plates was 3.10 mm. This deflection was considered too large, so two stainless

steel beams were clamped to the outside of the top and bottom of the flow conditioner, effectively dividing the top and bottom plates into three separate sections. The deflection was then reduced to a maximum of 0.046 mm.

The majority of the components of the flow conditioner were glued together. To ensure that the components would not break apart, a central groove was initially designed into the edges of each of the components to increase the surface area that the glue could bond to. An example of this type of groove can be seen in figure 3.8. Unfortunately this design required intricate machining and led to situations where the thickness of the edges of the components became too small. An alternative inter-locking method was then designed where a stepped groove was machined along each edge of the components (see figure 3.9). This reduced the complexity of the design and provided enough surface area to ensure that the flow conditioner would remain glued together.

## 3.5 Particle Image Velocimetry (PIV) System

### 3.5.1 Background of PIV

In the 1980's an experimental technique was developed that allowed quantitative measurements of a fluid flow to be obtained when observing objects flowing along with the fluid. Particle image velocimetry (PIV) is an imaging technique that infers the velocity of a fluid by determining the velocity of particles that are suspended in the fluid. These particles have a size and density that allow them to follow the same path as the fluid. Dual Nd:YAG lasers are used to illuminate the particles and a digital camera is used to capture images of the moving particles. A computer and software are then used to process the images and measure the velocity of the particles. This provides instantaneous two-dimensional velocity vector measurements of the fluid. PIV is an indirect velocity

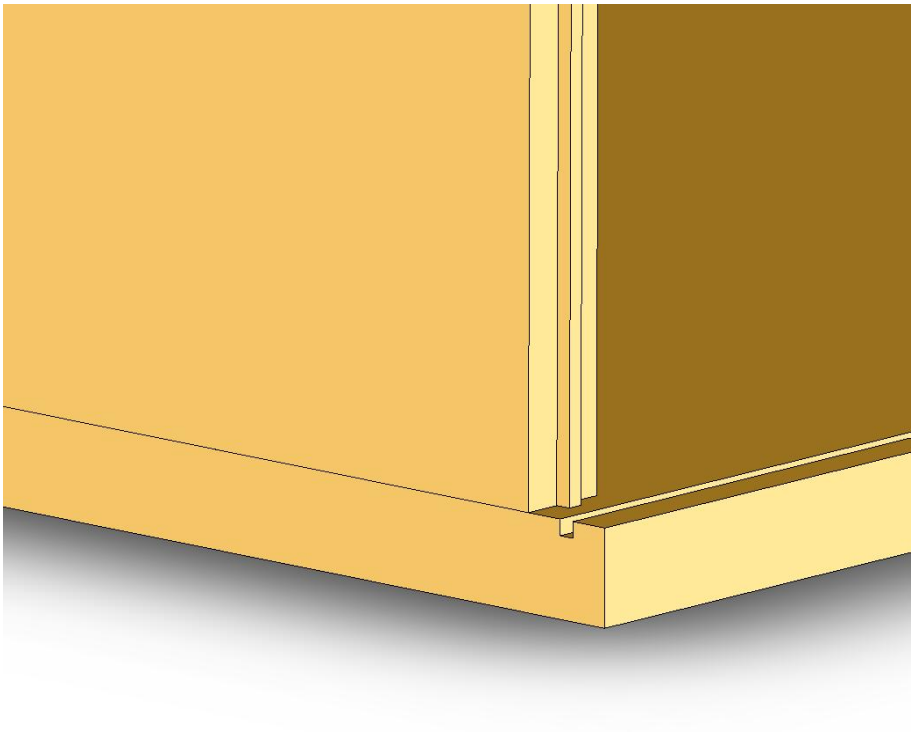

Figure 3.8: Central groove inter-locking method.

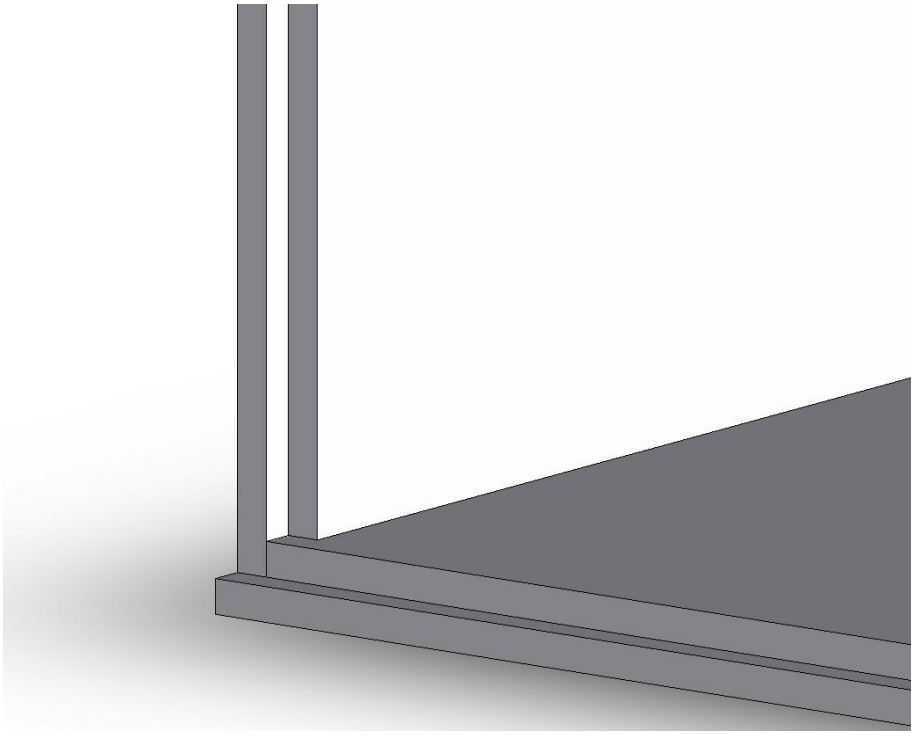

Figure 3.9: Stepped groove inter-locking method used in final design.

measurement technique that allows both large and small-scale spatial structures to be detected.

### 3.5.2 PIV System Components

The four main components of the PIV system used in this study are the laser source used to illuminate the tracking particles that were added to the water, the digital camera and lens used for image acquisition of the illuminated particles, the computer that was used to control the lasers and camera using in-house software, and a BNC Model 505 pulse/delay generator (see figure 3.10). The computer was also used to process the images in order to obtain the velocity vectors for each pair of images.

### 3.5.3 Illumination of Tracking Particles

Hollow glass spherical beads with a specific gravity of 1.0 were added to the water near the inlet of the pumping system. The pump was left to run for thirty minutes to allow complete mixing of the particles throughout the water tank so that a homogenous distribution would be obtained. The illumination system used dual Nd:YAG lasers with a pulse energy of 200 mJ as well as two lenses to modify the laser beam into a light sheet. The lasers were pulsed in order to freeze the motion of the particles. The maximum repetition rate was limited to 15 Hz so dual lasers had to be used to achieve short time delays between the images. Downstream of the laser beam a 1000-mm spherical lens was used to reduce the diameter of the beam and therefore the thickness of the light sheet. Reducing the thickness of the laser sheet increased the spatial resolution in the direction perpendicular to the light sheet. A plane light sheet was created by placing a -12.7-mm cylindrical lens downstream of the spherical lens. The direction of the light sheet was then converted from horizontal to vertical using a mirror inclined at 45°.

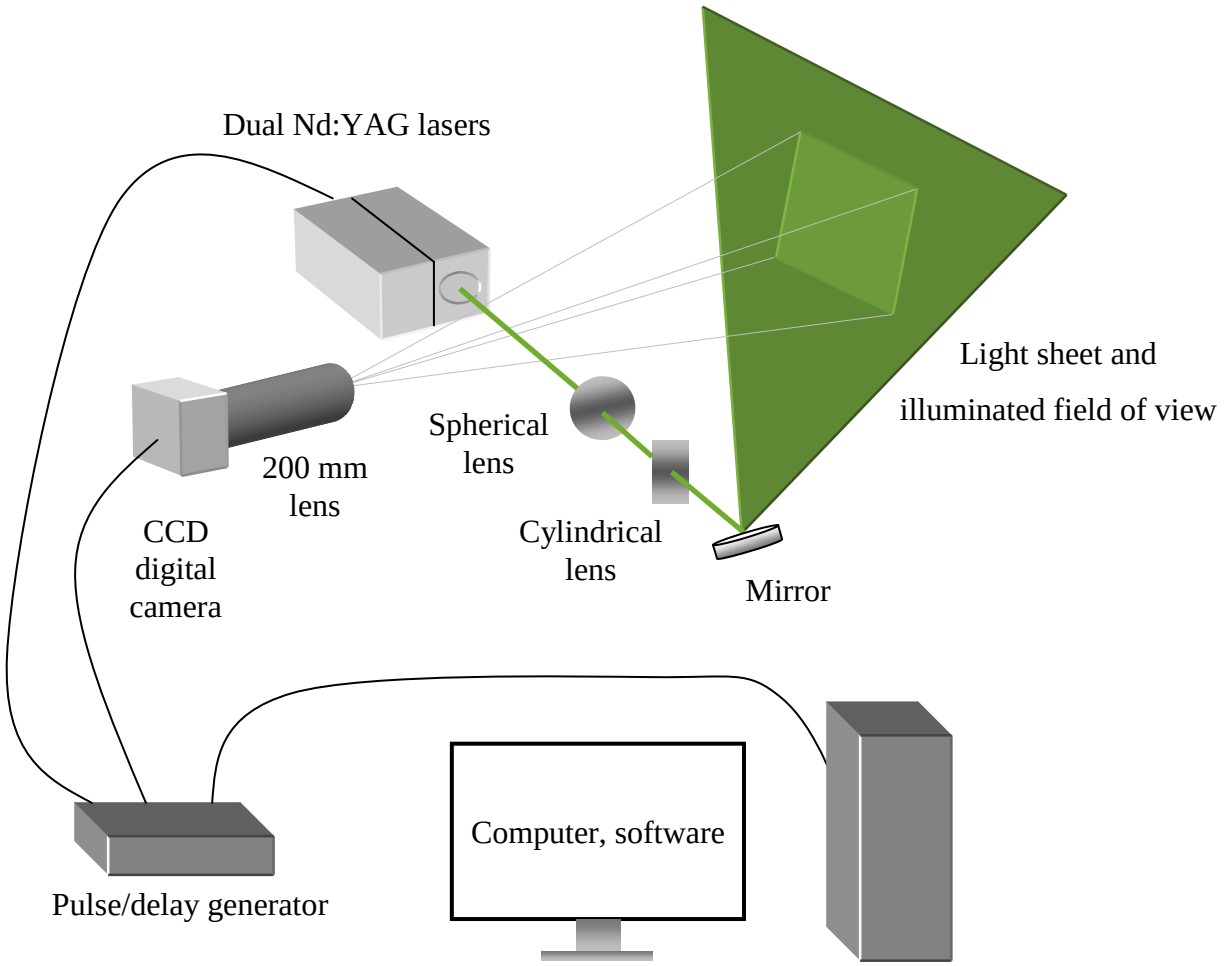


Figure 3.10: Schematic of a PIV system.

The lasers, lenses and mirror were secured to an optical table below the water tank. The equipment was positioned on the table such that the laser sheet was close to the desired location, and the table itself was then moved to finely position the field of view. The light sheet was aligned to either the centerline of the jet or 0.275 m off the centerline by carefully positioning a flat metal ruler on the glass plate using temporary guide blocks, and then manually moving the laser sheet until it was in line with the ruler. An image of the ruler and guide block can be seen in figure 3.11. The light sheet was aligned in the streamwise direction by first moving it to the desired approximate location, and then

moving the lenses and mirror to the precise location that would fully illuminate the desired field of view. The distance between the cylindrical lens and the mirror was adjusted to get the correct width of the laser sheet. The sheet had to be wide enough to cover the entire field of view however the intensity of the laser sheet would be diminished if it was made too wide.

### 3.5.4 Image Acquisition

A MegaPlus ES 4020 digital camera with a 2048 x 2048 pixel sensor was attached to a 200-mm Nikon lens and used to capture pairs of images of the illuminated particles. The camera and lens were mounted on a tripod and positioned so that the light sheet was visible through the side of the tow tank. The camera had to be positioned at the proper streamwise location and at a spanwise distance from the light sheet that provided an appropriately sized field of view. The vertical position of the camera was chosen so that the glass wall would be near the bottom of the field of view. A calibration image was then taken with a ruler placed on the glass wall that was in line with the laser sheet in order to determine the scale and dimensions of the field of view. The ruler had divisions of 1 mm and 1/16 in. Care was taken to keep the edge of the image aligned to the horizontal glass wall in order to minimize the amount of rotation the image required during processing. The ruler was then removed and the pump was turned on.

The lasers had an intensity setting that allowed a manual focusing of the camera lens on the particles. After manually focusing on the particles the lasers were returned to full power and five test images were obtained using the same in-house software used to control the lasers. The images were saved to the hard drive as ".raw" files. Test images

were required to ensure there were enough particles and that they were in focus, as well as to ensure the correct time delay between images was chosen. A displacement of approximately 8 pixels was desired, as will be explained in the next section. This was checked using in-house software. After verifying the particles were in focus and that a proper time delay was chosen, 2000 pairs of images in groups of 50 pairs of images were recorded at a frequency of 4 Hz and saved to the hard drive.

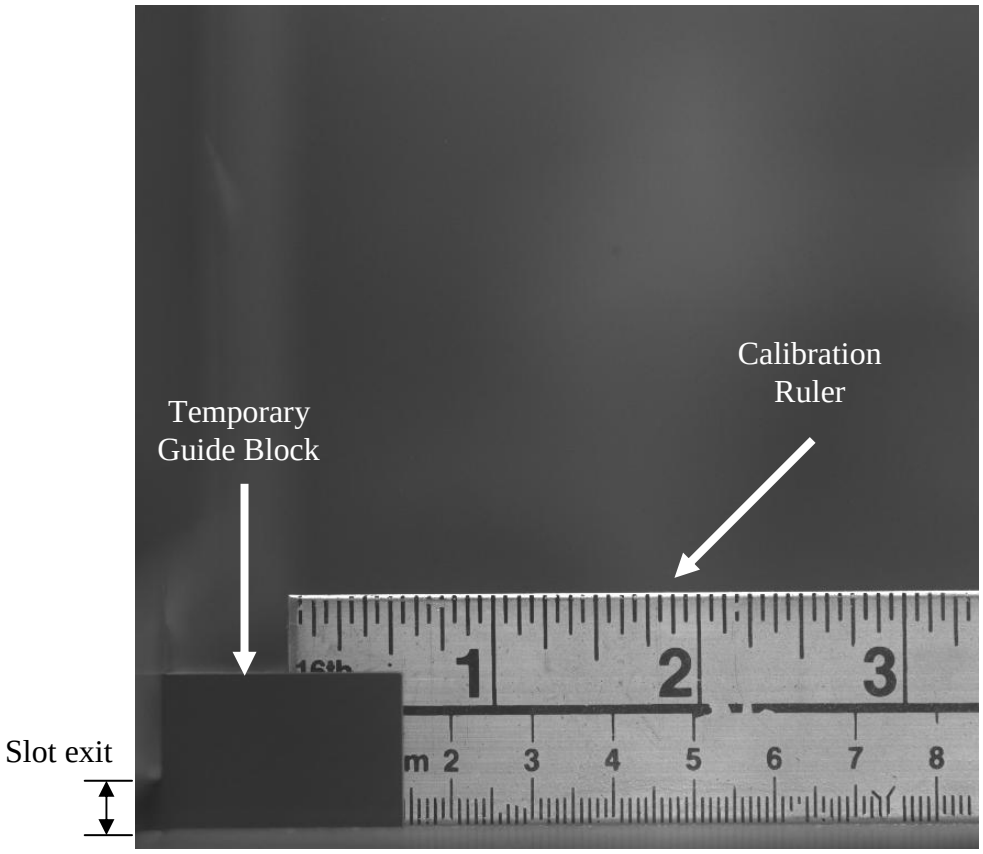


Figure 3.11: Calibration image showing the guide block located at the slot exit.

### 3.5.5 Image Processing

The velocity of the illuminated particles in the images had to be determined in order to measure the velocity of the fluid. This was accomplished by dividing the pairs of

images into a grid of square interrogation areas (see figure 3.12), and determining the displacement of the particles within each interrogation area. The streamwise, $\Delta x$, and vertical, $\Delta y$, particle displacement were divided by the time delay, $\Delta t$, between images to obtain two components of the velocity, $u$ and $v$. By keeping the size of the interrogation area small, a high spatial resolution of the fluid velocity throughout the entire field of view was obtained.

Due to the large number of particles that are present in the flow, it is not feasible to calculate the displacement of each particle in the field of view. By breaking up the image into smaller interrogation areas and calculating the displacement of the pattern that the particles made within that area, a single velocity vector for the interrogation area could be obtained. This was accomplished using a method of statistical analysis known as a half-padded fast Fourier transform (FFT) cross-correlation. The cross-correlation method works by comparing the first image to each possible displacement of the second image in order to determine where the particle images overlap. Each interrogation area of the first image remained at its original position while the corresponding interrogation area of the second image was moved pixel by pixel to each displacement in both the $x$ and $y$ directions. The displacement location where the images matched to the highest degree was found using an FFT algorithm; this displacement was the distance that the group of particles had travelled between images. Figure 3.13 shows a typical correlation plane. The peak in the image shows the $x$ and $y$ displacements where the images matched to the highest degree.

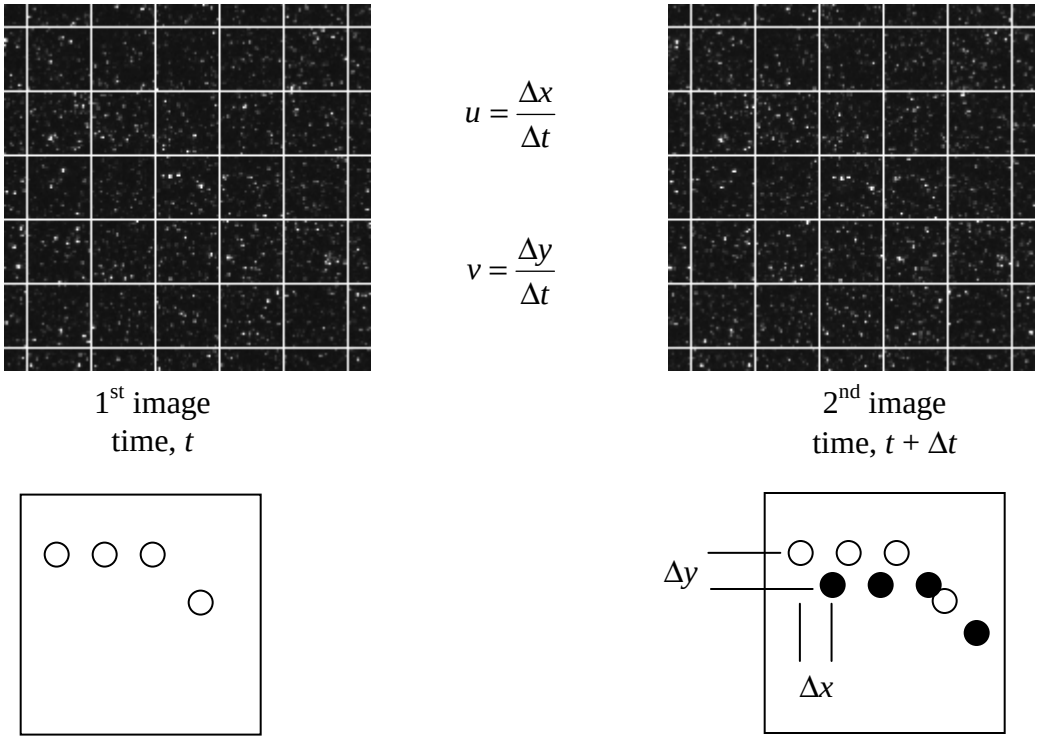


Figure 3.12: Illuminated particle images with 32 x 32 pixel interrogation areas and a schematic of the displacement of a pattern of particles.

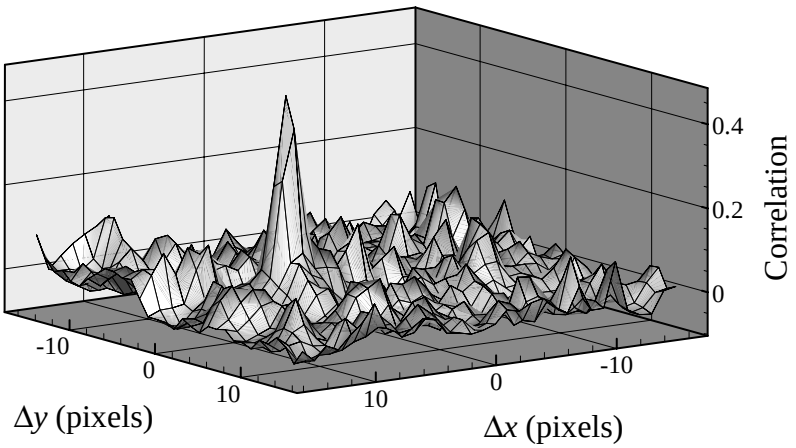


Figure 3.13: Correlation plane (the maximum correlation occurs at $\Delta x$ = 5 pixels and $\Delta y$ = -1 pixels).

In-house software was used to perform the processing of the image pairs. This study used interrogation areas of 32 x 32 pixels with a 50% overlap and half-padded FFT cross-correlation. This provided velocity vectors at 16 pixel intervals throughout the field of view for a total of 16,129 vectors for each image pair. The time delay that provided a displacement of approximately 8 pixels in the test images was chosen because a displacement of ¼ of the width of the interrogation area was desired. The pixel coordinates where the pattern of both images matched most closely was found using a relative maxima peak finding algorithm. A Gaussian curve-fitting method was used to improve the accuracy of the pixel displacement to the sub-pixel level.

Hart's (2000) correlation-based-correction (CBC) algorithm was used to improve the signal-to-noise ratio and to reduce the number of spurious vectors. Errors in the calculation of the particle displacement can occur when the particle density is either too high or too low in a particular area of the field of view, or if there is an abnormally large velocity gradient in a portion of the flow field. Additional in-house post-processing software was then used to identify vectors that differed greatly from their neighboring vectors using a cellular neural network (CNN) method (Shinneeb et al., 2004). An erroneous vector was replaced with an estimated vector that was calculated based on the values of the neighboring vectors using a Gaussian filter with a filter width of 8 pixels and a width of 2 interrogation windows.

The post-processing software was also used to properly scale the images by converting the local camera coordinates to global coordinates using the calibration image.

Also, the velocity field was aligned by rotating an amount calculated from the original image using the glass wall as a reference.

After post-processing all 2000 pairs of images, a file was created that contained the mean velocity vectors and turbulence statistics for that field of view. Files of instantaneous velocity vectors could also be created for any of the 2000 pairs of images. Figure 3.14 shows images of instantaneous velocity vectors for an entire field of view. In figure 3.14(b) only every fourth vector is shown to provide a better sense of the vector direction.

### 3.5.6 Experimental Uncertainty Analysis

Shinneeb (2006) was able to determine the experimental uncertainty of PIV velocity measurements by analyzing simulated images with a known pixel displacement and comparing that displacement to the one obtained using PIV analysis software. Shinneeb began this process by determining the characteristics of measured PIV images (see Table 3.1). The values for background noise and particle intensity are based on a grey scale from 0-255, where 0 and 255 correspond to pure black and white, respectively. Shinneeb (2006) then generated simulated images based on these characteristic values. The generated images were displaced by a specific pixel value and analyzed using the same PIV analysis software and settings as the real images. The difference between the known and measured pixel displacement provided Shinneeb (2006) with an absolute experimental uncertainty of 0.29 pixels for the PIV velocity measurements from that study. Shinneeb (2006) analyzed various particle displacements and found that the uncertainty was independent of the displacement.

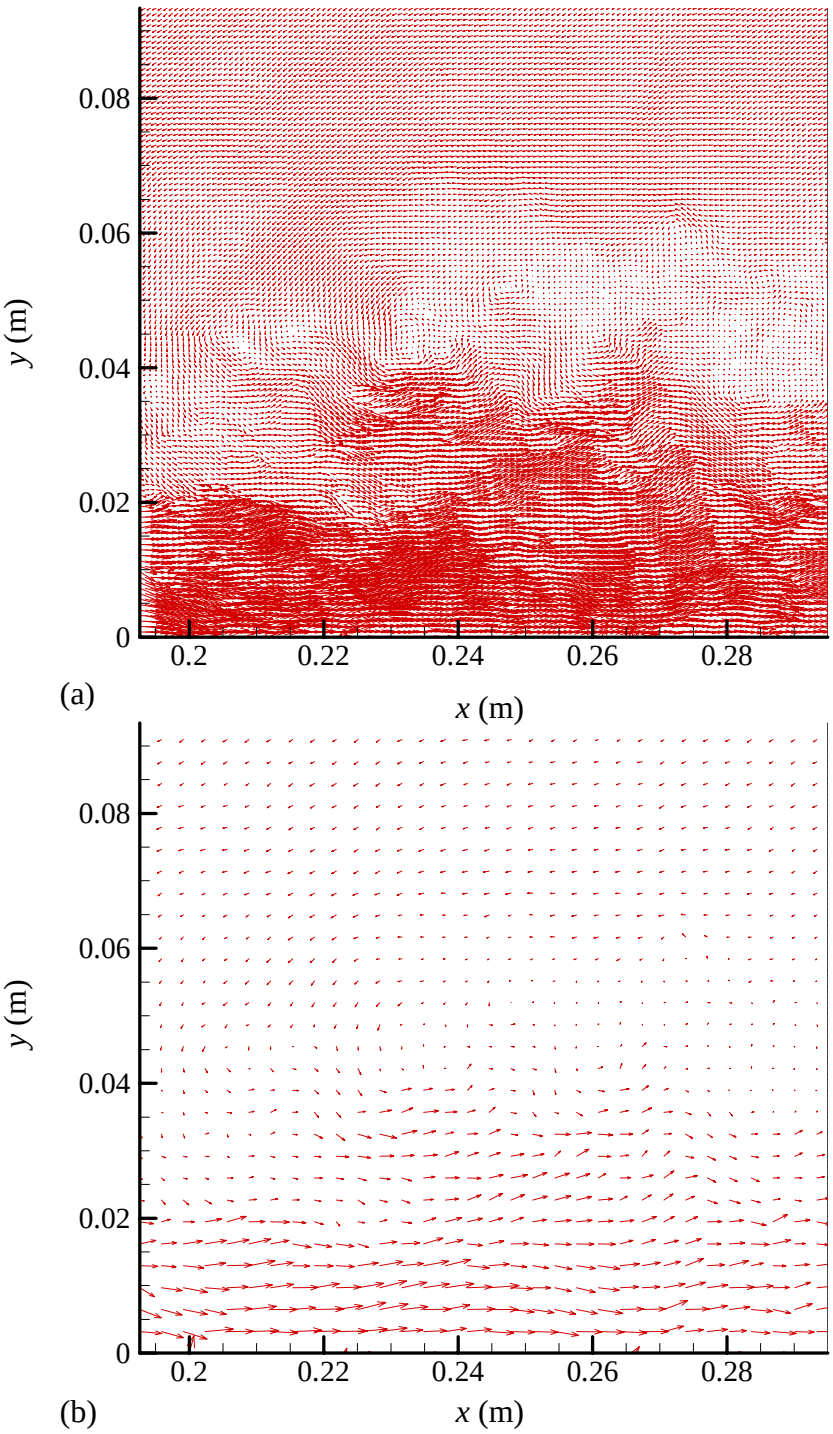


Figure 3.14 (a), (b): Example image of instantaneous velocity vectors for the field of view for test C3. Every fourth vector is shown in (b) to give a sense of the vector direction.

Table 3.1 Image characteristics obtained by Shinneeb (2006) and the present study.

| | Shinneeb (2006) | | Present Study | |
|---|---|---|---|---|
| Characteristic | Mean | Standard Deviation | Mean | Standard Deviation |
| Background noise | 23 | 11 | 13 | 2 |
| Particle intensity | 254 | 1 | 255 | 1 |
| Particle diameter (pixels) | 1.33 | 1.04 | 1.55 | 1.40 |
| Number of paired particles | ~79,000 | | ~84,000 | |

The image characteristics obtained by this study were assessed to determine if these results should use the same absolute uncertainty used by Shinneeb (2006). A random image was selected at a downstream location from the slot and the following characteristics were assessed: background noise, particle intensity, particle diameter and number of paired particles. The background noise was measured by determining the intensity of the image where there are no particles. Thirty measurements were taken and the background noise was determined to have a grey scale value of 13 with a standard deviation of 2. Thirty measurements of the particle intensity were also taken and the average value was determined to be 255 with a standard deviation of 1. Matrox Inspector® software was used to determine the average particle diameter as well as the number of paired particles. The mean particle diameter was 1.55 pixels with a standard deviation of 1.40 pixels, and the total number of paired particles for the entire image was approximately 84,000. All four of these image characteristics are similar to the characteristics measured by Shinneeb (2006). Given that this study also used the same water tank, particles, analysis software, outlier rejection software and similar software

settings, Shinneeb's (2006) absolute experimental uncertainty value of 0.29 pixels for PIV velocity measurements will be used. The time delay between images was chosen to provide particle displacements of about 8 pixels, which corresponds to a relative uncertainty of 3.6% for the PIV measurements of the streamwise velocity.

### 3.6 Run Matrix

A preliminary series of measurements were taken along the width of the slot without the horizontal glass wall in place and with a slot height of 0.009 m. The purpose of these measurements was to determine the uniformity of the streamwise mean velocity and turbulence intensity in the spanwise direction. Five horizontal fields of view were taken that provided data at $x = H$ along the entire slot width.

The two main series of measurements were taken with the glass wall in place and with a slot height of 0.006 m, as shown in figure 3.15. The first main series of measurements were along the centerline from the slot exit to a streamwise distance of 110 slot heights. The second main series of measurements were taken in a plane displaced a spanwise distance of 0.275 m from the centerline. These off-centerline measurements were located at that spanwise distance in order to allow comparison to LDA measurements. With the present optics, the LDA equipment was limited to measurements relatively close to the wall. The off-centerline measurements were taken at the slot exit and downstream of the slot to a streamwise distance of 100 slot heights. Each of the latter series of measurements required 12 hours to complete. This included the time needed to set up the lasers and digital camera and then acquire 2000 images for each field of view. Additional measurements were taken at the slot exit for both series of measurements

using a magnified field of view to obtain higher resolution data near the exit. These measurements at the slot exit helped to verify whether or not a uniform profile of the streamwise velocity with a low turbulence intensity was achieved. These additional measurements required 4 hours to set up and acquire.

Tables 3.2 and 3.3 summarize the measurements that were obtained. The preliminary measurements are listed as P1-P5. Test runs P1 and P2 were performed on the same day, as were test runs P3, P4 and P5. While the flow-rate was only measured for P1 and P4, all five test runs were performed with the pump valve fully open which should have produced a similar velocity at the slot exit for all five measurements. The main series of measurements performed along the centerline and off-centerline are listed as tests C0-C7 and OC0-OC7, respectively (see figure 3.15). Measurements of the water temperature and orifice voltage were obtained at the start and end of each test run. These measurements were then averaged so that an accurate temperature and flow rate would be used to determine the Reynolds number for each field of view.

### 3.7 Chapter Summary

The experimental facility and instrumentation used by this study was described in this chapter. This included the design and construction of the flow conditioner, the pump and piping system, the orifice plate, as well as background information on PIV and the components that were used to acquire the images for each field of view. An outline of the measurements that were taken was then provided. Chapter 4 will now provide a description of the results that were obtained by this study.

Table 3.2 Outline of preliminary measurements.

| Test Run | $z_{min}$ (m) | $z_{max}$ (m) | $\Delta t$ (μs) | $\Delta P$ (kPa) | $Q$ (L/s) | $Re$ |
|---|---|---|---|---|---|---|
| P1 | 0.220 | 0.392 | 1200 | 24.8 | 5.871 | 7594 |
| P2 | 0.048 | 0.220 | 1200 | - | - | - |
| P3 | -0.116 | 0.056 | 1200 | - | - | - |
| P4 | -0.275 | -0.104 | 1200 | 24.8 | 5.871 | 7594 |
| P5 | -0.425 | -0.254 | 1200 | - | - | - |

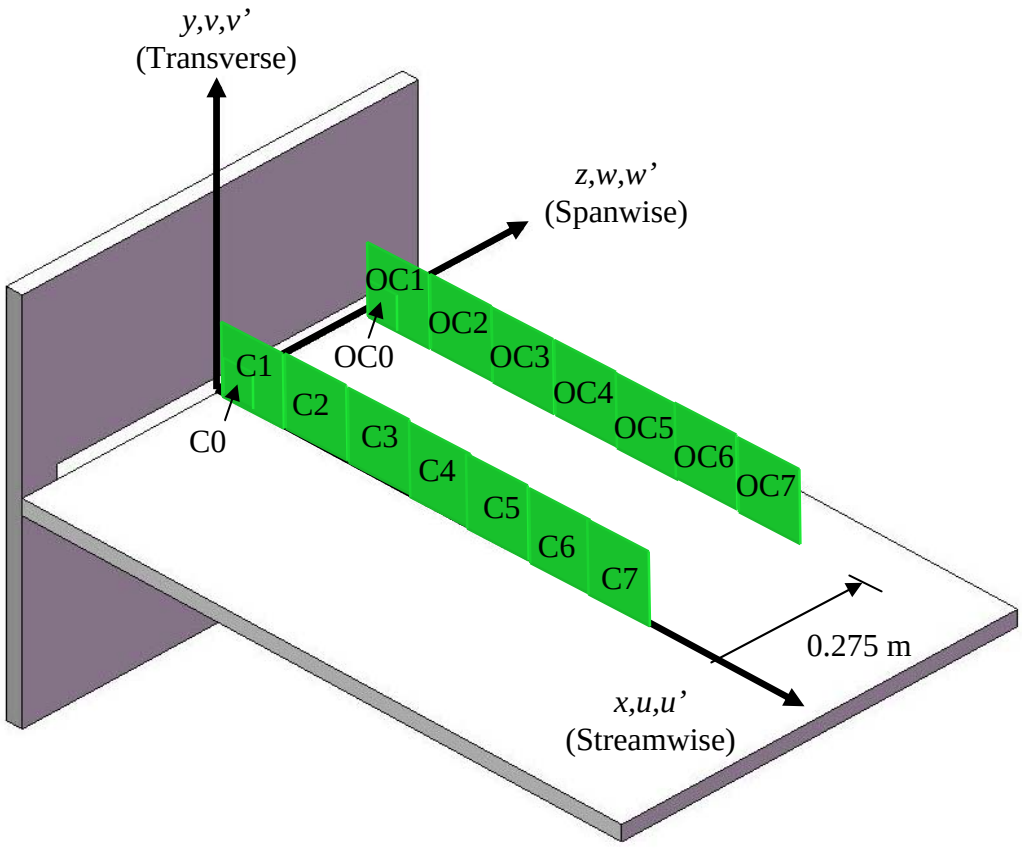


Figure 3.15: Location of each field of view for the main series of measurements.

Table 3.3 Outline of main series of measurements.

| Test Run | $(x/H)_{min}$ | $(x/H)_{max}$ | $\Delta t$ (μs) | Temperature (°C) | | |
|---|---|---|---|---|---|---|
| | | | | $T_1$ | $T_2$ | $T_{avg}$ |
| C0 | 0 | 4 | 80 | 21.8 | 21.9 | 21.9 |
| C1 | 0 | 15 | 250 | 20.8 | 21.0 | 20.9 |
| C2 | 15 | 32 | 300 | 21.0 | 21.2 | 21.1 |
| C3 | 32 | 49 | 350 | 21.2 | 21.4 | 21.3 |
| C4 | 49 | 65 | 450 | 21.4 | 21.6 | 21.5 |
| C5 | 66 | 82 | 550 | 21.6 | 21.8 | 21.7 |
| C6 | 82 | 98 | 625 | 21.8 | 22.0 | 21.9 |
| C7 | 99 | 115 | 625 | 22.1 | 22.2 | 22.2 |
| OC0 | 0 | 7 | 100 | - | - | 21.4 |
| OC1 | 0 | 17 | 250 | 21.4 | 21.6 | 21.5 |
| OC2 | 16 | 32 | 300 | 21.7 | 21.9 | 21.8 |
| OC3 | 31 | 46 | 350 | 22.0 | 22.1 | 22.1 |
| OC4 | 47 | 62 | 450 | 22.2 | 22.3 | 22.3 |
| OC5 | 61 | 77 | 550 | 22.3 | 22.5 | 22.4 |
| OC6 | 78 | 93 | 600 | 22.5 | 22.7 | 22.6 |
| OC7 | 93 | 108 | 625 | 22.6 | 22.8 | 22.7 |

| Test Run | Orifice Voltage (volts) | | | $Q$ (L/s) | $U$ (m/s) | $Re$ |
|---|---|---|---|---|---|---|
| | $V_1$ | $V_2$ | $V_{avg}$ | | | |
| C0 | 2.558 | 2.557 | 2.558 | 5.80 | 1.279 | 8093 |
| C1 | 2.564 | 2.563 | 2.564 | 5.81 | 1.281 | 8107 |
| C2 | 2.570 | 2.563 | 2.567 | 5.81 | 1.281 | 8107 |
| C3 | 2.561 | 2.560 | 2.561 | 5.80 | 1.279 | 8093 |
| C4 | 2.567 | 2.563 | 2.565 | 5.81 | 1.281 | 8107 |
| C5 | 2.576 | 2.568 | 2.572 | 5.82 | 1.283 | 8121 |
| C6 | 2.571 | 2.568 | 2.570 | 5.81 | 1.281 | 8107 |
| C7 | 2.572 | 2.569 | 2.571 | 5.82 | 1.283 | 8121 |
| OC0 | - | - | 2.547 | 5.79 | 1.276 | 8080 |
| OC1 | 2.564 | 2.561 | 2.563 | 5.81 | 1.281 | 8107 |
| OC2 | 2.567 | 2.564 | 2.566 | 5.81 | 1.281 | 8107 |
| OC3 | 2.568 | 2.568 | 2.568 | 5.81 | 1.281 | 8107 |
| OC4 | 2.573 | 2.571 | 2.572 | 5.82 | 1.283 | 8121 |
| OC5 | 2.575 | 2.572 | 2.574 | 5.82 | 1.283 | 8121 |
| OC6 | 2.579 | 2.573 | 2.576 | 5.82 | 1.283 | 8121 |
| OC7 | 2.574 | 2.572 | 2.573 | 5.82 | 1.283 | 8121 |

# Chapter 4

## Evaluation of Wall Jet Based on Flow Measurements

### 4.1 Introduction

The plane wall jet produced by this experimental apparatus is assessed in this chapter. Preliminary measurements of the streamwise velocity and turbulence along the width of the slot are presented first. The inlet boundary conditions for the wall jet are then documented by plotting streamwise mean velocity profiles and streamwise turbulence intensity profiles near the slot exit. The initial development of the jet is described by examining streamwise velocity profiles in the region from one to six slot heights from the exit, as well as by determining the length of the potential core. The fully developed region is identified by determining the region where the streamwise mean velocity and turbulence intensity profiles are self-similar. The growth and decay rates are then compared to established results. An initial assessment of the degree to which this experimental facility produces a two-dimensional flow is performed throughout the chapter using the method recommended by Gartshore & Hawaleshka (1964) of comparing spanwise measurements. This is accomplished by comparing various flow characteristics obtained along the centerline ($z$ = 0 m) to those obtained near the lateral edge of the horizontal glass wall ($z$ = 0.275 m). Hereafter, the measurements taken at $z$ = 0 m will be referred to as the centerline measurements, and the measurements taken at $z$ = 0.275 m will be referred to as the off-centerline measurements. The effect that return flow has on the development and two-dimensionality of the wall jet is also examined.

## 4.2 Initial Conditions

### 4.2.1 Streamwise Velocity and Turbulence Along the Slot Width

Measurements of the streamwise mean velocity and turbulence were initially performed without the glass wall in place in order to determine the uniformity of the flow in the spanwise direction (see figure 4.1). The laser sheet was aligned horizontally with the middle of the slot, which had a height of 0.009 m, and data was obtained along the entire slot width. The measurements from $z$ = -0.275 m to 0.327 m show a very uniform streamwise velocity. The small amount of scatter in this region is due to the lower quality PIV measurements that are obtained near the edges of the fields of view. The average streamwise velocity in this spanwise region is 0.894 m/s. The maximum deviation of the streamwise velocity (when ignoring the three data points near $z$ = 0.2 m that are below 0.8 m/s) is 3.2%, which is within the experimental uncertainty limits of the PIV measurements. The average streamwise turbulence is 2.5% of the average streamwise velocity. The measurements along this portion of the slot suggest that the flow conditioner is initially producing a two-dimensional flow in the spanwise region from $z$ = -0.275 m to 0.327 m.

The increased values for the streamwise velocity in the spanwise region from $z$ = -0.358 m to -0.254 m suggest that the flow is not two-dimensional across the entire slot width. However, it is important to note that this region of elevated $u$ corresponds to one field of view (i.e. one set of PIV measurements). Within this field of view, $u$ is still very uniform. This discrepancy is believed to be a result of an error in recording the flow rate or $\Delta t$ rather than a physical feature of the flow produced by the flow conditioner.

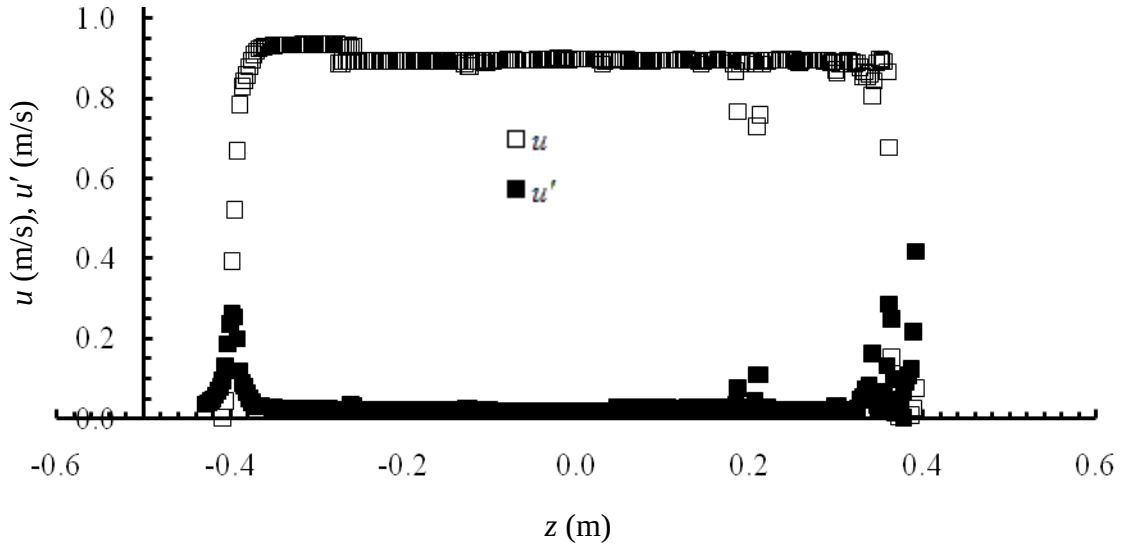


Figure 4.1: Streamwise mean velocity and turbulence at $x = H$ along the slot width.

4.2.2 Slot Exit Velocity Profiles

George et al. (2000) determined that the conditions at the slot exit affect the development of a wall jet. The streamwise mean velocity profile and streamwise turbulence intensity at the jet exit was documented to enable more meaningful comparisons to other experiments and to provide computational studies with accurate boundary conditions. Measuring the streamwise mean velocity profile at the slot exit also allows the initial jet momentum to be calculated, which is required when performing a momentum balance and also for certain types of scaling.

Figure 4.2 shows the streamwise mean velocity profiles for the centerline measurements at five locations at or near the slot exit ($x/H$ = 0, 1/6, 1/3, 1/2 and 2/3). At $x/H$ = 0 and $x/H$ = 1/6 the streamwise velocity profile is not uniform. At $x/H$ = 2/3 the velocity profile has a maximum velocity deviation of 0.3% over 71% of the slot height

(see figure 4.3). This deviation is less than the experimental uncertainty of 3.6%, confirming that a uniform streamwise velocity profile has been produced. The streamwise turbulence within the flat part of the jet is 1.45% of the mean streamwise velocity. The peak values for the streamwise turbulence occur at locations of maximum shear due to interactions with both the stagnant fluid and the wall. The shape of the profiles verifies that the experimental apparatus is satisfactorily conditioning the flow by producing a uniform streamwise velocity profile with a low turbulence level, although it is important to note that this does not occur exactly at the slot exit.

These results compare well with Eriksson et al. (1998), who obtained uniform streamwise velocity profiles with a turbulence intensity of less than one percent in the flat part of the profile, and Schneider & Goldstein (1994) who obtained a uniform profile with a turbulence intensity of 0.3%. Some previous experiments did not produce a top-hat profile, such as Tachie (2000) who obtained a flat profile over only 30-40% of the slot height with a turbulence intensity that varied from 3-5%.

The maximum velocity at $x/H = 2/3$ is 1.42 m/s, which differs from the value of 1.28 m/s that was measured by the flow meter. This discrepancy is due to not accounting for the lower velocities in the wall shear and free shear regions. The average velocity across the height of the slot based on the profile shown in figure 4.3 is equal to 1.29 m/s, which agrees well with the value measured by the flowmeter.

Figure 4.4 shows the transverse mean velocity and turbulence profiles at $x/H = 2/3$ for the centerline and off-centerline measurements. In both profiles the mean velocity is close to zero; however the positive velocity near the wall indicates that the wall jet has

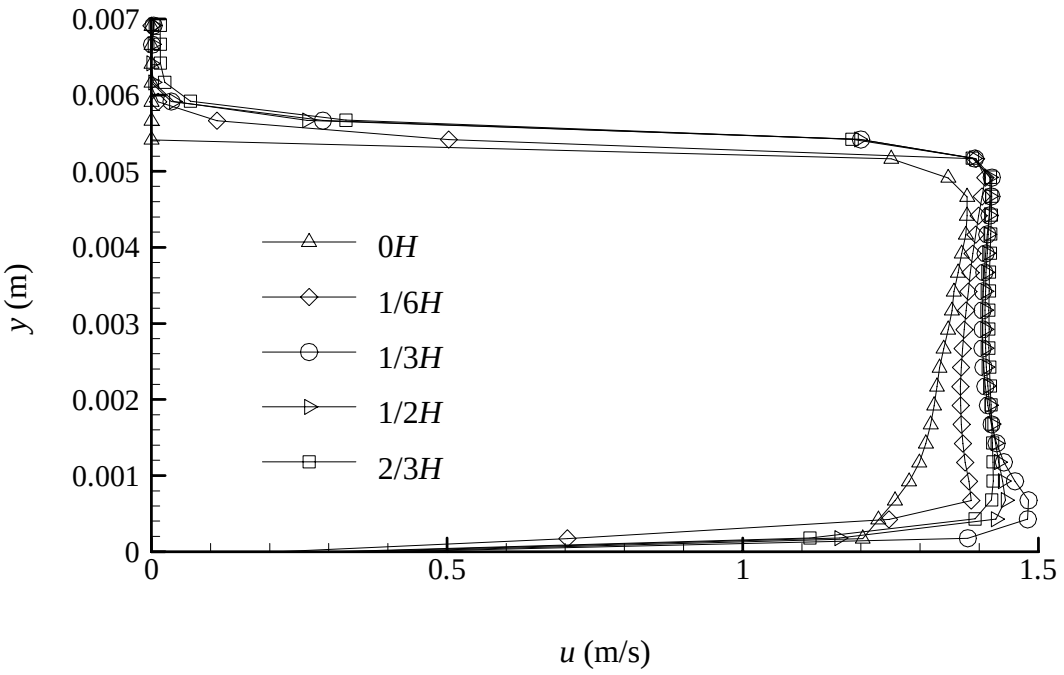


Figure 4.2: Streamwise mean velocity profile development along the centerline for $0 \leq x/H \leq 2/3$.

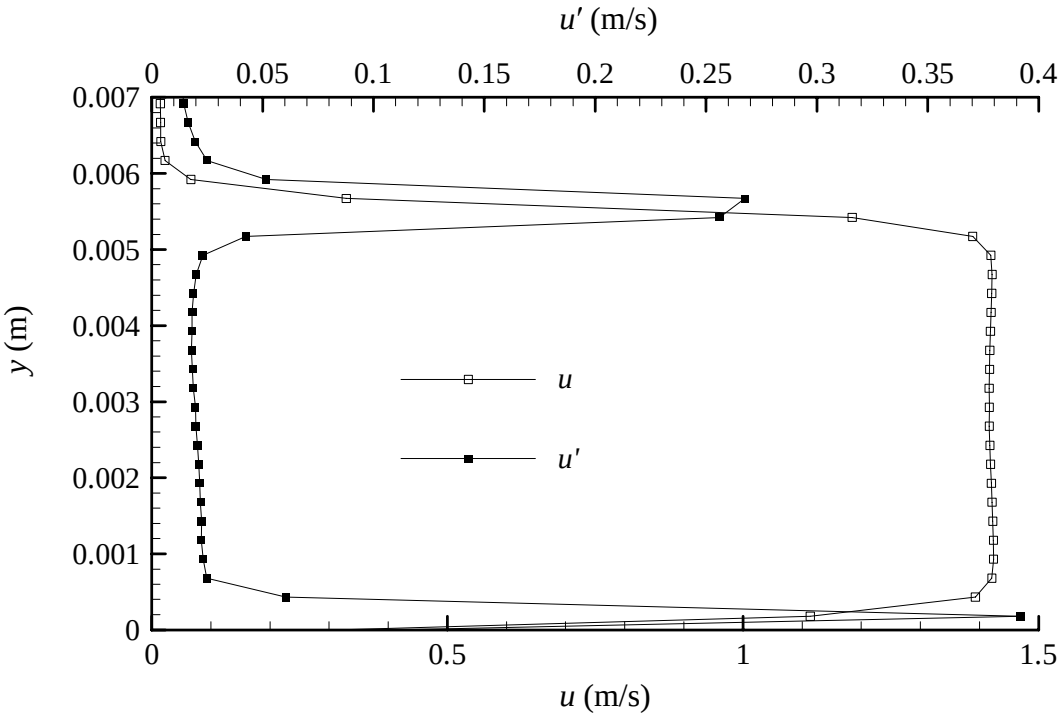


Figure 4.3: Streamwise mean velocity profile and streamwise turbulence intensity at $x/H = 2/3$ and $z = 0$ m.

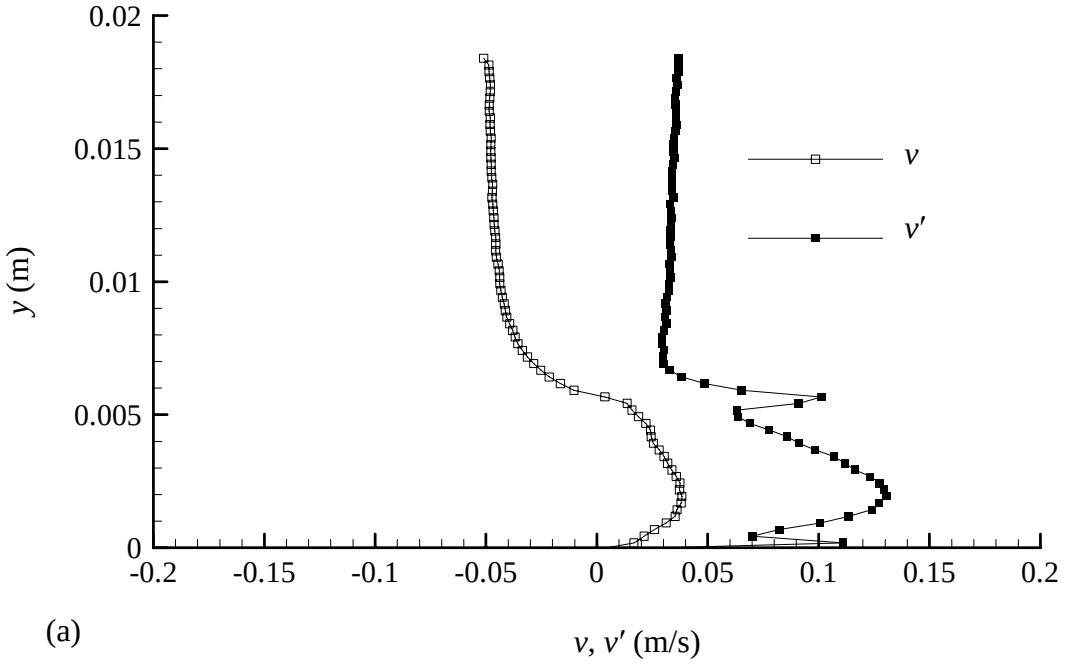


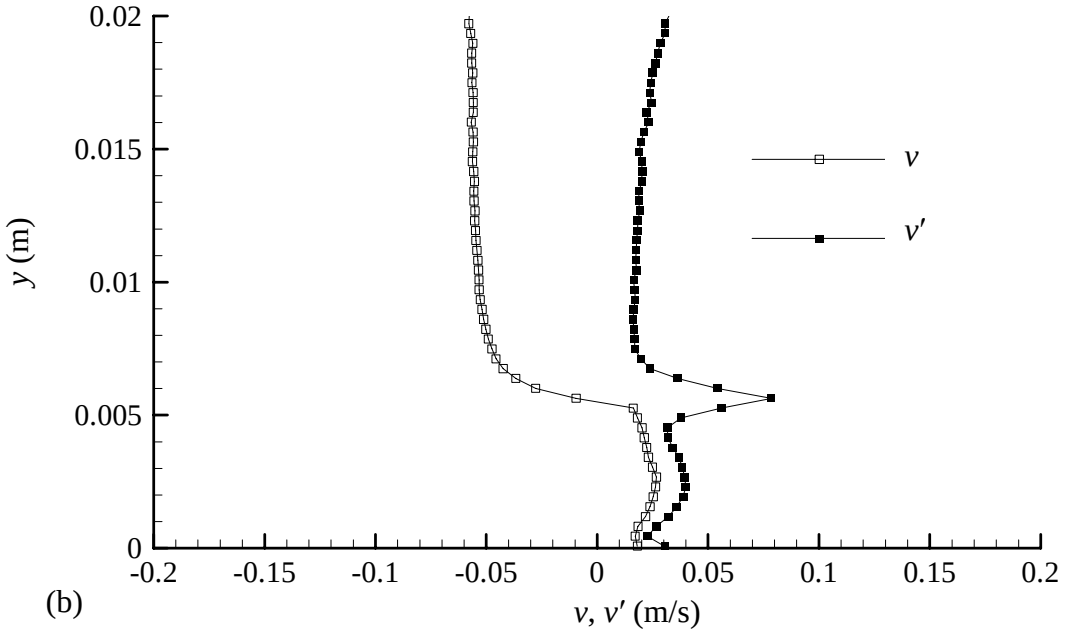


Figure 4.4: Transverse mean velocity and turbulence profiles for *x/H* = 2/3 at (a) *z* = 0 m, and (b) *z* = 0.275 m.

begun to spread and the negative velocity in the outer region indicates entrainment of fluid. The transverse turbulence levels are larger than the streamwise turbulence level along the centerline. The maximum transverse turbulence occurs where the positive mean velocity is maximum for $z = 0$ m and occurs where the mean velocity is zero for $z = 0.275$ m.

#### 4.2.3 Comparison of Streamwise Mean Velocity Profiles Near the Slot Exit

Figure 4.5 compares the streamwise mean velocity profiles obtained at $x/H = 5/6$ for the centerline and off-centerline locations. The similar shape of the profiles and the maximum velocity difference of less than 1% show that the experimental apparatus is initially creating a flow that is similar at the centerline and 0.275 m off of the centerline.

### 4.3 Initial Development Region

#### 4.3.1 Velocity Profiles For $1 \leq x/H \leq 6$

The initial development region of the plane wall jet is located where the jet undergoes transition from having a uniform streamwise velocity profile with a low turbulence intensity to being self-similar and turbulent downstream of the slot. Figure 4.6 shows streamwise velocity profiles at streamwise distances of $1 \leq x/H \leq 6$. At one slot height the profile has a flat shape. As the streamwise distance increases the velocity gradients in the shear layers decrease due to the interaction with both the wall and the stagnant fluid. The shear force at the wall causes the inner layer of the jet to take on the shape of a boundary layer. As this boundary layer grows, the velocity in the inner core of the jet decreases. The shear force present at the interface between the jet and the stagnant

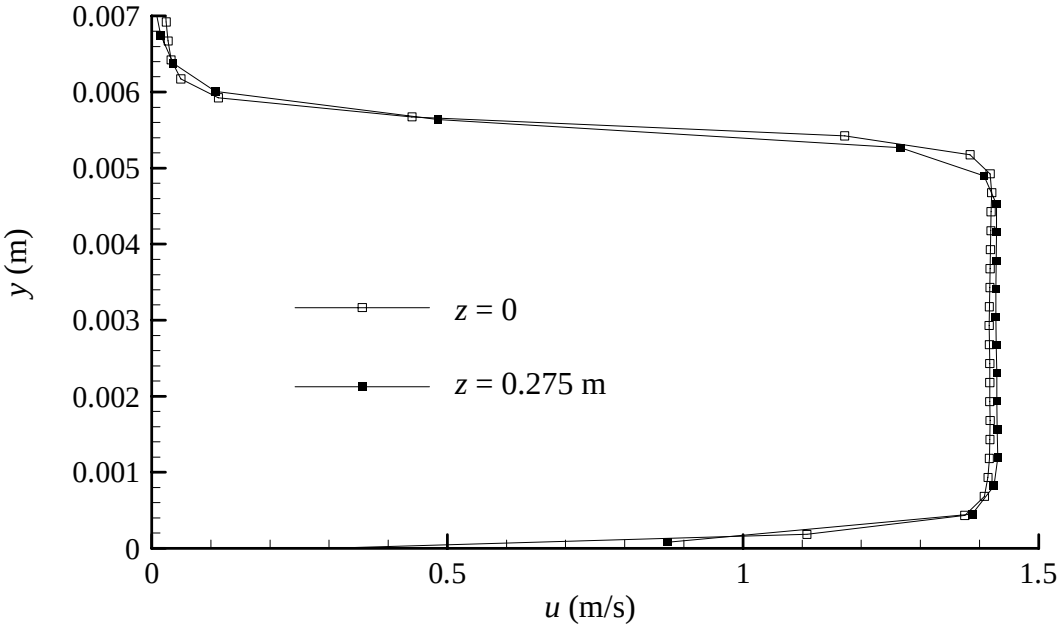


Figure 4.5: Two-dimensional comparison of streamwise mean velocity profiles at $x/H = 5/6$.

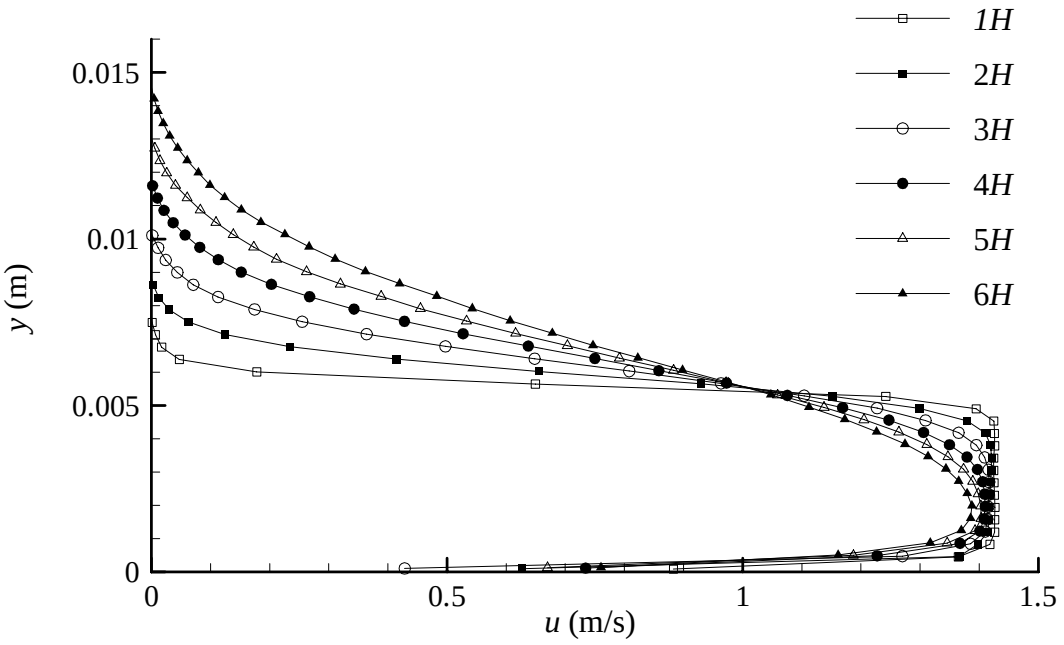


Figure 4.6: Initial development of streamwise mean velocity profiles for $1 \leq x/H \leq 6$ at $z = 0.275$ m.

fluid causes entrainment of additional fluid into the jet as it flows downstream. This causes the jet to grow in size, and the momentum that has been transferred to the entrained fluid causes a decrease in the maximum velocity of the jet.

### 4.3.2 Comparison of Streamwise Mean Velocity Profiles at $x/H = 4$

Figure 4.7 compares streamwise mean velocity profiles for the centerline and off-centerline measurements at a streamwise distance of $x = 4H$. This figure shows that the experimental apparatus has produced a flow that is similar at both spanwise locations. Both profiles have a similar shape and the difference between the maximum velocities is less than 1%, which is within experimental uncertainty limits. This figure also shows that return flow has not yet begun to affect the development of the wall jet since the velocities approach zero even at relatively large distances away from the wall.

### 4.3.3 Potential Core

The potential core is characterized by the preservation of the initial maximum streamwise velocity. When the maximum streamwise velocity has become less than the initial maximum streamwise velocity the potential core has been consumed (Rajaratnam, 1976). As seen in figure 4.8, the initial maximum velocity of the jet was 1.43 m/s. The jet adequately maintains this velocity until $x/H = 6$. There is a noticeable drop in the maximum velocity at $x/H = 7$. This suggests that the length of the potential core is $6H$. The next section will look at self-similarity to verify the region of fully developed flow.

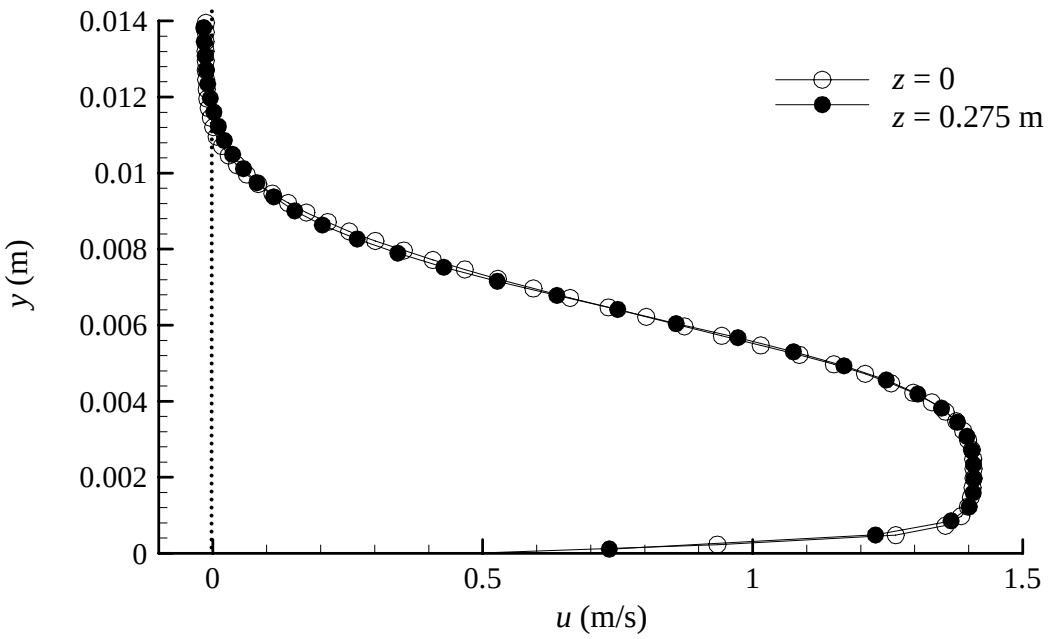


Figure 4.7: Spanwise comparison of streamwise mean velocity profiles at 4*H*.

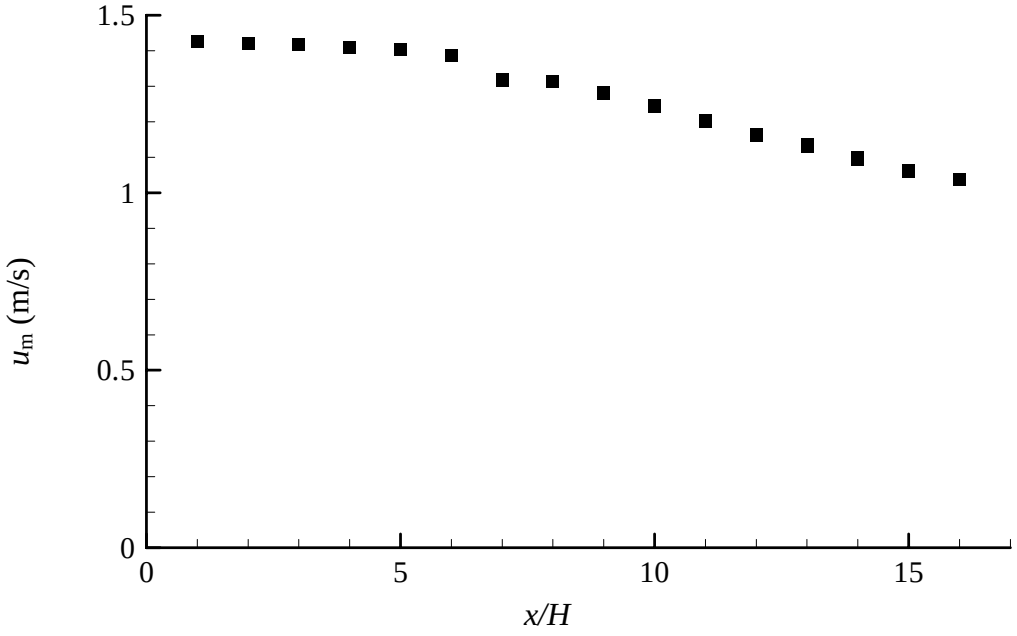


Figure 4.8: Decay of the maximum velocity for $1 \leq x/H \leq 16$ at $z = 0.275$ m.

## 4.4 Fully Developed Region

### 4.4.1 Development of Wall Jet Velocity Profiles For $1 \leq x/H \leq 100$

Figure 4.9 shows streamwise mean velocity profiles at $x/H$ from 1 to 100 for both the centerline and off-centerline measurements. The transition from a uniform velocity profile to a fully developed wall jet is evident. The flatness of the velocity profile at $x/H = 1$ has been lost at $x/H = 5$. At $x/H = 10$ the wall jet has further interacted with both the stagnant fluid and the wall, causing the wall jet to expand, the boundary layer to increase in size, and the maximum velocity to decrease. This trend continues as the wall jet flows downstream, and eventually a fully developed turbulent wall jet is reached. The region of fully developed flow will be further explored in the next section by scaling the velocity and turbulence profiles using the outer scales $y_{1/2}$ and $u_m$, and then qualitatively describing the region of self-similarity.

### 4.4.2 Normalized Streamwise Mean Velocity Profiles For $10 \leq x/H \leq 100$

Researchers such as Eriksson et al. (1998) define fully developed flow as the region of self-similarity, which is the criterion that this study will use. Figures 4.10 and 4.11 show the streamwise mean velocity profiles at $x/H = 10$ - 100 in dimensionless form for the centerline and off-centerline measurements, respectively. These profiles have been scaled using the outer coordinates based on $y_{1/2}$ and $u_m$.

Figure 4.10(a) shows that the profile at $x/H = 10$ does not collapse onto the other profiles, which indicates that the wall jet is still developing at this location. This lack of

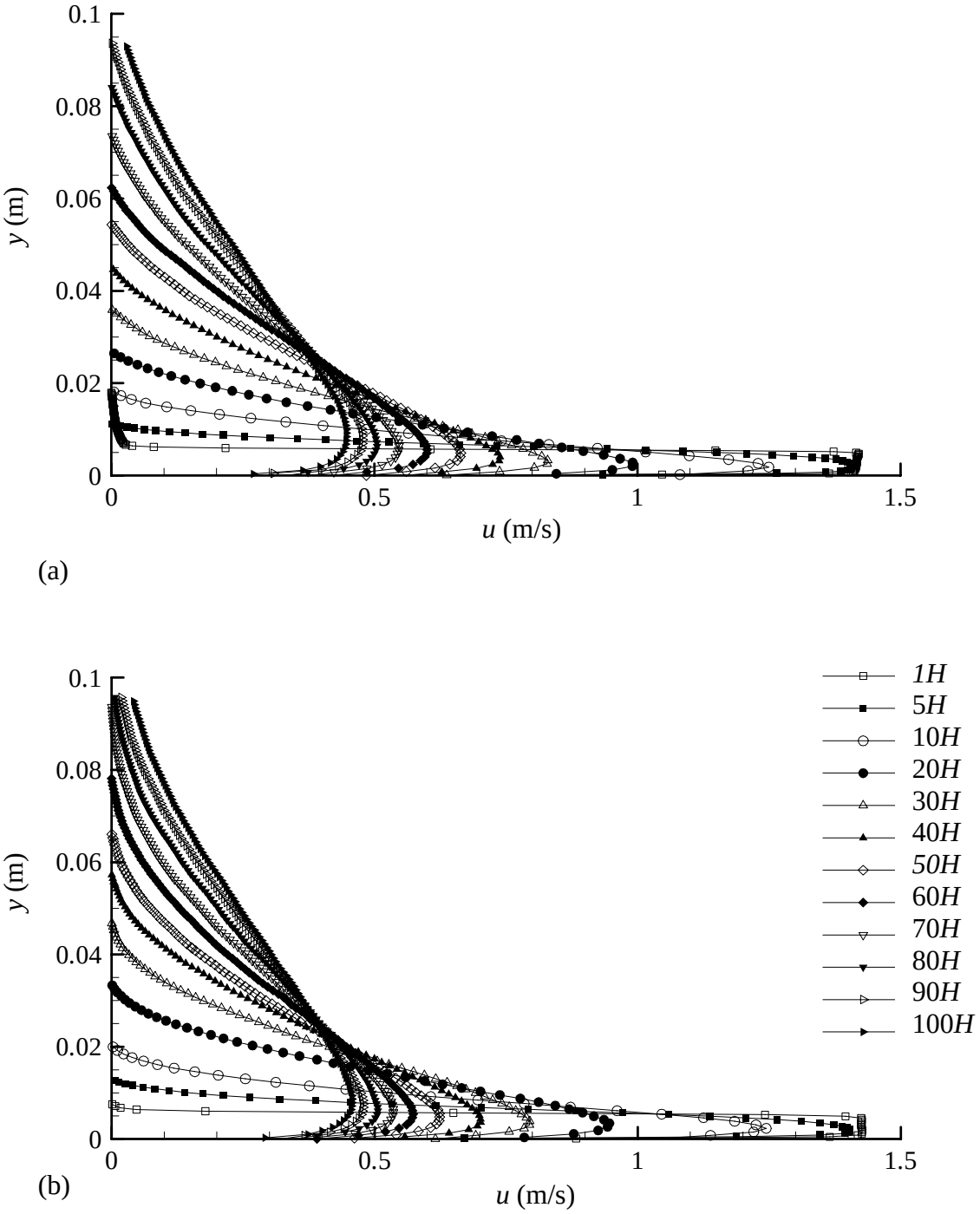


Figure 4.9: Wall jet development of streamwise mean velocity profiles for $1 \leq x/H \leq 100$ at (a) $z = 0$ m, and (b) $z = 0.275$ m.

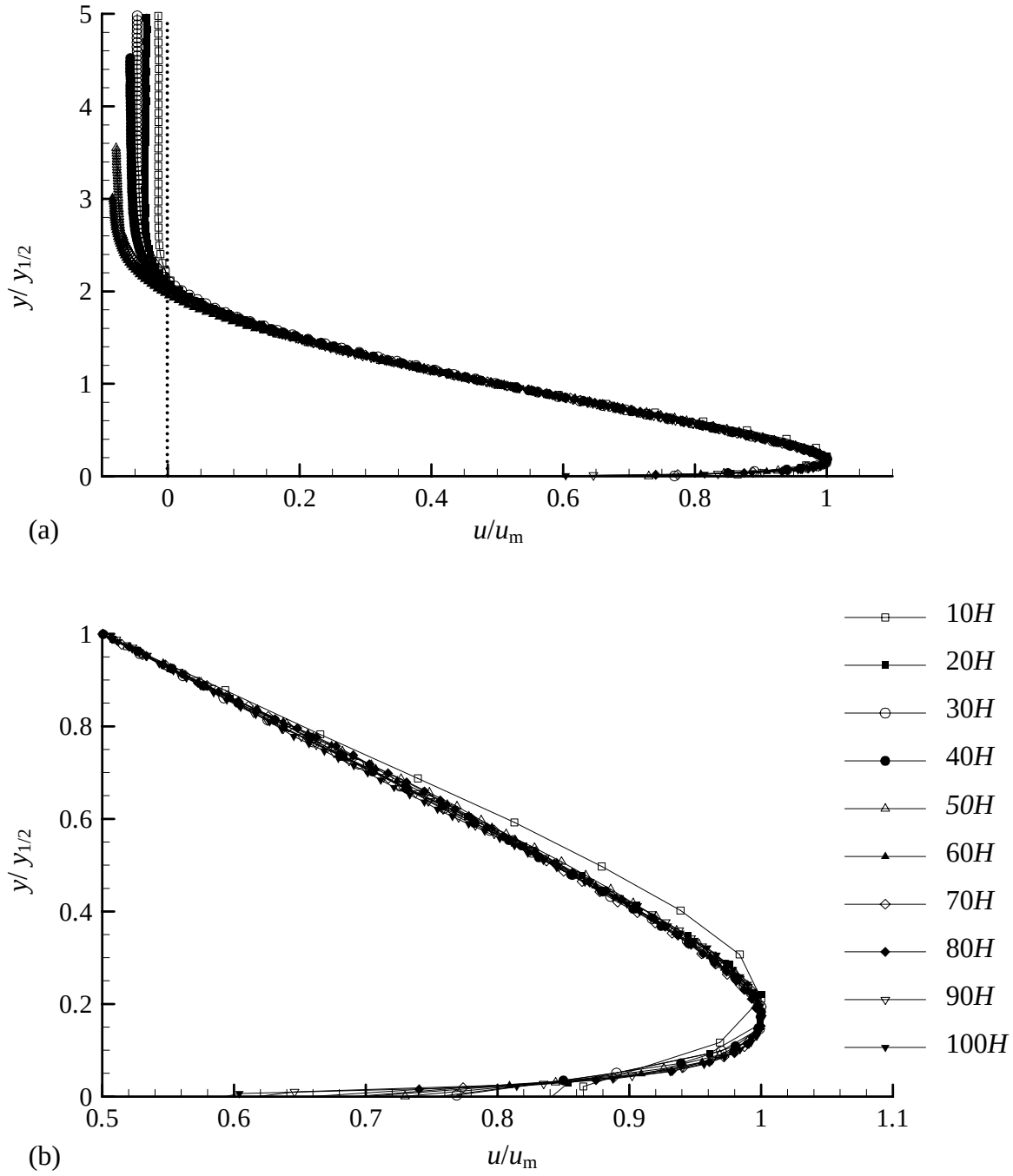


Figure 4.10: Non-dimensionalized streamwise mean velocity profiles for $10 \leq x/H \leq 100$ at $z = 0$ m (a) complete profiles, (b) enlarged view of maximum velocity region.

collapse can clearly be seen in figure 4.10(b), where the profiles in the range $0 \leq y/y_{1/2} \leq 1$ have been enlarged. In this region of the wall jet along the centerline, self-similarity is achieved from $x/H$ = 20 to 100. However, the profiles in the outer region do not achieve the same level of collapse. The effect of a return flow for $y/y_{1/2} > 2.0$ can be seen in figure 4.10(a). The velocity profiles should ideally approach zero as the distance from the wall increases. However, the return flow has caused the wall jet to have a negative velocity in this outer region. The profiles eventually attain self-similarity (from $x/H$ = 50 to 100) in this outer region of the wall jet, but they have a value less than zero.

For the off-centerline measurements, figure 4.11(a) shows that the profile at $x/H$ = 10 does not collapse. The off-centerline wall jet does not appear to be significantly affected by a return flow since all of the profiles approach a value of approximately zero in the outer region of the wall jet. Figure 4.11(b) shows an enlarged view of the profiles in the transverse range of $0 \leq y/y_{1/2} \leq 1$. The mean velocity takes longer to develop a self-similar profile in this transverse range when compared to the centerline measurements. The profiles along the off-centerline collapse well from 40*H* to 100*H*, suggesting that the flow is fully developed in this region.

### 4.4.3 Comparison of Streamwise Mean Velocity Profiles in the Fully Developed Region

The previous section showed that the self-similar regions for the centerline and off-centerline measurements were $x/H$ = 50 to 100 and $x/H$ = 40 to 100, respectively. Figure 4.12 compares the centerline and off-centerline measurements at streamwise locations of 50*H*, 80*H*, and 100*H*. The profiles have a relatively similiar shape when

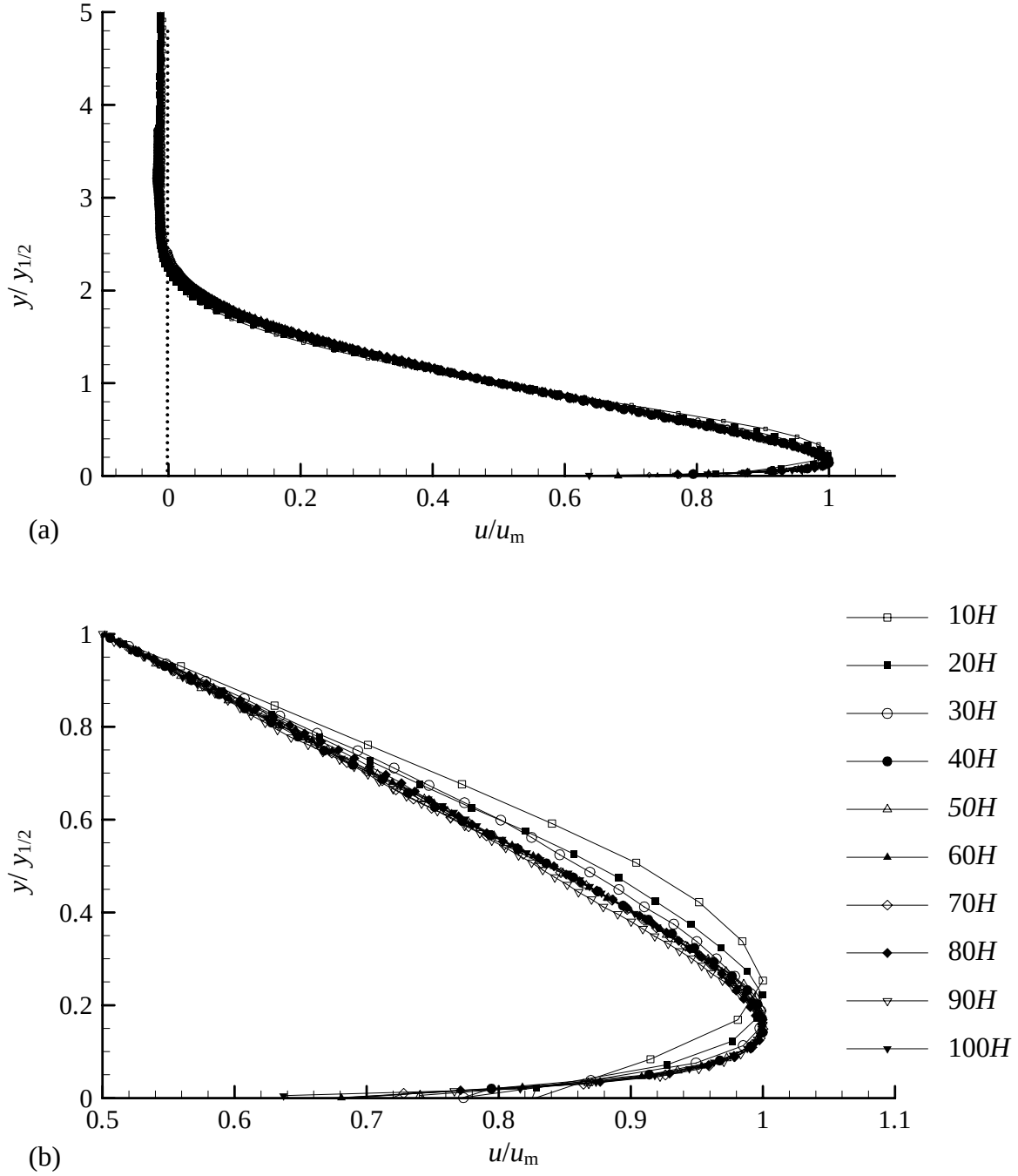


Figure 4.11: Non-dimensionalized streamwise mean velocity profiles for $10 \leq x/H \leq 100$ at $z = 0.275$ m (a) complete profiles, (b) enlarged view of maximum velocity region.

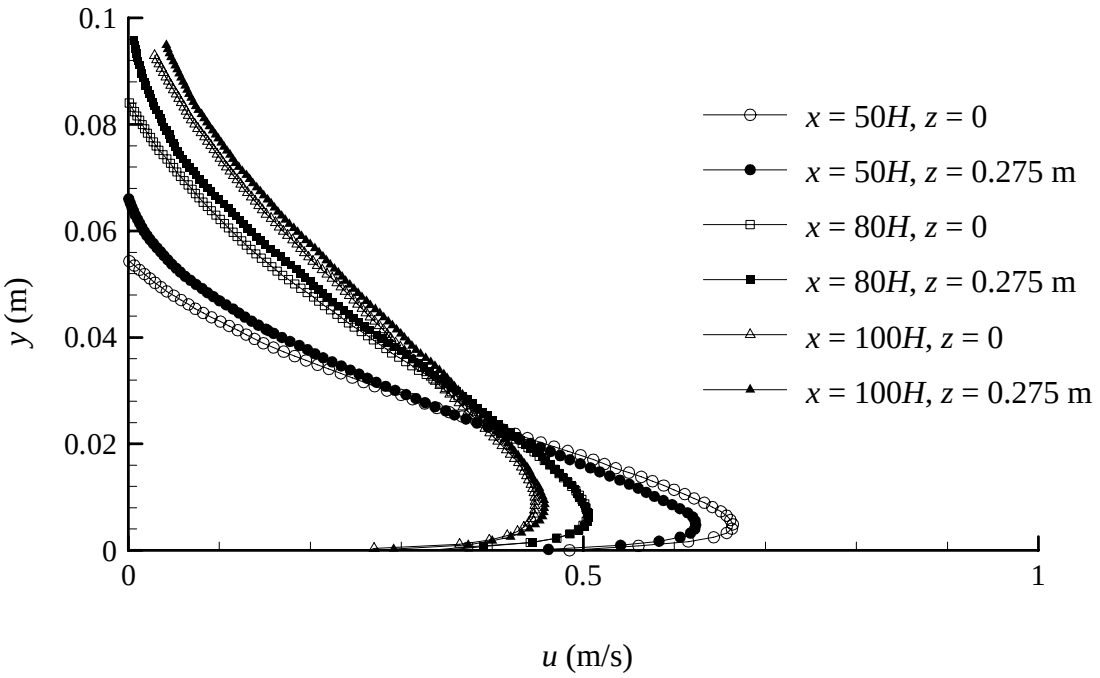


Figure 4.12: Comparison of streamwise mean velocity profiles at 50*H*, 80*H*, and 100*H*.

compared at the same streamwise location, however the effect of a return flow on the centerline measurements can be seen. This is shown by the reduced velocity in the outer region of the wall jet along the centerline. While the velocity of the centerline wall jet is reduced in the outer region, its maximum velocity is larger than the off-centerline wall jet at 50H. Whether or not this is a consequence of return flow is unknown. The maximum velocities differ by 6%, 2%, and 2% at $x/H$ = 50, 80, and 100, respectively.

### 4.4.4 Transverse Velocity Profiles in the Fully Developed Region

Figure 4.13 shows the transverse velocity profile at $x = 50H$ for the centerline and off-centerline measurements. A profile obtained using the continuity equation is also plotted as a comparison. The continuity equation profile was obtained by subtracting the integral of the streamwise velocity profile at 51*H* from the integral of the streamwise

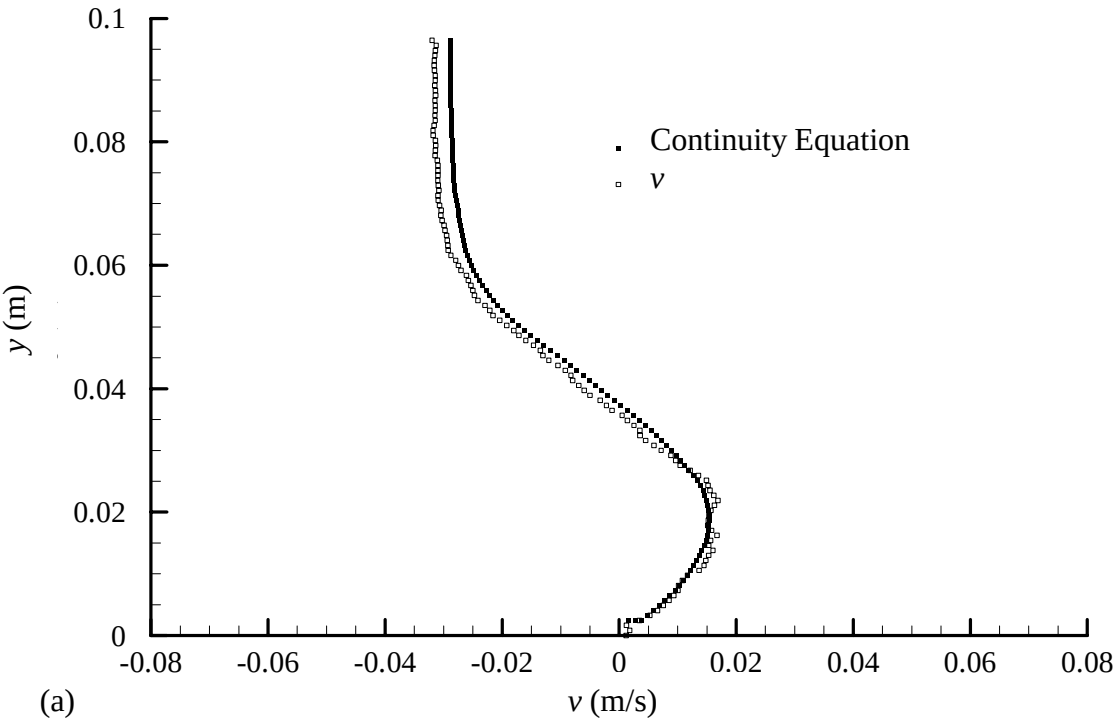


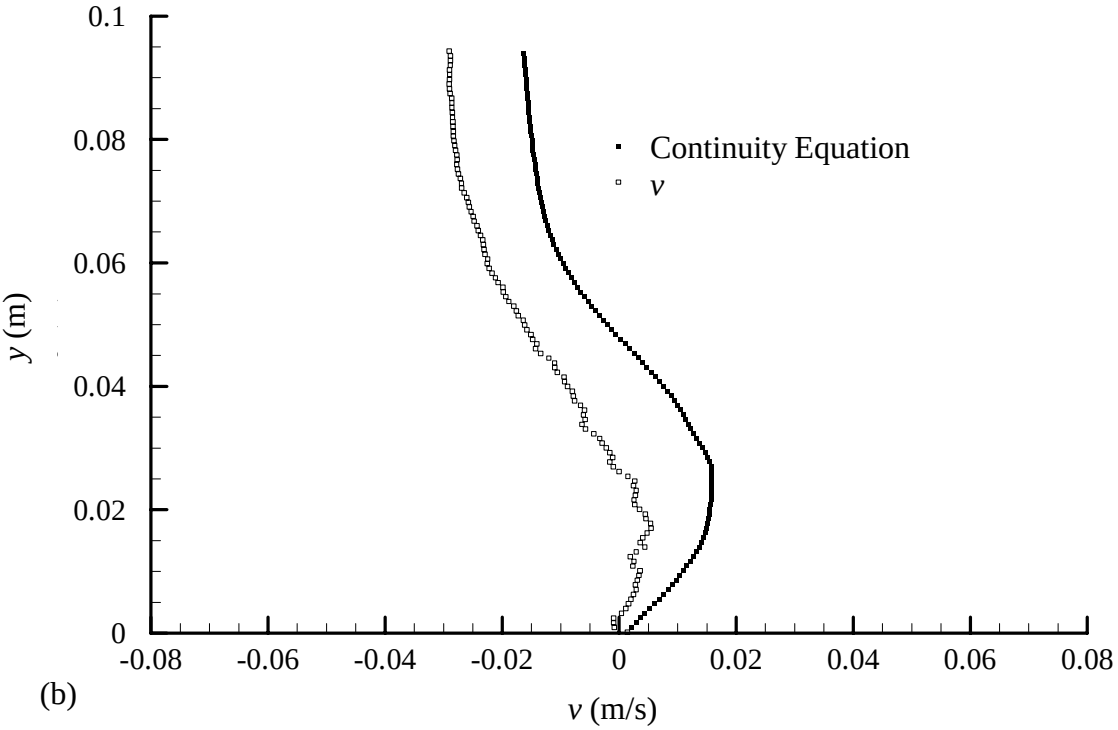


Figure 4.13: Comparison of transverse velocity profiles to continuity equation profiles for (a) centerline measurements and (b) off-centerline measurements.

velocity profile at 49*H*. The close agreement between both profiles for the centerline measurements indicates that the spanwise velocity gradient, $\partial w/\partial z$, is close to zero. Conversely, the lack of agreement between the off-centerline profiles indicates that the spanwise velocity gradient is not zero at that location. This result indicates that spanwise spreading of the wall jet is occurring at $x = 50H$ for the off-centerline measurements.

## 4.5 Growth Rate of the Wall Jet

### 4.5.1 Growth Rate

As the fluid flows downstream from the slot, the surrounding stagnant fluid becomes entrained in the outer portion of the wall jet, causing it to slow down and also increase in transverse extent. The extent of the wall jet is normally quantified by the value of the jet half width. It has been reported by multiple previous experiments, making it an excellent characteristic for comparison.

Figure 4.14 plots the normalized jet half-width, $y_{1/2}/H$, as a function of the normalized streamwise position, $x/H$, for the centerline and off-centerline meaurements, respectively. The growth for the centerline data appears to be linear from $x/H = 10$ to 100, whereas the growth for the off-centerline data only appears to be linear from $x/H = 50$ to 100. The growth rate, $A$, and normalized virtual origin, $x_0/H$, were found using equation (2.1), i.e. $\frac{y_{1/2}}{H} = A\left(\frac{x}{H} + \frac{x_0}{H}\right)$, by performing linear regressions over multiple ranges of $x/H$. The growth rate for each range of values can be seen in Table 4.1.

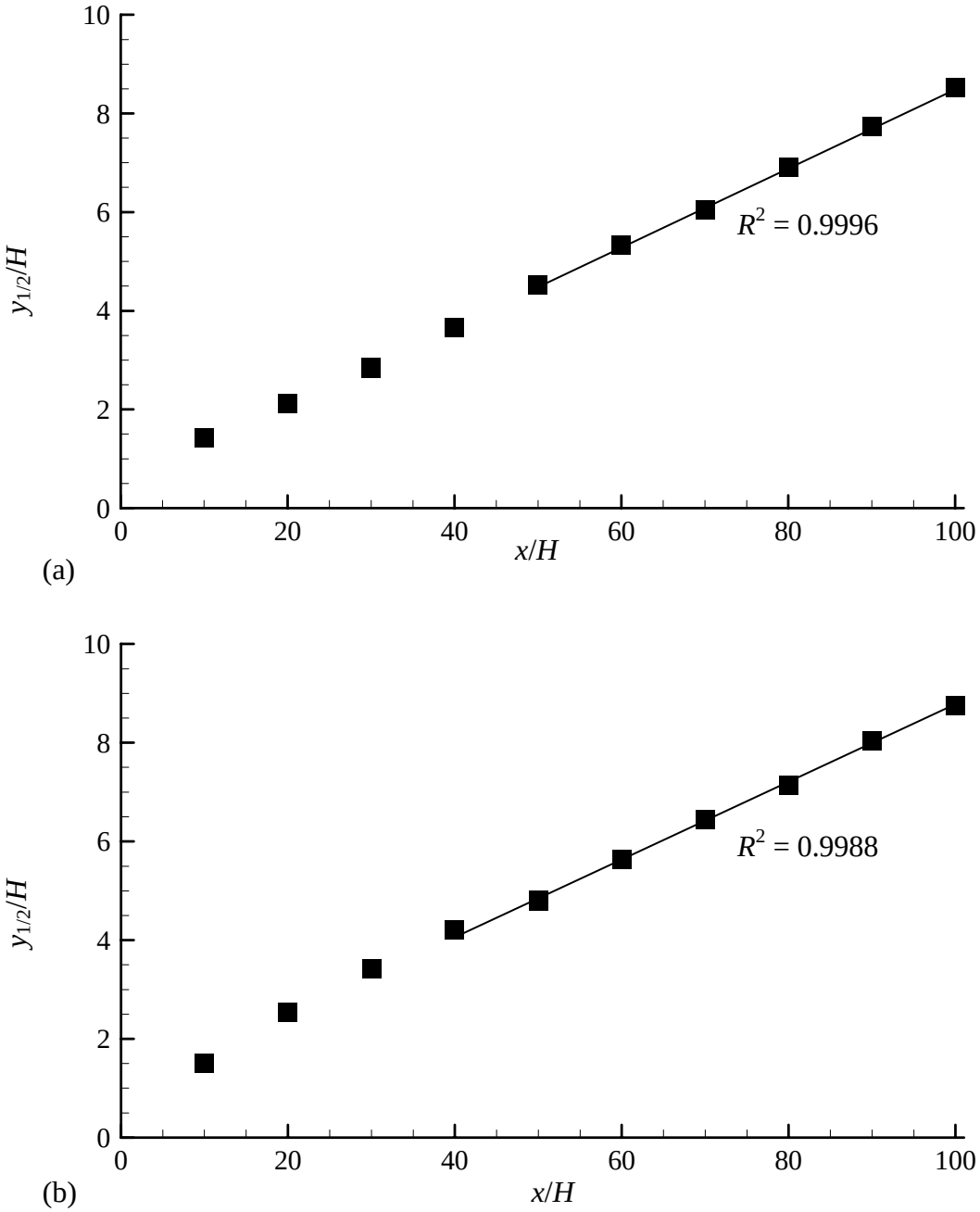


Figure 4.14: Growth of jet half-width from 10-100$H$ along (a) $z$ = 0 m, (b) $z$ = 0.275 m.

Table 4.1: Jet half-width growth rates and virtual origin values for several ranges of $x/H$.

| Region ($x/H$) | $z$ = 0 m | | $z$ = 0.275 m | |
|---|---|---|---|---|
| | $dy_{1/2}/dx$ | $x_0/H$ | $dy_{1/2}/dx$ | $x_0/H$ |
| 10-100 | 0.080 | -6.6 | 0.079 | -11.7 |
| 20-100 | 0.081 | -5.8 | 0.077 | -13.5 |
| 30-100 | 0.081 | -5.3 | 0.077 | -14.0 |
| 40-100 | 0.081 | -5.6 | 0.077 | -13.3 |
| 50-100 | 0.080 | -6.3 | 0.079 | -11.0 |

The self-similar region of the centerline plane ($x/H$ = 50 to 100) had a growth rate of 0.080 and a normalized virtual origin of -6.3$H$. The squared value of the correlation coefficient, $R^2$, was 0.9996. The off-centerline self-similar region ($x/H$ = 40 to 100) had a growth rate of 0.077 and normalized virtual origin of -13.3$H$, with an $R^2$ value of 0.9988. The virtual origin obtained by Schneider & Goldstein (1994) was -8.7$H$, which is between the values obtained by this study. The growth rates along the centerline and off-centerline fall outside the range of values of $0.073 \pm 0.002$ proposed by Launder & Rodi (1981); however they compare well with the more recent results of Eriksson et al. (1998), who obtained a growth rate of 0.078. Another recent result is that of Tachie (2000), who obtained growth rate values from 0.85 to 0.090. He partly attributed his higher values to a return flow that was present. The larger growth rate along the centerline of this study is also possibly due to return flow.

The discrepancies between the different growth rate values could be attributed to different conditions such as the slot exit profile, Reynolds number, the degree to which a return flow is present, or lateral spreading. When comparing to Eriksson et al. (1998), this experiment had a similar Reynolds number and similar exit profiles, which could explain

why the growth rates were within 2.5% of each other. These results support that similar exit conditions correspond to similar growth rates.

### 4.5.2 Spanwise Comparison of Growth Rates

The difference between the centerline and off-centerline growth rates was between 1% and 5%, depending on the range of streamwise values that were used. An additional growth rate at a third spanwise location needs to be obtained before the two-dimensionality of the flow can be confirmed.

## 4.6 Decay Rate of the Maximum Streamwise Velocity

### 4.6.1 Decay Rate

As the wall jet grows it transfers momentum to the entrained fluid, causing the maximum velocity of the wall jet to decrease. This decay of the wall jet's maximum velocity is another characteristic that can be compared to previous experimental results. Figure 4.15 shows the decay of the maximum streamwise mean velocity as a function of the streamwise distance. From this figure it is evident that the rate of decay of the maximum streamwise velocity is not linear.

Figure 4.16 shows the maximum velocity as a function of the jet half-width in logarithmic form at $x/H$ distances from 10 to 100. The logarithmic decay rate of the wall jet appears to be linear in the region from $x/H$ = 50 to 100 for both sets of measurements. Table 4.2 provides the decay rate, $n$, for multiple ranges of values that were obtained by applying a linear regression in the form of equation (1.8) to figures 4.16(a) and 4.16(b).

The decay rate varies considerably depending on the range of streamwise values that are used. A decay rate of -0.624 was obtained along the centerline in the self-similar region from $x/H$ = 50 to 100. The off-centerline had a linear decay rate of -0.562 in the self-similar region from $x/H$ = 40 to 100. The squared value for the correlation coefficient, $R^2$, was 0.9979 and 0.9876 for the centerline and off-centerline decay rates, respectively. The off-centerline results compare well with the results of Eriksson et al. (1998) who measured a decay rate of -0.573 in the region from $x/H$ = 40 to 150. Schneider & Goldstein (1994) obtained a decay rate of -0.608.

As was the case with the wall jet growth rate, the discrepancies between the different decay rate values could be attributed to different conditions such as the Reynolds number, initial conditions, the degree to which a return flow is present, or

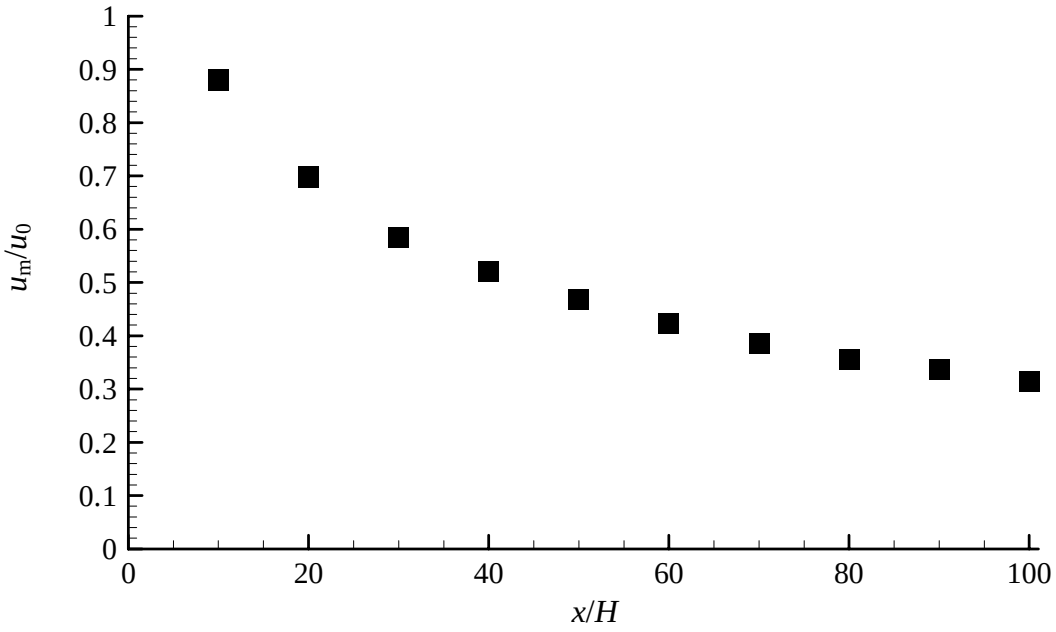


Figure 4.15: Decay of the maximum streamwise velocity from 10-100$H$ along $z$ = 0 m.

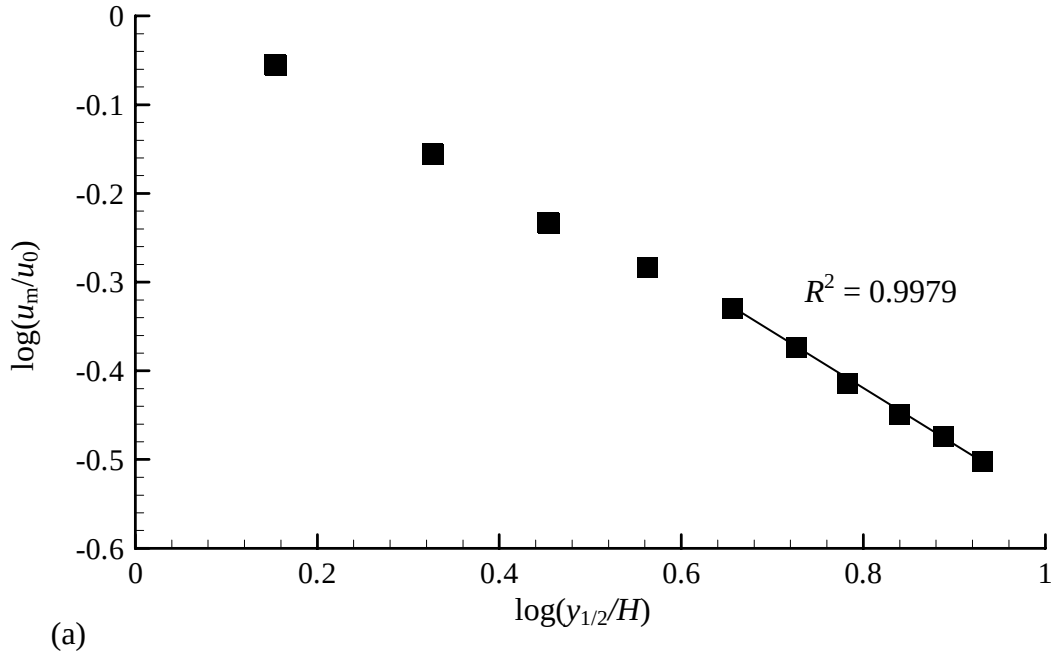


(a)

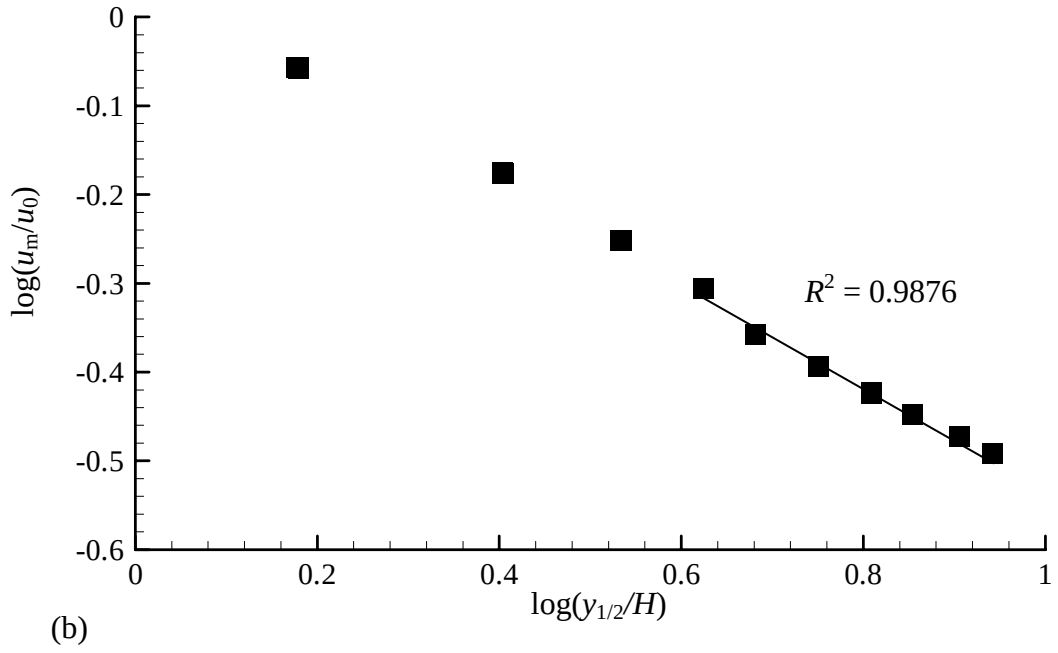


(b)

Figure 4.16: Decay of maximum streamwise velocity from 10-100$H$ along (a) $z$ = 0 m, (b) $z$ = 0.275 m.

Table 4.2: Decay rates, $n$, of the maximum streamwise mean velocity, $u_m$, for multiple streamwise regions.

| Region ($x/H$) | Decay rate, $n$ | | % difference |
|---|---|---|---|
| | $z$ = 0 m | $z$ = 0.275 m | |
| 10-100 | -0.569 | -0.584 | 3 |
| 20-100 | -0.569 | -0.595 | 4 |
| 30-100 | -0.574 | -0.586 | 2 |
| 40-100 | -0.602 | -0.562 | 7 |
| 50-100 | -0.624 | -0.515 | 17 |

lateral spreading. The spread in decay rate values obtained when using different streamwise ranges showcases the importance of including a full description of how the decay rate was obtained.

### 4.6.2 Spanwise Comparison of Decay Rates

The difference between the decay rates for the centerline and off-centerline measurements varied from 2% to 17%. This is possibly due to the effect of return flow on the development of the centerline wall jet. Comparison of the decay rates does not support the two-dimensionality of the wall jet being maintained downstream of the slot.

## 4.7 Normalized Turbulence Intensity Profiles For $10 \leq x/H \leq 100$

The turbulence intensity at $x/H$ = 10 - 100 is presented in figures 4.17 and 4.18 for the centerline and off-centerline measurements, respectively. These profiles are scaled using the outer coordinates of $y_{1/2}$ and $u_m$.

The centerline turbulence intensity profiles do not collapse, possibly due to the greater influence that the return flow appears to have along the centerline. The profiles at

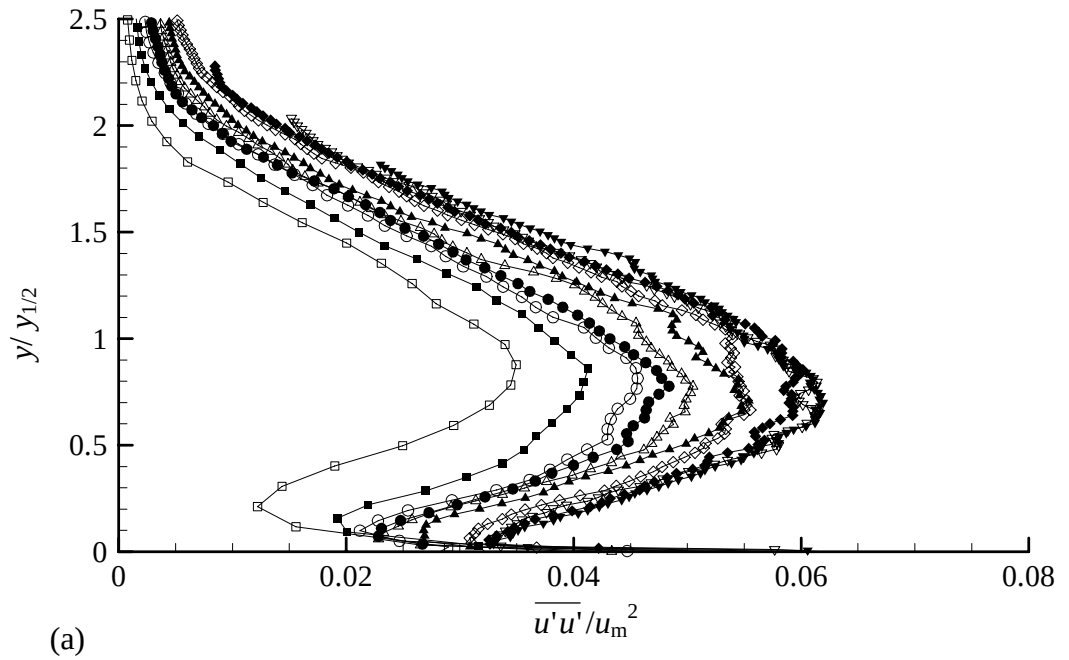
2.5
2
1.5
1
0.5
0
y/ y1/2
0
0.02
0.04
0.06
0.08
u'u'/um2

(a)

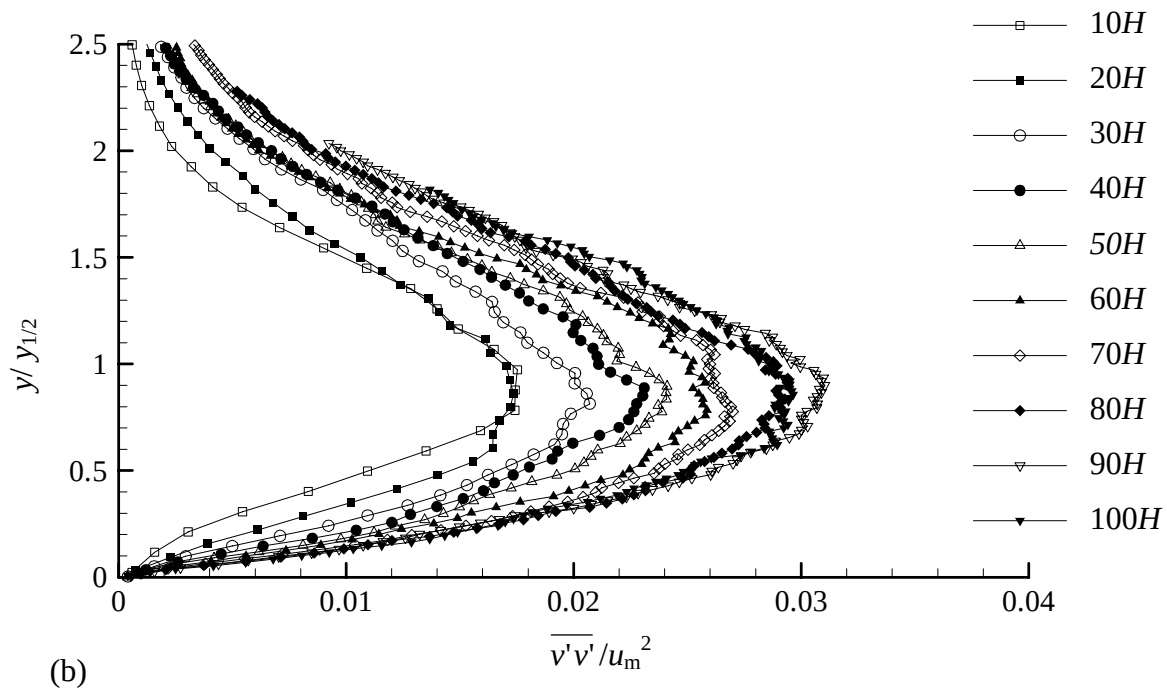
2.5
2
1.5
1
0.5
0
y/ y1/2
0
0.01
0.02
0.03
0.04
v'v'/um2
10H
20H
30H
40H
50H
60H
70H
80H
90H
100H

(b)

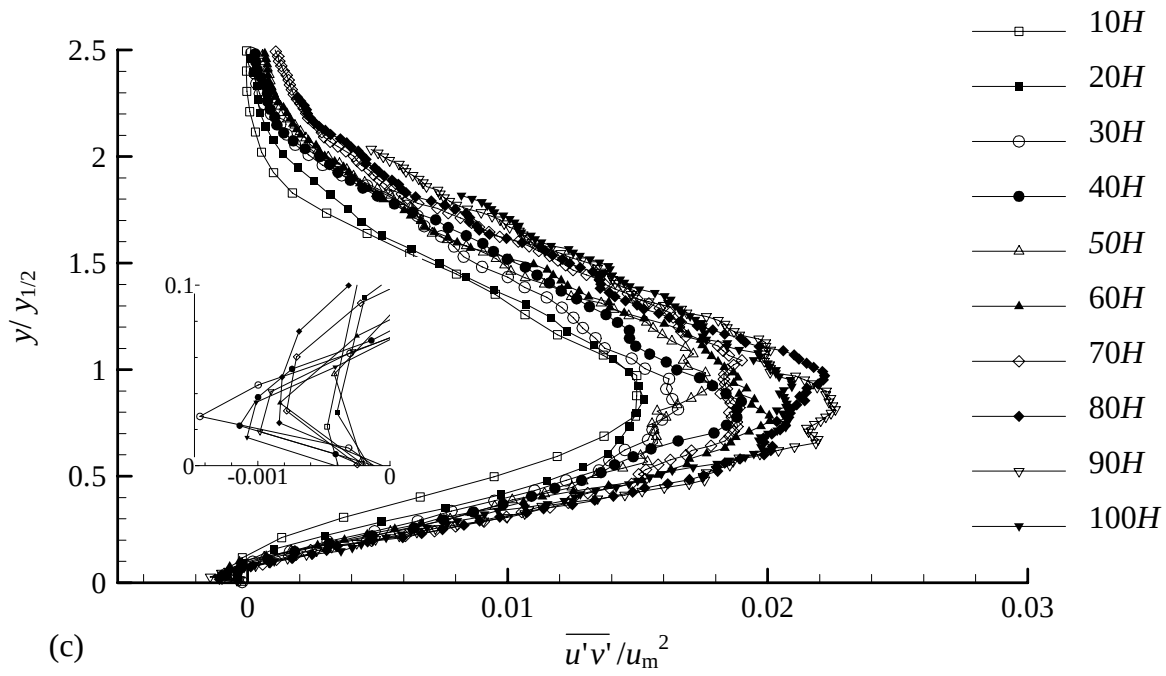


(c)

Figure 4.17: Non-dimensionalized profiles along $z$ = 0 m from 10-100$H$ for (a) streamwise turbulence intensity, (b) transverse turbulence intensity, (c) Reynolds shear stress.

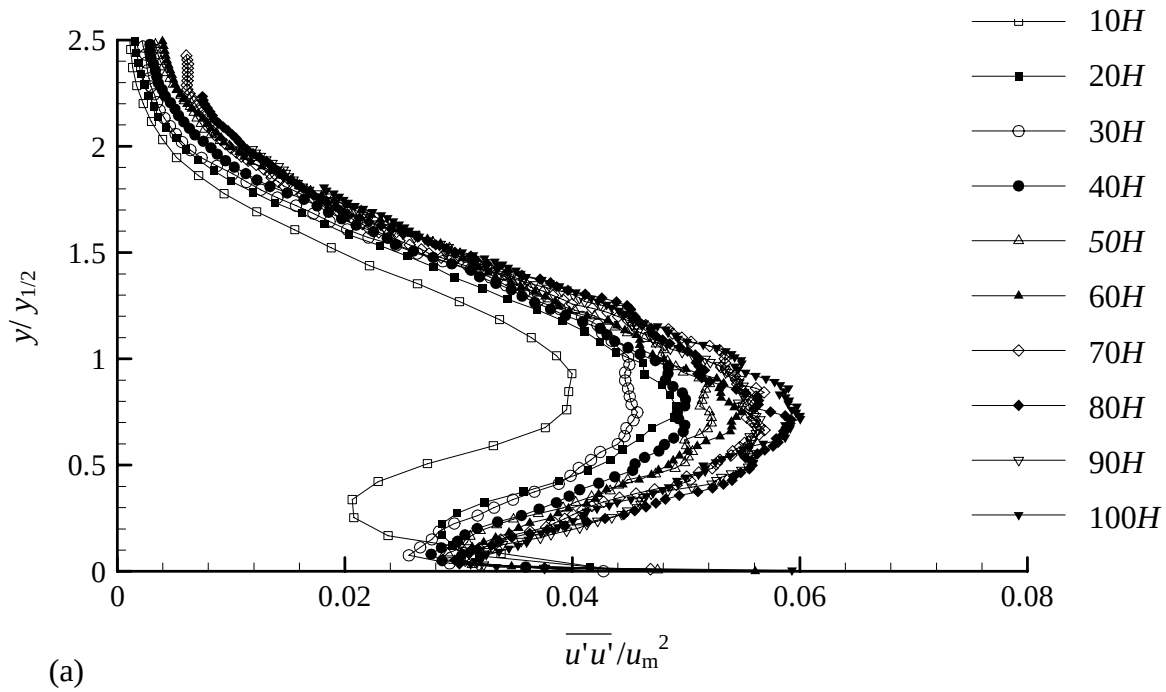


(a)

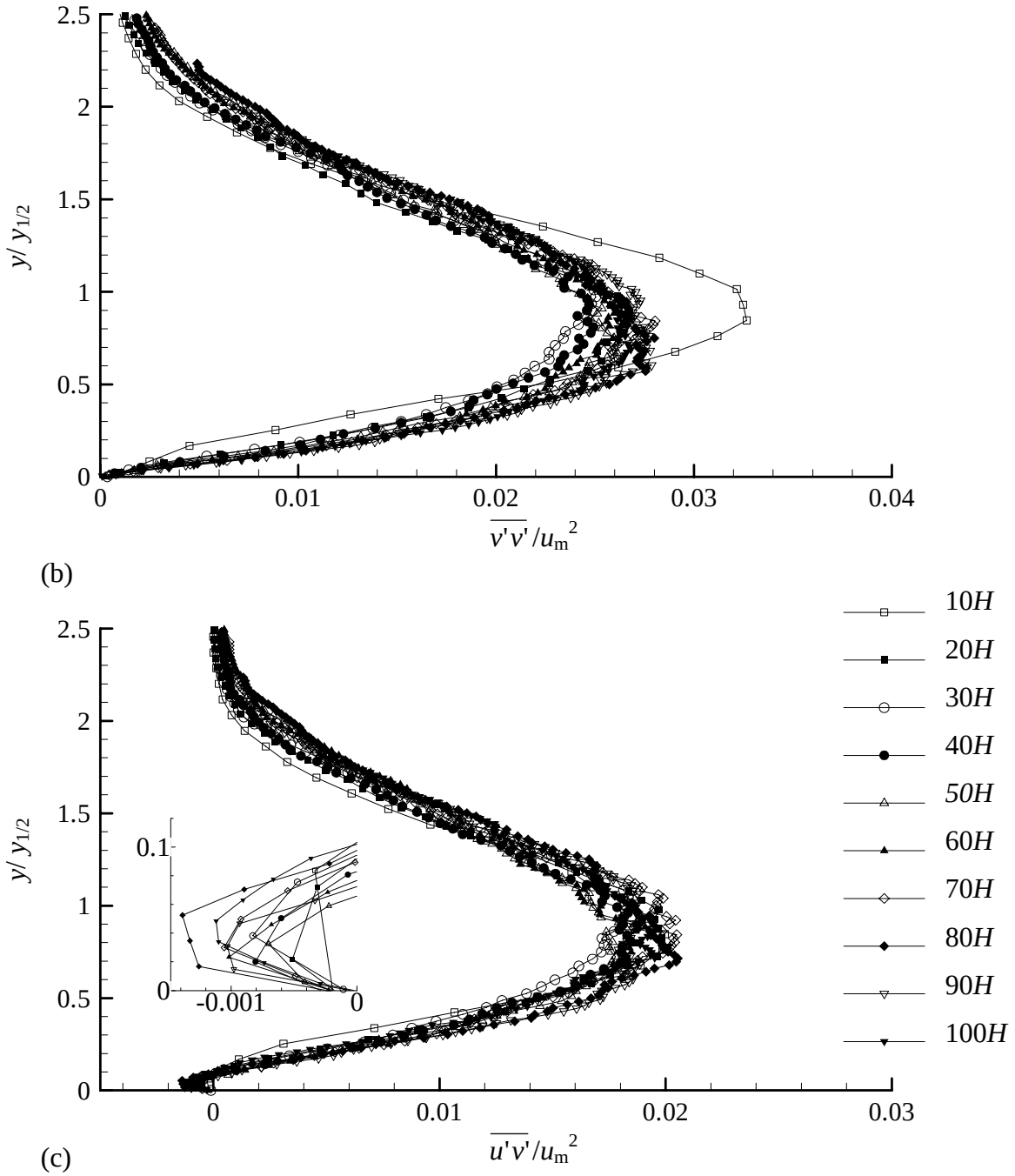


Figure 4.18: Non-dimensionalized profiles along $z$ = 0.275 m from 10-100$H$ for (a) streamwise turbulence intensity, (b) transverse turbulence intensity, (c) Reynolds shear stress.

$x/H$ = 10 and 20 appear to be still developing as they do not have a similar shape to the other profiles. The maximum turbulence intensity values ranged from approximately 0.045 to 0.06 for the normalized streamwise turbulence, $\overline{u'u'}/u_m^2$, 0.02 to 0.03 for the normalized transverse turbulence, $\overline{v'v'}/u_m^2$, and 0.016 to 0.022 for the normalized Reynolds shear stress, $\overline{u'v'}/u_m^2$. The lack of collapse when using the outer scaling coordinates was also noted by Eriksson et al. (1998), who had to subtract the "extra" turbulence in the outer region of the jet in order to achieve a collapse of the turbulence profiles.

The off-centerline profiles achieve a greater degree of collapse. This further suggests that the return flow has less effect away from the centerline. The turbulence profiles collapse to a similar range of values in the region from $x/H$ = 40 to 100 for the streamwise and transverse turbulence, and $x/H$ = 20 to 100 for the Reynolds stress. The range of maximum turbulence values were from approximately $\overline{u'u'}/u_m^2$ = 0.05 to 0.06 for the streamwise turbulence, $\overline{v'v'}/u_m^2$ = 0.024 to 0.028 for the transverse turbulence, and $\overline{u'v'}/u_m^2$ = 0.016 to 0.022 for the Reynolds shear stress.

The lack of collapse of the turbulence intensity profiles could be due to the presence of return flow as discussed, or it could signify that they do not achieve self-similarity until further downstream of the slot. Future studies could take additional measurements at larger $x/H$ values to determine if self-similarity of the turbulence intensity profiles can be achieved.

Figure 4.19 presents the turbulence intensity profiles for the components of the Reynolds stress at $x/H$ = 90 for $z$ = 0.275 m. The normal stress in the streamwise direction, $\overline{u'u'}$, contributes more turbulent kinetic energy to the flow than the normal stress in the transverse direction, $\overline{v'v'}$. The jaggedness of the turbulence intensity profiles indicates that two thousand images were not enough to obtain proper turbulence measurements. Acquiring additional images for each field of view would provide smoother profiles; however, these results still provide a good representation of the Reynolds stresses present in this wall jet flow.

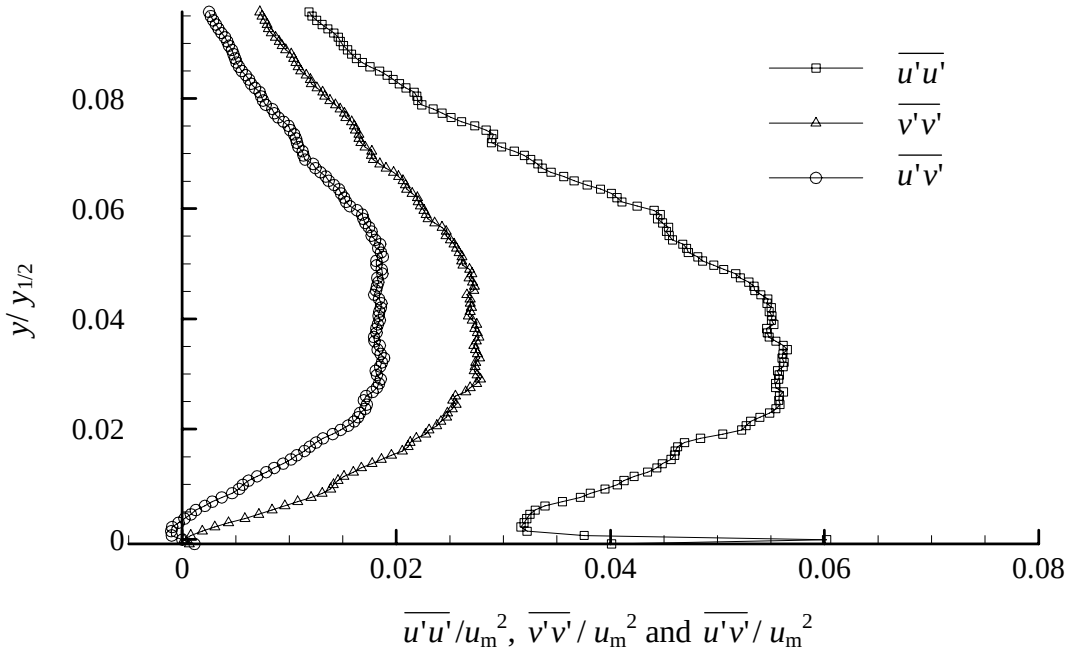


Figure 4.19: Turbulence intensity profiles of the normal stresses, $\overline{u'u'}$ and $\overline{v'v'}$, and the Reynolds shear stress, $\overline{u'v'}$ at $x/H$ = 90 for $z$ = 0.275 m.

## 4.8 Chapter Summary

This chapter evaluated the wall jet that was produced by this experimental facility using multiple methods. Preliminary measurements along the slot width suggest that a two-dimensional flow was initially produced; however there was a discrepancy in the streamwise velocity values for one of the fields of view. The initial conditions near the slot exit were documented by determining the degree to which the profile of the mean streamwise velocity was uniform and by measuring the level of the streamwise turbulence. The initial development region was analyzed, and the region of fully developed flow was found by determining which streamwise mean velocity profiles achieved self-similarity. The rate of spread of the wall jet and the decay rate of the maximum streamwise velocity were determined in the fully developed region and compared to previous results. The profiles of the Reynolds stresses were then presented as preliminary information on the turbulence structure within the wall jet. An initial assessment of the two-dimensionality of this wall jet was performed near the slot exit and downstream of the slot by comparing spanwise measurements of the streamwise mean velocity profiles, the turbulence intensity profiles, and the rates of spread and decay. Chapter 5 will make conclusions about the performance of this wall jet facility, and provide recommendations for future work.

# Chapter 5

# Conclusions and Recommendations

## 5.1 Summary

This study involved the design and construction of an experimental facility to produce a plane turbulent wall jet. A flow conditioning apparatus was built that discharged a horizontal jet of water from a curved channel with a slot height of either 0.009 m or 0.006 m and slot width of 0.756 m. The jet of water flowed across a smooth ground plane that was positioned flush to the bottom of the slot exit. The flow conditioning apparatus was designed to align the flow in the streamwise direction, reduce the turbulence of the flow, and evenly distribute the flow across the width of the slot. There was a vertical wall present above the slot exit, and the apparatus and ground plane were contained within a tank filled with stagnant water. The water was transported from the far end of the tank to the inlet of the flow apparatus using a piping system and a 1.1-kW centrifugal pump. The jet had a Reynolds number, based on the slot height and jet exit velocity, that varied from 7594 to 8121. A particle image velocimetry system was used to take three series of measurements. The first series of measurements were in the horizontal plane at the slot exit and provided data along the entire slot width. The second and third series were in the vertical plane along the slot centerline and 0.275 m off the centerline. These latter measurements provided data from the slot exit to $x/H = 100$ for the streamwise and vertical components of velocity and the three associated Reynolds stress components.

The criteria provided by Launder & Rodi (1981) for assessment of the quality of a turbulent wall jet were used as the basis for verifying the quality of the wall jet produced with this facility. The first criterion was evidence of good two-dimensionality. While Launder & Rodi (1981) recommended the use of the momentum integral equation, this study did not obtain measurements of the wall shear stress so a comparison of spanwise measurements as recommended by Gartshore & Hawaleshka (1964) was used. The second criterion was the proper documentation of the author's work, including the flow conditions. This study provided documentation of the measurements that were performed and presented data for the initial streamwise velocity and turbulence level at the slot exit. The third criterion recommended by Launder & Rodi (1981) was that the data should be consistent throughout all measurements and that turbulence data should be provided where possible. The data presented in this study had a consistent Reynolds number, was able to achieve self-similar profiles of the streamwise velocity, and included extensive measurements for the streamwise turbulence, vertical turbulence, and Reynolds shear stress. The final criterion was that the wall jet should be generally credible when compared to previous established results. This study was able to achieve similar growth and decay rates as previous studies with similar initial conditions, and was able to achieve a collapse of the streamwise velocity profiles when using the traditional outer coordinates of $u_{\mathrm{m}}$ and $y_{1/2}$.

## 5.2 Conclusions

The specific conclusions as to the performance of the wall jet facility are as follows:

1. This experimental facility was able to produce a uniform profile of the streamwise mean velocity with low turbulence near the slot exit. The design criteria that were used to achieve this were a contraction ratio of 36:1, having the radius of the inside corner of the slot be nearly equal to the slot height, and the use of straightening vanes and mesh screens. The centerline profile of the streamwise mean velocity at $x/H$ = 2/3 was uniform over 71% of the slot height with a streamwise turbulence level that was equal to 1.45% of the mean streamwise velocity. These initial profiles were documented to provide a proper description of the flow conditions at the slot exit; satisfying Launder & Rodi's (1981) second criterion for assessment of a wall jet's quality. The documentation also included a description of the initial development from $x/H$ = 0 to 2/3 to show how the uniform streamwise velocity profile initially developed.

2. An initial assessment at the slot exit suggests that the flow conditioner was able to initially produce a two-dimensional wall jet. The preliminary measurements along the slot width provided a mean streamwise velocity at $x/H$ = 1 that was uniform in the spanwise region from $z$ = -0.275 m to 0.327 m. The measurements along the centerline and off of the centerline provided streamwise mean velocity profiles at $x/H$ = 5/6 that had maximum velocity values that were equal within experimental uncertainty limits. Additional spanwise measurements of the mean velocity profile would help to confirm the degree to which this facility is producing a two-dimensional wall jet.

3. The fully developed region for the centerline and the off-centerline ($z/H$ = 46) measurements was determined to extend from $x/H$ = 50 to 100 and $x/H$ = 40 to 100, respectively. The criteria for determining the region of fully developed flow was self-similarity of the profiles for the mean streamwise velocity. This self-similar region was determined by scaling the streamwise mean velocity profiles with $u_m$ and $y_{1/2}$, and identifying the profiles that achieved collapse. The length of the potential core was determined to be 6$H$, which was close to the values provided by Rajaratnam (1976) of 6.1$H$ to 6.7$H$.

4. The downstream flow appeared to be affected by return flow and spanwise spreading. The self-similar streamwise velocity profiles along the centerline had values less than zero at $y/y_{1/2}$ values greater than 2; while the off-centerline profiles had a value close to zero in the outer region. This suggests that a return flow is affecting the centerline measurements more than the off-centerline measurements. The comparison at $x/H$ = 50 of the transverse mean velocity profiles to profiles obtained using the continuity equation show that the spanwise velocity gradient, $\partial w/\partial z$, is close to zero at the centerline; however it has a finite value for the off-centerline measurements. This indicates that spanwise spreading of the wall jet is occurring at 50$H$ for the off-centerline measurements.

5. The growth rate, $d(y_{1/2})/d(x)$, along the centerline was determined to be equal to 0.080 in the self-similar region from $x/H$ = 50 to 100. The off-centerline growth rate was 0.077 in the self-similar region from $x/H$ = 40 to 100. Both of these values compare well with Schneider & Goldstein (1994), and Eriksson et al.

(1998), who obtained growth rates of 0.077 and 0.078, respectively. Schneider & Goldstein (1994) and Eriksson et al. (1998) considered Reynolds numbers of 14,000 and 9,600, respectively, and measured similar profiles for the streamwise velocity and similar turbulence intensities at the slot exit as in this study. These results suggest that similar inlet conditions produce a similar wall jet growth rate. The difference in growth rates along the centerline and off-centerline could potentially be attributed to return flow and/or possible spanwise spreading.

6. The decay rate, $d(\log(u_m/u_0))/d(\log(y_{1/2}/H))$, was found to be -0.624 along the centerline self-similar region, and -0.562 along the off-centerline self-similar region. Schneider & Goldstein (1994), and Eriksson et al. (1998) obtained growth rates of -0.608 and -0.570, respectively. The differences between the decay rates could be partially attributed to the differing values for the virtual origin, which were -6.3$H$ and -13.3$H$ for the centerline and off-centerline measurements of this study, respectively, compared to -8.7$H$ for Schneider & Goldstein (1994). Proper documentation of the decay rate should include the inlet conditions, the value for the virtual origin, $x_0/H$, and the streamwise region that was used to obtain the decay rate. The difference between the centerline and off-centerline measurements of this study could potentially be attributed to return flow and/or possible spanwise spreading.

7. The off-centerline profiles achieved a greater degree of collapse than the centerline profiles in the region from $x/H$ = 40 to 100 for the streamwise and transverse turbulence intensities, and from $x/H$ = 20 to 100 for the Reynolds shear

stress when scaled using the outer coordinates of $u_m$ and $y_{1/2}$ The turbulence profiles along the centerline did not collapse when using the same coordinates, which suggests that a return flow is affecting the wall jet development. The similarity theory proposed by George et al. (2000) stated that the Reynolds shear stress does not scale with $u_m$ and $y_{1/2}$. The results from this study are inconclusive in verifying this statement. The turbulence profiles were presented to provide a more detailed description of the wall jet flow, satisfying Launder & Rodi's (1981) third criterion for assessment of the quality of a wall jet.

8. An initial assessment of the downstream flow showed that the two-dimensionality of the wall jet was affected by the presence of return flow and possible spanwise spreading. The two-dimensionality of the wall jet was analyzed by comparing measurements at the centerline and off of the centerline. In order to further assess and confirm the degree to which the downstream flow is two-dimensional, additional spanwise measurements should be performed. The experimental apparatus was found to maintain similar streamwise mean velocity profiles in the initial development region at $x/H$ = 4. Downstream of the slot at $x/H$ = 80 and 100 the maximum velocity of the streamwise mean velocity profiles were found to be in relative agreement; however the profiles at $x/H$ = 50 were not. The comparison of the growth rate of the wall jet and the decay of the maximum streamwise velocity further show that the two-dimensionality of the wall jet is affected by a return flow and possible spanwise spreading. The difference between the growth rate values varies between 1 to 5% depending on the range of streamwise values that are used. The difference between the decay rate values are

even more pronounced, with a variation between 2 to 17% depending on the range of streamwise values that are used.

## 5.3 Contributions

The main contributions of this research project are as follows:

1. This study was successful in designing and constructing an experimental facility capable of producing a plane turbulent wall jet with a spread rate and decay rate that are similar to other well regarded studies in the literature. This facility can be used to further study both plane wall jets and free jets. For the wall jet, the finite size of the tank appears to produce a lack of strict two-dimensionality in the far field of the jet.

2. This study used particle image velocimetry to provide extensive full-field velocity and turbulence data for a plane turbulent wall jet that can be used to: (a) investigate plane wall jet theory, including the complex interaction between the inner and outer regions of the flow, by studying the coherent structures present in the turbulent flow, and (b) provide benchmark data for computational studies.

## 5.4 Recommendations for future work

The following recommendations are made based on the conclusions reached in this study:

1. Study the structure of the return flow that is present in this experimental set-up, and its precise effect on the characteristics of the wall jet produced by this facility. The

degree to which spanwise spreading occurs should also be studied by obtaining measurements of the spanwise velocity in the *z*-*y* plane.

2. Use the data produced by this study to look at the coherent structures present in a plane turbulent wall jet through the use of the proper orthogonal decomposition (POD) technique (Shinneeb, 2006). These structures could potentially provide insight into the complex interactions between the inner and outer regions of a wall jet.

3. Study the influence of initial conditions on the evolution of wall jet characteristics by adjusting the slot height and Reynolds number.

4. Perform an in-depth analysis of the initial development region where a uniform profile of the streamwise velocity with low turbulence evolves into a fully developed turbulent wall jet.

5. Obtain measurements that attempt to determine the wall shear stress using a technique such as LDA. This would provide the momentum loss at the wall and allow the momentum integral equation to be calculated. The wall shear stress would also provide the skin friction which could then be used to apply the inner scaling coordinates of $u_*$ and $u_*/\nu$. This inner scaling could be used to verify scaling theory presented by other researchers such as George et al. (2000) and Barenblatt (2005).

# References

Abrahamsson, H., B. Johansson and Loefdahl, L. (1994), A turbulent plane two-dimensional wall jet in a quiescent surrounding, *European Journal of Mechanics B-Fluids*, **13**, 533-556.

Barenblatt, G.I, Chorin, A.J. and Prostokishin, V.M. (2005), The turbulent wall jet: A triple-layered structure and incomplete similarity, *Proceedings Of The National Academy Of Sciences Of The United States Of America – Physical Sciences*,**102**(25), 8850-8853.

Bradshaw, P. and Gee, M. (1960), Turbulent wall jets with and without an external stream, *Aeronautical Research Council*, Report and Memoranda 3252.

Dejoan, A. and Leschziner, M.A. (2004), Large eddy simulation of a plane turbulent wall jet, *Physics Of Fluids*, **17**, 025102.

Eriksson J.G., Karlsson, R.I. andPersson, J. (1998), An experimental study of a two-dimensional plane turbulent wall jet, *Experiments In Fluids*, **25**, 50-60.

Farell, C. and Youssef, S. (1996), Experiments on turbulence management using screens and honeycombs, *Journal of Fluids Engineering – Transactions Of The ASME*, **118**, 26-32.

Gartshore, I. and Hawaleshka, O. (1964), The design of a two-dimensional blowing slot and its application to a turbulent wall jet in still air, *Technical Note 64-5*, Department of Mechanical Engineering, McGill University, Montreal.

George, W.K., Abrahamsson, H., Eriksson, J., Karlsson, R.I., Loefdahl, L. and Wosniak, M. (2000), A similarity theory for the turbulent wall jet without external stream, *Journal of Fluid Mechanics*, **425**, 367-411.

Giles, J.A., Hays, A.P. and Sawyer, R.A. (1966), Turbulent wall jets on logarithmic spiral surfaces, *Aeronautical Quarterly*, **17**, 201.

Guitton, D.E. (1968), Correlation of hot wire data for high intensity turbulence, longitudinal cooling and probe interference, *Report Number 68-6*, Department of Mechanical Engineering, McGill University, Montreal.

ISO 5167-1 (1991), *Measurement of fluid flow by means of pressure differential devices – Part 1: Orifice plates, nozzles and Venturi tubes inserted in circular cross-section conduits running full*, International Organization for Standardization, Switzerland.

Irwin, H. (1973), Measurements in a self-preserving plane wall jet in a positive pressure gradient, *Journal of Fluid Mechanics*, **61**, 33-63.

Kundu, P.K. and Cohen, I.M. (2008), *Fluid Mechanics, Fourth Edition*, Elsevier Inc., Amsterdam.

Karlsson, R.I., et al. (1991) *ERCOFTAC Database: Classic Collection at University of Surrey*. Available at http://cfd.me.umist.ac.uk/ercoftac/database/cases/case55/case_data.

Launder, B.E. and Rodi, W. (1981), Turbulent wall jet, *Progress In Aerospace Sciences*, **19**, 81-128.

Launder, B.E. and Rodi, W. (1983), The turbulent wall jet – measurements and modeling, *Annual Review of Fluid Mechanics*, **15**, 429-459.

Mehta, R.D. (1985), Turbulent boundary layer perturbed by a screen, *AIAA Journal*, **23**, 1335-1342.

Morel, T. (1975), Comprehensive design of axisymmetric wind tunnel contractions, *Journal of Fluids Engineering – Transactions Of The ASME*, **97**, 225-233.

Patel, R.P. (1962), Self-preserving, two-dimensional turbulent jets and wall jets in a moving stream, *M. Eng. Thesis*, Department of Mechanical Engineering, McGill University, Montreal.

Raffel, M., Willert, C. and Kompenhans, J. (1998), *Particle Image Velocimetry: A Practical Guide*, Springer, Berlin.

Rajaratnam, N. (1976), *Turbulent Jets*, Elsevier Scientific Publishing Company, Amsterdam.

Schneider, M.E. and Goldstein, R.J. (1994), Laser Doppler measurement of turbulence parameters in a two-dimensional plane wall jet, *Physics Of Fluids*, **6** (9), 3116-3129.

Shinneeb, A.-M., Bugg, J.D. and Balachander, R. (2004), Variable threshold outlier identification in PIV data, *Measurement Science & Technology*, **15**, 1722-1732.

Shinneeb, A.-M. (2006), Confinement effects in shallow water jets, *Ph.D. Thesis*, Department of Mechanical Engineering, University of Saskatchewan, Saskatoon.

Sigalla, A. (1958), Measurements of skin friction in a plane turbulent wall jet, *Journal of Royal Aeronautical Society*, **62**, 873-877.

Tachie, M.F. (2000), Open channel turbulent boundary layers and wall jets on rough surfaces, *Ph.D. Thesis*, Department of Mechanical Engineering, University of Saskatchewan, Saskatoon.

Tailland, A. and Mathieu, J. (1967), Jet Parietal, *Journal de Mecanique*, **6**, 03-131.

Tavoularis, S. (2005), *Measurement In Fluid Mechanics*, Cambridge University Press, New York.

Timoshenko, S.P. (1955), *Strength Of Materials, Part II: Advanced Theory And Problems, Third Edition*, D. Van Nostrand Company, Inc., New York.

Verhoff A. (1970), Steady and pulsating two-dimensional turbulent wall jets in a uniform stream, *Princeton University Report Number 723*.

White, F.M. (1999), *Fluid Mechanics – Fourth Edition*, WCB/McGraw-Hill, United States of America.

Wilson, D.J. and Goldstein, R.J. (1976), Turbulent wall jets with cylindrical streamwise surface curvature, *Journal of Fluids Engineering – Transactions Of The ASME*, **96**, 550